Production and Characterization of Electrospun Metal Nanofibers for Applications in Nanoaerosol Filtration

by

Joerg Ahne

A thesis

presented to the University of Waterloo

in fulfillment of the

thesis requirement for the degree of

Doctor in Philosophy

in

Mechanical and Mechatronics Engineering

Waterloo, Ontario, Canada, 2019

Examining Committee Membership

The following served on the Examining Committee for this thesis. The decision of the Examining Committee is by majority vote.

External Examiner   Alex De Visscher, Professor, Department of Chemical and Materials Engineering, Concordia University

Supervisor(s)   Zhongchao Tan, Professor, Department of Mechanical and Mechatronics Engineering

Eric Croiset, Professor, Department of Chemical Engineering

Internal Member   Amir Khajepour, Professor, Department of Mechanical and Mechatronics Engineering

Internal Member   Roydon Fraser, Professor, Department of Mechanical and Mechatronics Engineering

Internal-external Member   Sheshakamal Jayaram, Professor, Department of Electrical and Computer Engineering

Authors Declaration

I hereby declare that I am the sole author of this thesis. This is a true copy of the thesis, including any required final revisions, as accepted by my examiners.

I understand that my thesis may be made electronically available to the public.

Abstract

Airborne particles have a large impact on human health and the environment. They can be as small as a few nanometers. Electrospun nanofibrous materials have shown strong potential in filtering airborne nanoparticles for their high efficiency and low energy consumption. Electrospinning has been investigated for decades. Unlike polymeric fibers, the production of fibers made from non-polymeric materials is limited. Additionally, the effects of single parameters on the fiber size are not well understood. To better understand the effects of electrospinning parameters on nanofiber size, the following tasks have been conducted:

1. Understand electrospinning using polymer-based samples for air filtration
2. Determine a reliable way of producing metal-based fibers, focusing on composition of the electrospinning solution and calcining atmosphere
3. Conduct a parametric study using metal-based fibrous filter samples
4. Conduct dimensionless parametric studies aiming at predicting the size of the fibers produced by electrospinning

Before producing metal-based fibers, polymer fibers were produced using an existing apparatus in the lab. CA solutions were prepared by diluting various concentrations of CA in a 2:1 (w:w) ratio of N,N-dimethylacetamide (concentration 10 wt.% to 20 wt.%). The electrospinning voltages ranged from 8 to 12 kV with distances from 10 to 15 cm and deposition times of up to 30 minutes. The produced nanofibrous filter samples were then analyzed in terms of fiber size distribution and filter quality factor using nanosized NaCl particles ranging from 4 to 240 nm in diameter. The maximum filtration efficiency measured was 99.8 % for filter samples obtained with an overall deposition time of 30 minutes. The maximum filter quality factor was 0.14 Pa^{-1} for a CA concentration of 20 wt.% and a tip-to-collector distance of 15 cm. The average fiber diameters of the fibers were between 175 and 890 nm, and CA concentrations below 15 % led to the formation of beads.

Then ceria and alumina-based filters were fabricated using the same setup with different operating parameters. Results showed that a solution mix with a ratio of 2:1 ethanol:water with a solid concentration of 15% in a weight ratio of 1:2 w:w metal nitrate:polymer yields the best

fibers in terms of size distribution. The average fiber diameter was reduced by calcination due to the loss of polymer. The average diameter of the fibers was as small as 200 nm after calcination. Additionally, the produced metal-based fibers were tested for filtration and the filtration quality was 0.07 Pa^{-1}, which is comparable to those of polymeric fibers.

The importance of different solution and operating parameters were evaluated. The trial series was planned according to orthogonal two factorial experimental design. Four parameters, each with two levels were chosen for this study. The solution parameter chosen was concentrations of polymer and salt; process parameters included voltage, nozzle size and feed rate of the solution. It was found that the concentration of the precursor solution had a dominant effect on the fiber size, while the effects of electric field strength, flow rate and needle diameter were comparable in their effect on the fiber size.

Dimensionless numbers have been developed using the Pi-theorem aiming at the prediction of electrospinnablitiy. The development of the dimensional tables and the identification of suited parameters for the dimensional table show that the processing parameters electric field strength, needle diameter and solution feed rate; the solution parameters, including viscosity, surface tension and solution conductivity, are the most appropriate for characteristic numbers describing the electrospinning process.

Acknowledgments

I would like to thank my co-supervisors Drs. Zhongchao Tan and Eric Croiset for their guidance, support and inspiration. Their support and trust in my capabilities enabled me to conduct this research. I would also like to thank them for their ongoing advices and support. I also want to thank my PhD committee members, Professor de Visher from Concordia University, and Professors Amir Khajepour, Roydon Fraser, and Sheshakamal Jayaram.

I would like to thank the staff members of the Faculty of Engineering at the University of Waterloo for their technical and administrative support; foremost, Jason Benninger, Andy Barber, James (Jim) Merli, Greg Friday, and Louise Green. Furthermore, I am extremely grateful to the current members and alumni of the Green Energy & Pollution Control Lab during my PhD studies, foremost Raheleh Givehchi, Haiming Wang, Maryam Razavi, Chao Yan, Wala Bkari, Qiang Zhou, Ben Tan and Fangyan Sun. I would also like to thank the undergraduate research assistants, Noelle Wong and Allison Irvine, whom I had the pleasure to work with. I would also like to thank Hassan (Moses) Moussa for the training and insight on operating an electron microscope. Financial support from NSERC, CFI and the University of Waterloo are also acknowledged.

I would like to thank the track and field teams of the University of Waterloo and the University of Guelph; my coaches and teammates, who helped me to keep smiling throughout difficult times far from home and teaching me that hard work and dedication make anything possible.

I wish to thank my parents Heike and Gerd. Thank you for your unconditional love, support and understanding throughout my whole life, especially the last few years. I owe you everything.

Above all, I wish to thank my friend, advisor, English teacher, training partner, motivator and partner in good and bad times, Erika Fiedler. You know this thesis would not exist without you.

Dedication

To

Wolfgang Mertsching

You are missed

Table of Contents

List of Figures

List of Tables

Nomenclature

Roman Symbols

c_e	Entanglement Concentration (%)
C_W	Concentration with Filter
$C_{W/O}$	Concentration without Filter
D	Parameter "Concentration"
$d_a \dots d_{abcd}$	Fiber Diameter with Parameter A … ABCD high (nm)
df	Fiber Diameter (nm)
dN	Needle Diameter
E	Electric Field Strength (kV/m)
F	Droplet Form Correction Factor
F	Free Matrix of M
g	Gravitational Acceleration (m/s²)
K	Constant
K	Kernel Matrix
m	Mass (kg)
M	Metal
M	Dimensional Matrix in Reduced Echelon Form
n	Number of Runs
QF	Quality Factor (Pa^{-1})
r	Radius (m)

R	Physical Quantity
s	Distance (m)
t	Time (min)
U	Voltage (kV)
V	Volume (m³)
V	Flow rate (ml/hr)
Z	Dimensional Matrix
ΔP	Pressure Drop (Pa)

Greek Symbols

γ	Surface Tension (mN/m)
ε	Permittivity (F/m)
η	Filtration Efficiency (%)
θ	Temperature (°C)
κ	Electric conductivity (S/m)
μ	Dynamic Viscosity (cp)
ν	Kinematic viscosity (mm²/s)
Π	Dimensionless Group
π	Pi=3.14159
ρ	Density (kg/m³)
Φ	Effect of a Parameter (-)

T(x)	Contribution of a Parameter x (%)

Abbreviations

CA	Cellulose Acetate
COV	Correlation
DMAc	N,N-Dimethylacetamide
DMF	N,N-Dimethylformamide
FE	Field Emission
PM	Particulate Matter
PM10	Particulate Matter 2.5-10 µm
PM2.5	Particulate Matter 0.1 - 2.5 µm
PVA	Polyvinylalcohol
PVP	Poylvinylpolindrone
RH	Relative Humidity
SEM	Scanning Electron Microscope
SMPS	Scanning Mobility Particle Sizer
v:v	Volume to Volume
w:w	Weight to Weight
X	Multitude

Chapter 1 Introduction

1.1. Problem Statement

Particulate matter (PM) is one of the most critical air pollutants. It is generated from different sources including volcanic emission, fuel combustion, agriculture crop burning, cooking, and house cleaning. PM can be classified according to the particle size in the air. Micron particles have a diameter between 0.1 and 100 µm. They are further divided into coarse, fine and ultrafine particles. Ultrafine particles are also referred to as nanoparticles in the air. Coarse particles are those in the range of 2.5-10 µm (PM10), fine particles are sized between 0.1 and 2.5 µm (PM$_{2.5}$), and nanoparticles are those with at least one dimension in the range of 1-100 nm (0.001-0.1 µm). [1,2]

Airborne nanoparticles are more toxic than larger ones because of their small sizes and large surface to volume ratios [3,2,4]. They have considerably high deposition rates (greater than 90%) in the alveolar region of the lungs. Nanoparticles are not completely removed from the upper parts of the respiratory system and penetrate deep into the lungs. They can enter the circular system [5-7,3]. Nanoparticles are smaller than the cells and thus can penetrate through them. Charged nanoparticles have 5-6 times greater deposition into lungs and cause more adverse health effects than larger ones [8]. Not only do nanoparticles have the greatest interactive capacity with biological systems due to their large surface areas [1], they also can transport toxic chemicals into the respiratory system [9].

Exposure to nanoparticle causes various adverse health effects such as ischemic heart disease, cardiovascular diseases, stroke, chronic bronchitis, asthma, and respiratory tract infections [10,11]. Adequate protection against exposure to nanoparticle includes minimizing nanoparticle exposure in enclosed buildings (house, workplace or nanotechnology lab) and personal exposure at an occupational level.

1

Air cleaning by filtration contribute greatly to effective reduction of exposure to airborne nanoparticles. The exact mechanisms for air filtration depend on the particle size. The filtration of micrometer-sized particles and larger ones are achieved by interception and impaction. Smaller ones are captured by diffusion. Filtration by diffusion requires a high surface area to volume ratio in contrast to conventional filters. Very fine fibers like nanofibers have a great potential in fulfilling the requirement of a large surface area while having a low overall volume. [12-14]

Nanofibers can be produced by electrospinning. Electrospinning technology was first developed in the 1930s [15], and it has been intensively investigated over the past decades. The process relies on the stretching of a polymer solution in an electric field, while the solvent evaporates on its way from the nozzle to the grounded collector. Since the initial product of electrospinning were polymers, the production of pure polymer nanofibrous materials has been well investigated. However, it is still challenging to electrospun non-organic materials. Generally speaking, the electrospinning of metal-based fibers relies on the production of polymeric fibers, which have been doped with metal-based materials like salts. After electrospinning, the organic material has to be removed. Meanwhile rigid crystals and fibers are produced. Through the addition of salts to the electrospinning solution, the solution properties change significantly, which poses new challenges to the electrospinning process.

The electrospinning process depends on a variety of parameters [16]. They can be classified into setup dependent parameters, like voltage and needle-to-collector distance, and solution properties such as viscosity and conductivity and environmental properties like air temperature and relative humidity. These parameters interact with each other. For example, the solution density and electrospinning temperature have a great impact on its viscosity. Through these interactions, a change of one parameter can affect the fiber size or, in a general term, electrospinnability. Electrospinnablitiy describes the capability of an electrospinning setup and the applied solution to produce fibers successfully.

Despite the interactions among these electrospinning parameters, most studies on electrospinning focused on the impact of a single parameter on the nanofiber size [17-25]. These single parameter studies make it challenging to compare the impact of the single parameter on

the fiber size with respect to others. Furthermore, the results of single parameter studies are often stand-alone results for specific research groups. A slight change, for example, in the setup (i.e. nozzle size, plate shape or size) with other parameters being constant, may yield dramatically different fiber sizes. For the polymer PVA (polyvinyl alcohol), researchers reported comparable concentrations and applied voltages but different collector types and different fiber sizes. Givehchi et al. [26] used a 10 cm x10 cm plate collector and collected fibers as thin as 150 nm, while Choi et al. [27] collected their PVA fibers on a rotating drum, with documented fiber sizes of 240 – 340 nm.

A small number of researchers conducted parametric studies to understand the relative impact of parameters on the fiber size, or to determine a complete model for the electrospinning process [28,17,29,30]. The research has been focusing predominantly on the absolute impact of parameters. For example that the increase of the viscosity leads to an increase in the fiber size, without considering the other parameters affected by the viscosity change. These studies show contradicting results. Furthermore, all studies failed in understanding the interactions among the electrospinning parameters, which have a major impact on the fiber size. At this point, it is challenging to predict the electrospinnability of a given solution in a certain setup.

1.2. Research Objectives

The main objective of this research is to better understand the interaction among multiple parameters on the electrospinning process. To achieve these goals, the following tasks have been completed:

1) Validation of basic impacts of parameters on fiber size
2) Feasibility of producing stand-alone metal-based nanofibers
3) Parametric study of key parameters of electrospinning on fiber diameter
4) Development and validation of a Pi-theorem model to predict the size of fiber produced by electrospinning

1.3. Research Approach

The overall structure of this thesis is shown in Figure 1-1. There are eight chapters in this thesis. Chapter 1 provides an overview of the research problem and describes the motivation, opportunities and objectives of the thesis. A comprehensive literature review is presented in chapter 2, including the relevant knowledge about electrospinning and the related parameters. Chapter 3 describes the methodology of the experimental and analytical works of the thesis research. It focuses on the production and analyses of nanofibers, as well as the analyses of the electrospinning process in terms of solution properties, fiber characterisation and statistical methods. A 2k factorial design and the Pi-theorem are introduced in this chapter. The Pi-theorem is a method for computing sets of dimensionless parameters from given variables, even if the form of their interaction is still unknown. It provides a way of generating sets of dimensionless parameters for further analysis.
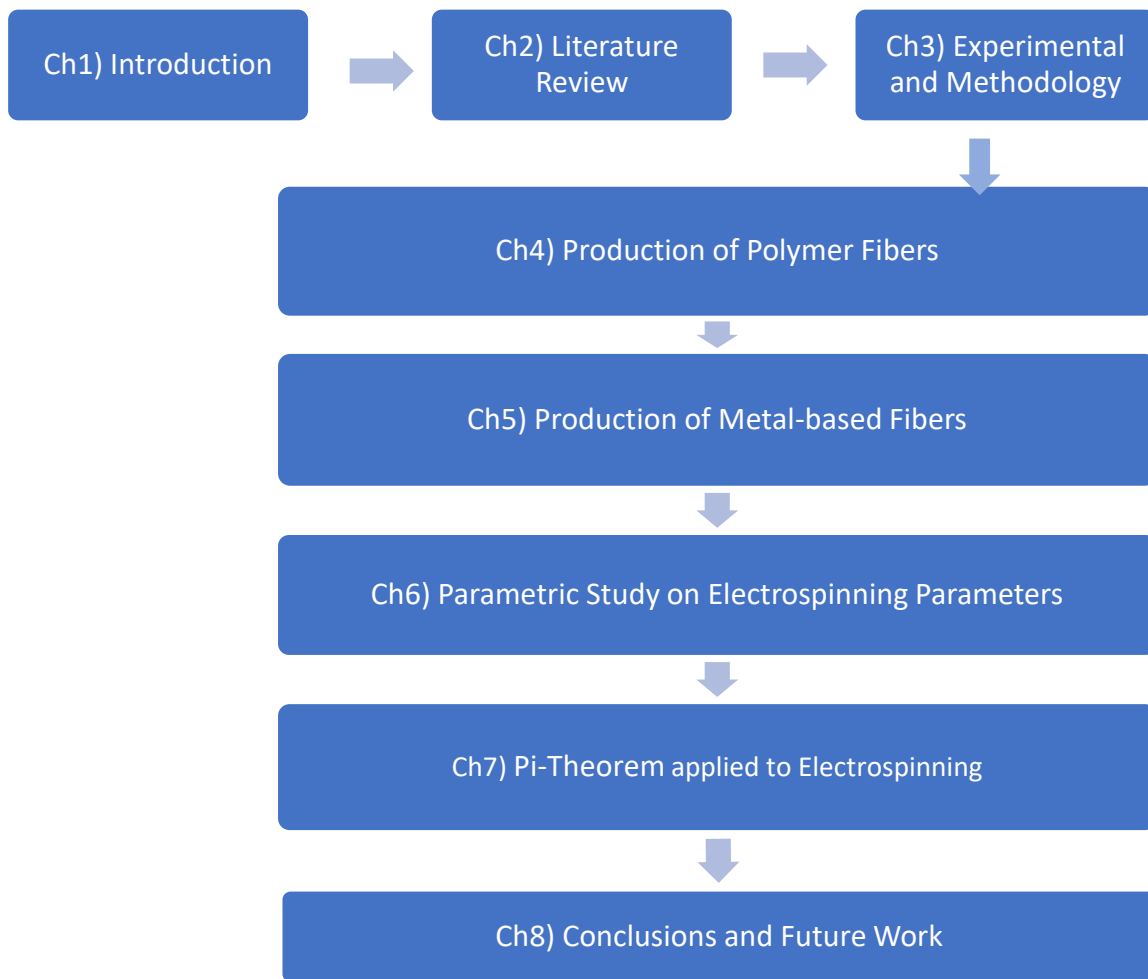
Figure 1-1 Thesis structure

Chapter 4 describes the process of the production of pure polymer fibers made of cellulose acetate. This chapter introduces an electrospinning setup for the research and presents single parameter studies on the following parameters, applied voltage, concentration and distance. Results are compared with those in literature. Also confirmed was the filtration behaviour of the nanofibrous materials for nanosized particles. Chapter 5 is an extension of chapter 4 by metal-based nanofibers. The first part of the chapter discusses the development of an operational precursor solution for metal-based fibers. The fibers for the rest of the research were produced using poylvinylpolindrone (PVP) as a precursor polymer and hydrate nitrate salts as metal source. The electrospinning takes place in the same way as in the previous chapter. However, after electrospinning, the filter samples were calcined in order to remove the polymer and to

form metal-based fibers. Chapter 6 uses the results from this research to conduct a parametric study on the relative impact of electrospinning parameters on the fiber size, comparing the polymeric electrospinning process with the calcined fibers. Applying the findings of the previous chapters, Chapter 7 describes the development of a model for electrospinning using the Pi-theorem. The process led to the final dimensionless number, considering all parameters relevant for electrospinning. In conclusion, the developed dimensionless numbers can be used to predict the calculated fiber diameter or the electrospinnability.

Chapter 2 Literature Review

2.1. Introduction

This chapter provides first an overview of recent studies on airborne nanoparticles and their impact on society. Control mechanisms of nanoparticles are then described briefly without elaboration, because the focus of this thesis work is on electrospinning for nanofibrous materials for air filtration purposes. The literature review has shown a variety of parameters that impact the quality of the electrospinning process, as well as the fiber size of the produced fibers. However, it was challenging to determine relationships between parameters to predict electrospinning outcomes. Furthermore, many researchers have presented contradicting results regarding the effects of electrospinning parameters on the fiber morphology. As a conclusion of this chapter, nanofibers produced by different research groups differ strongly from each other, even for identical materials. This is a challenge for the effective transfer of knowledge from laboratory to industry.

2.2. Nanoparticles

Nanoparticles can cause considerable harm to an organ. [31] Nanoparticles (with sizes in the range of 1-100 nm) can enter and damage organisms because of their small sizes. Many nanoparticles can breach the defence barriers of humans, reaching the deepest parts of the body. They can cause disorders to cellular processes. Nanoparticles can enter the respiratory tract and start accumulating in the lungs, which increases the risk for cancer, bronchitis and asthma. However, the toxicity of nanoparticles depends on the materials they are made of and the exact arrangement of their atoms. Considering the possible variations of atom arrangement in nanoparticles yields different physical and toxicological properties for the same materials. [2]

Nanoaerosols are nanoparticles suspended in a gas. These nanoparticles could be liquid droplets but are usually solid particles with at least one dimension in the range of 1-100 nm. Most researchers consider nanoaerosol as another name of ultrafine aerosol or ultrafine particulate

matter. There is a slight difference between ultrafine aerosol or particulate matter and nanoaerosol. The former is commonly used to describe airborne nanoparticles that are produced incidentally without intention. The latter has a broader coverage, including both environmental and engineered nanoparticles in any carrier gas. A nanoaerosol can be either organic or inorganic and generated in nature or by engineering processes. [32]

What distinguishes nanomaterials from other materials is their size. The physical behaviour of nanoparticles falls within the transitional zone between individual atoms/molecules to their equivalent bulk materials [33]. The reduction of the particle size leads to modifications of the physical and chemical properties from the bulk and molecular counterparts of nanoparticles. For a group of airborne particles with a fixed bulk density ($10 \, mg/m^3$) and unit density ($1 \, g/cm^3$), the number of particles increases exponentially, along with the surface area, as the particle size decreases to less than 100 nm. This allows for a greater proportion of atoms or molecules on the surface, allowing adjacent atoms and substances to interact more readily. The surface-to-volume ratio determines the potential number of reactive groups; the intrinsic properties of materials at the scale are emphasized compared to their larger bulk counterparts. The enhanced activities could be either beneficial (e.g., antioxidation, carrier capacity for drugs, increased uptake and interaction with biological tissues) or disadvantageous (e.g., toxicity, instability, induction of oxidative stress), depending on the intended use [34-36]. The charges carried by the materials in contact with membranes, tissues and its chemical reactivity play a dominant role when particles react with other substances, but these charges are mostly independent of the particle size. [37,36].

Nanomaterials have been used in a variety of applications, including fillers, opacifiers, catalysts, semiconductors, cosmetics, microelectronics, and drug carriers [34]. With the increase in production and usage of engineered nanomaterials, the potential environmental and health impacts have increased and must be investigated and confirmed [38,36]. The health impacts are summarized in the following section.

2.3. Impacts of Nanoparticles on Human Health

The particle size and surface area of nanomaterials are important characteristics from a toxicological point of view. For example, inflammation, genotoxicity, and histology are related to surface area instead of particle mass. It can be shown that the occurrence of tumors correlates more with surface area than with the particle mass [39,40]. It is established that the available surface area is the most critical parameter for the (health) effects of nanoparticles, together with surface chemistry, biodegradability, number, shape and solubility. [41,33,42,36]. Studies show that an increase of nanoparticle concentration correlates with short term increases in morbidity and mortality [43,44].

Out of all exposure paths, inhalation is the most important entry route for nanoaerosols [33,34]. The respiratory zone consists of all structures that participate in gas exchange and it begins with the respiratory bronchioles [45]. The human lungs contain approximately 2300 km of airways and 500 million alveoli [46]. The surface area of the human lungs is estimated to be between 75–140 m^2 in adults [47,48]. The pseudostratified epithelia that constitute the barrier to absorption into the bloodstream are markedly different in airways and alveoli of the lungs. In the tracheobronchial region the epithelium is protected by a mucus layer [49]. Any particle deposited in this area is transported away from the lung by mucociliary clearance [50], or diffused through the thick mucus to reach the epithelium cells. In contrast, the alveoli have a thin, single cell layer. The distance from the air in the alveolar lumen to the capillary blood flow is less than 400 nm. The large surface area of the alveoli and the intimate air–blood contact in this region make the alveoli less protected against inhaled substances, such as nanoparticles, as compared to the airways [49].

Depending on the size and shape, the deposition of nanoparticles can occur in all regions of the lung, reaching from the airways to alveoli. Table 2-1 shows the site and size of particles that can deposit in the lung. With particles smaller than 500 nm, the deposition rate increases everywhere in the lung, due to an increase of diffusional mobility [51]. Fibers with small diameters penetrate deeper, while long fibers (over 20 μm) can be found predominantly in the upper airways. [52,53,36]

9

Table 2-1 Mechanism of aerosol deposition [49,51]

Site	Size (µm)	Mechanism	Comment
Large airways	5–9 (slow inhalation), 3–6 (fast inhalation)	Impaction	Most deposition in segmental airways
Smaller airways	1–5	Gravitational sedimentation	Improved with slow and deep breathe
Respiratory bronchioles	1–3	Gravitational sedimentation	Improved with slow and deep breathe
Alveoli	≤0.5	Brownian diffusion	Most exhaled

Particles need to be small enough to avoid the initial deposition in the upper airways and go through to the lower airways. On the other hand, particles need to be large enough to avoid exhalation [54,55]. Therefore, particles around 1 µm have the highest deposition efficiency [51]. Smaller particles are mostly exhaled after inhalation without deposition [56,57]. However, the deposition of particles smaller than 100 nm appears to have a deposition efficiency of around 50% [51,49,58]. Their effects were even greater on people with asthma or other obstructive pulmonary diseases. [36,59,60]

2.4. Filtration of Airborne Nanoparticles

Filtration is the most effective way to capture airborne particles for the protection of environment and health. If the particulate matter is not separated, the membrane will lose its function due to clogging [12]. This section summarizes different mechanisms which are applied to filter particles from an airstream.

Considering a particle dispersed in a gas stream moving towards a target, the particle is likely to stick to the target on impact due to inter-surface forces. The most dominant mechanisms describing possible ways of the particle touching the target are impaction, interception and diffusion. For nanoparticles, diffusion is the dominant mechanism.

Nanofibrous filters have been shown to be a more affordable option for the filtration of nanoparticles [61-63]. Nanofibrous materials have two distinct advantages over microfibers: they have 1) a higher filtration efficiency, due to slip flow and 2) a larger surface area to volume ratio, which increases the deposition of particles, and through that the filtration efficiency. Research has shown that nanofibers have a long lifetime, can be loaded with a larger particle mass, have a lower air resistance and are relatively light [64]. Over the last decades, the relevance of nanofibrous materials in the industry grew and is expected to reach a market size of USD 700 billion in the next few years [65].

The characteristic difference of nanofibers compared to larger fibers is the slip flow. Due to their size, nanoparticles are small enough to pass through the mean free path of gases under normal conditions. The slip flow allows more particles to approach target surfaces, through which the capture due to Brownian diffusion, interception and impaction is greatly increased [66,67]. As a side effect, the slip flow also reduces the air resistance, since the drag force on the nanoparticles is reduced [68,69]. Research has shown that the interception efficiency can be further improved, when the fiber size is similar to that of the particle size. Overall, nanofibrous filters are an efficient and affordable alternative to current micro fibrous filters [66,70,71]. Considering the potential of nanofibrous materials compared to the conventional fiber technology, a more efficient and controllable production of nanofibrous materials is desirable.

2.5. Nanofiber Production Technologies

Nanofibers can be produced by melt blowing, forcespinning, and electrospinning. Each of them have pros and cons. Melt blowing is a method of producing non-woven fibrous materials, which has been used in commercial production [72,73]. It relies on the extrusion of molten polymer through a fine orifice into a high velocity hot air stream [72-74]. Under the right conditions, the drag of the hot air causes the polymer to elongate into a fiber. This process can produce fibers with diameters ranging from 1 to 50 μm. It means that the method can produce fibers and is efficient for commercial use, however, the fibers are not real nano-sized. Furthermore, the materials are limited to thermoplastic polymers. [75]

The melt blow method can be improved with an assisting electric field. It can produce finer fibers than the sole melt blowing method. The produced fibers are roughly 1 μm and with a narrower fiber size distribution, which is qualitatively better than purely melt blown fibers. Therefore, these fibers tend to have a better filtration efficiency. [76]

Forcespinning is another method to produce polymeric nanofibers. It utilizes centrifugal forces, which allows for a much higher output than melt blowing and electrospinning. This method does not require any electric field. It can also be used with polymeric solutions or melts, if the viscosity is acceptable.

The forcespinning process begins with first loading the solution/melt into a spinneret, specially designed for this process. During the nanofiber production, the polymer solution is drawn from the orifice by rotating forces. As the polymer is drawn, the important parameters that need to be considered include spinneret angular velocity, orifice radius, polymer viscoelasticity (which includes viscosity and relaxation time of the material), surface tension, evaporation rate (for solvent in solution), temperature (melting and solidification), and distance between spinneret orifice to collector. The rate of solvent evaporation depends on polymer viscosity and elasticity. In the case of polymer solutions, it is important to determine the polymer-solvent compatibility to determine optimum concentration that enables the production of nanofibers with the desired size and morphology.

To produce a polymer jet, the rotating speed must be high enough to overcome the surface tension of the solution or melt. If the forces exerted on the jet are too high, the surface tension of the polymer solution can cause the jet to break up, resulting in beads. This may occur under certain conditions where the angular velocity of the spinneret is low (low centrifugal forces) and/or the viscosities are not too high. [77]

Electrospinning by itself is an old technique, which was first described by Rayleigh in 1897 and studied further by Zeleny in 1914 [78]. Later on it was patented by Formhals in 1934 [72]. The fundamental scientific work has been conducted by Taylor and has continuously advanced since [79,16]. The following section is focused on electrospinning process as it is the central scope of this thesis work.

2.6. Electrospinning and governing parameters

Electrospinning can be applied to the production of nanofibers. A good nanofiber filter consists of fine fibers, since the filtration efficiency increases with a decreasing fiber diameter [80]. Fiber diameter can be influenced by several solution and process parameters [81]. A narrow distribution of fiber diameter indicates a reproducible spinning process. A typical electrospinning process has a low output [82]. Problems often occurring during electrospinning are blocked nozzles causing uneven fibers and dripping of solution onto the spun fibers, destroying the web structure. Even if the fibers are used as a coating layer for filtration purposes, the challenges of an even distribution and good quality stay identical. [17]

In this research, electrospinning is chosen as the method for nanofiber production because it can produce the finest nanofibers in the range of 10s to 100s nm. Electrospinning is often seen as a simple and controllable procedure. In a standard experiment of electrospinning in a laboratory, a polymer solution, or melt, is pushed through a thin nozzle (also acting as an electrode), which has an internal diameter in the order of 100 nm (see Figure 2-1). An electric field of 100-500 kV/m is applied to the nozzle. In a laboratory setting, the distance between the collector and the needle tip is 10-25 cm. The corresponding currents can range from 100s nanoamperes to microamperes. The substrate on which the build-up of electrospun fibers takes place is commonly brought into contact with the counter electrode. The electrospinning process can be vertical or horizontal.
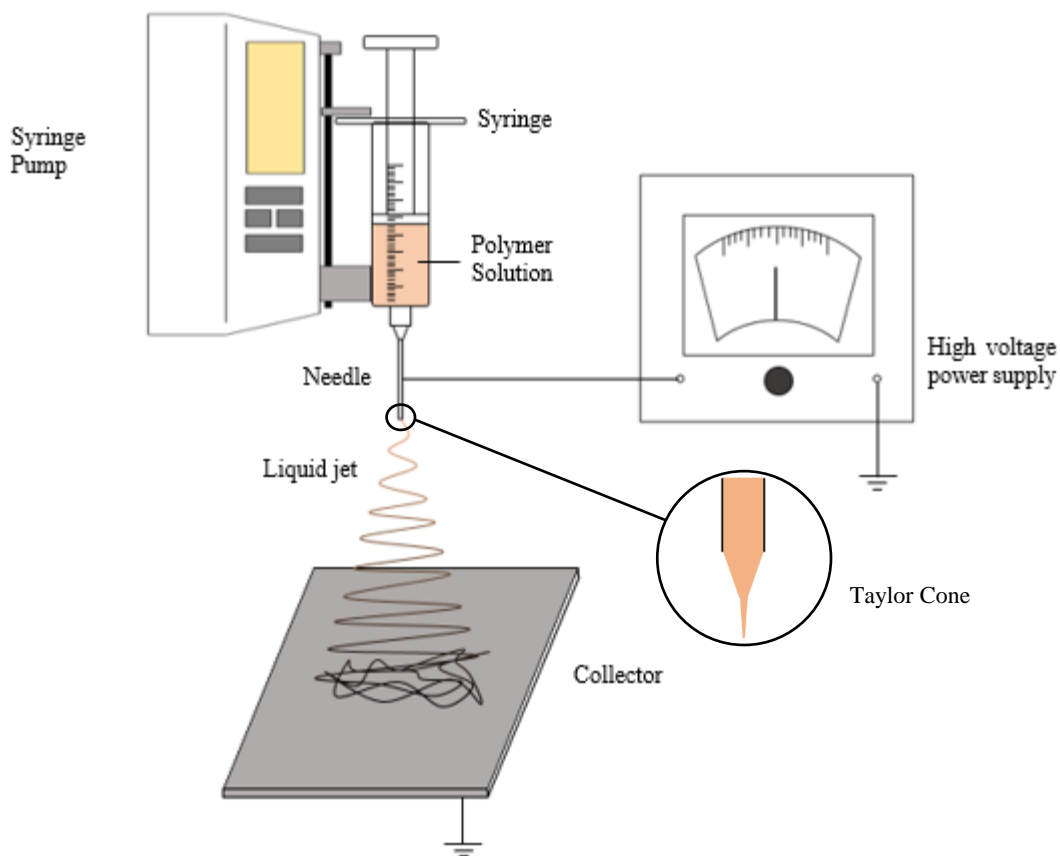
Figure 2-1 Electrospinning setup

The dissolution of polymers in the solution is crucial to successful electrospinning. The solution properties depend on the degree on entanglement of the polymer molecule chains. Furthermore, to obtain rigid polymer layers after electrospinning, the polymer chains need to be entangled enough to hook into each other. However, for the electrospinning process a liquid is needed, therefore it is necessary to have the polymer not entangled in the solution [83] (see Figure 2-2).

| (a) Polymer before dissolution | (b) Dissolved polymer | (c) Electrospun polymer |
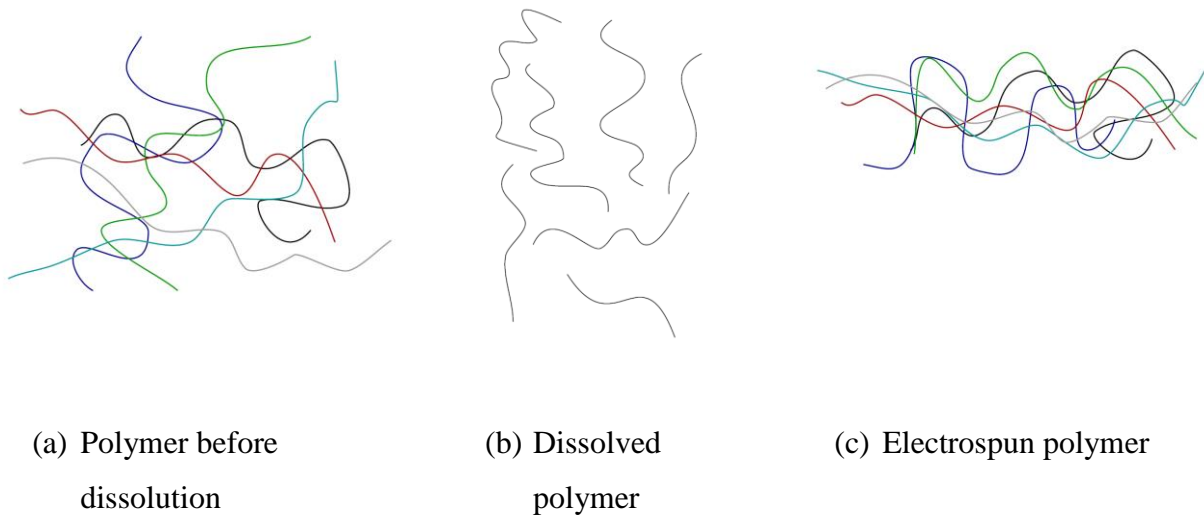
Figure 2-2 Stages of polymer entanglement

Dissolving polymers can take place in different ways. One model [84] considers the detangling and diffusion of the polymers in the solvent. In combination with the solvent, the polymer forms a gel-layer as a boundary, which is known as plasticization. The larger the polymer chain, the lower the dissolving rate, since the larger chains need more energy to be detangled, due to a larger entropy of disorientation [84]. Theoretically, polymer chains are straight. However, they are practically in amorphous states of random conformation. The hydration of polymers is either performed by direct H-bonds between the polymer and water or is achieved by water molecules surrounding hydrophobic groups of the polymer. If the solvent consists of more than one liquid, a competition for the H-bonds is taking place, where the solvents bind at different sections of the long polymer chain (see Figure 2-3). The literature assumes the solvent-solvent interaction to be relatively weak compared to the interaction between the solvent and the polymer
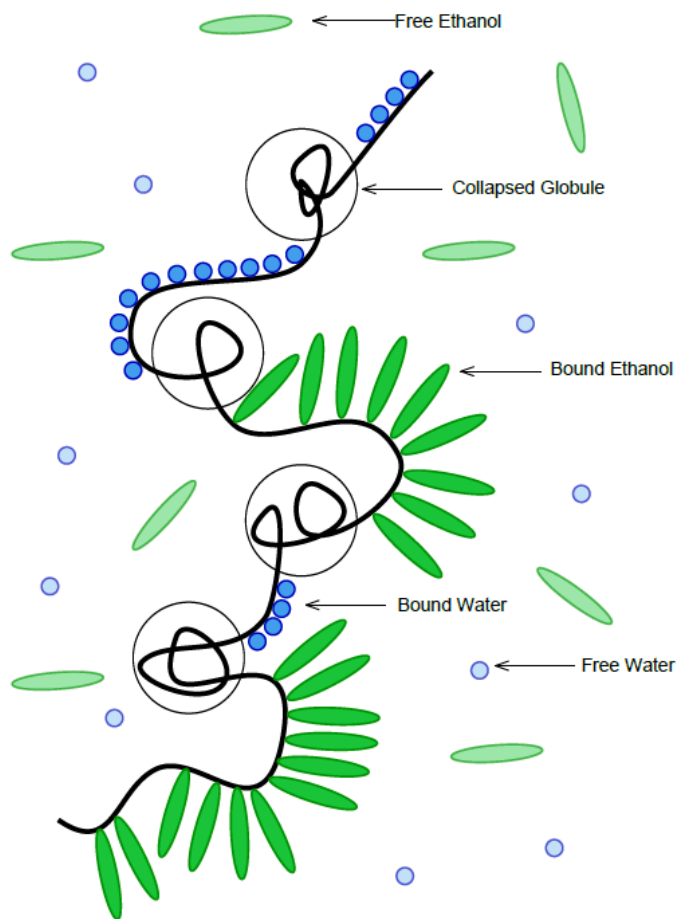
Figure 2-3 Dissolved polymer molecule and bonding of solvent molecules to the polymer

During the electrospinning process, the liquid solvent evaporates quickly due to the high travel speed of the jet. After deposition, some liquid is stored in the fiber membrane due polymer plasticization and incomplete evaporation, which leaves liquid between the chains [81,85]. The residual liquid can be removed with drying or aging of the polymer membrane. During the electrospinning process, the polymer chains change their orientation from random to uniform, while they are still entangled enough to form rigid mats (see Figure 2-2).

The applied electric potential difference causes a droplet of polymer solution to deform, producing a cone-shape towards the counter electrode as seen in Figure 2-1 [86]. The Taylor cone angle is approximately 30° in electrospinning. Upon increasing the voltage, the drop

becomes a jet, which moves in the direction of the counter electrode and becomes thinner [87,88]. Solvent evaporation or solidification of the jet occurs on route to the counter electrode. The evaporation process (diffusion speed of the solvent) depends on the humidity of the surrounding atmosphere. Research has found that the spinning process produces more fiber material fibers when the relative humidity is as low as possible [89]. These jets velocities can reach 40 m/s or higher. Medeiros et al. [90] found that the diameter of PVA electrospun fibers decreased as relative humidity increased and beads were formed on the fibers electrospun at 60% and 80% relative humidity (RH). This effect is opposite to that of fibers electrospun from organic solvents such as dimethylformamide (DMF), tetrahydrofuran, and toluene, in which fiber diameter generally increases as the relative humidity increases. PVA dissolved in water ranged from 230-540 nm at 20% relative humidity, and 100-400 nm for 80% RH; while poly (methyl methacrylate) dissolved in DMF ranged from 1000-1200 nm at 20% to 1900-2100 at 60% relative humidity.

It is important to control the configuration and external climate as they play a vital role in electrospinning. The process is controlled by the external electric field that is produced by the application of voltage as well as the induction of an electric field (which is due to the free and induced charges present on the surface of the jet). Furthermore, the diameter and morphology of the nanofibers are affected by surroundings and environments. These factors include the distance between the needle tip and target, the diameter of the needle, the shape of the collector, and the amount of potential difference that is applied. Other processing conditions are the feed rate and solution temperature. The upcoming subsections discuss these factors extensively. Electrospinning technologies have been introduced in the following papers [91-96]. A summary of electrospinning parameters can be separated into processing and material variables. [16]

Processing variables:

- Voltage
- Electrode arrangement
- Electrode material
- Electric field intensity
- Tip-to-collector distance

- Solution feed rate
- Needle diameter

Material variables:

- Solution viscosity
- Surface tension
- Solution conductivity
- Solution permittivity
- Polymer molar weight
- Solution concentration
- Solvent quality
- Charge density
- Chemical composition

Environmental variables

- Relative humidity
- Temperature

2.6.1. Voltage

A predominant factor that can be used to manipulate the electric field is the applied voltage between the needle and the collector, which act like two electrodes. In a typical setting, 6 kV is needed to make the jet form the Taylor cone [79]. The jet will gain velocity at a more rapid pace, and a greater amount of solution will be pulled out of the needle at a higher voltage applied as the amount of charge will be greater [97]. The change of voltage could impact the shape of the jet. At a specific voltage, the Taylor cone is no longer visible and the jet appears to come from the nozzle directly [98].

More stretching of the jet (because of greater columbic force faced by the surface charges) and a decrease in the diameter of the electrospun nanofibers [99,27,100] can be observed as the applied voltage increases. This change also causes the electric field between the needle and the

target to increase. Pawlowski et al. [101] have also shown that drier fibres can be produced at a higher voltage because the resulting solvent evaporates at a faster pace. In comparison, Zhao et al. [102] proved that a weaker electric field was produced at a lower voltage, which caused the jet to decelerate and increase its time of flight. This will result in thinner fibres. Furthermore, a voltage that is near to the minimum critical voltage is necessary for the initiation of electrospinning for thinner fibres. The effects of applied voltage on the average fiber size are not clear. Zhang et al. [103] found that an increase in voltage led to thick fibers. Some studies had mixed results showing a smoother fiber, but thicker fiber at low voltages, and thinner fibers with more defects at high voltages [104], with a minimum diameter depending on voltage [105,106]. Matabola and Moutloali [105] found a minimum voltage of 12 kV for polyvinylidene fluoride fibers and Tan et al. [104] found almost no impact on the fiber size of polylactic acid fibers, while a minimum of 10 kV was required to generate an electrospinning jet.

Another result of high voltage is the formation of beads. This is probably because a high voltage causes the jet to become more unstable when a recession of the Taylor cone into the syringe needle occurs. The shape of the bead changes according to the voltage from a spindle to a spherical shape. It is common for the beads to amalgamate to form thicker fibres since the amount of the beads has increased [107-109]. Nevertheless, according to Jarusuwannapoom et al., there will be increased solution stretching and the number of beads formed would be lower at higher voltages [110].

2.6.2. Electrode Arrangement

Using various electrode settings is another method to alter the electric field between the needle tip and the collector. Researchers used a needle and flat collector plate as electrodes. Later, technological advancements led to the changing of the electric field by altering the electrode arrangement, to attain the desired nanofiber morphologies.

Collector electrode configurations that have been scrutinized to form fibres that are highly aligned [111] include rotating tube collector with knife-edge electrodes, rotating wire drum collector, spinneret with knife-edge blade, disc collector, and drum collector with a wire wound. An arrangement of many spinnerets has also been used to mix fibres from different materials.

Balancing the electric field between the spinneret and the collecting plate can be done by the guard electrode arrangements.

Many researchers have used single-needled systems for laboratory studies of electrospinning, but it has a low throughput. To be more industrially relevant, other researches have reported multi-jet electrospinning. A model presented by Theron et al. [112] indicates that nine jets could electrospin from distinct nozzles with a pitch of 10 to 400 mm under appropriate conditions. Yarin et al. [113] used a ferromagnetic sub-layer in liquid form to produce approximately 26 jets/cm^2 in the vertically upward direction. The voltage used was about 32 kV. The diameter of the fibre was between 200 and 800 nm. Yang et al. [95] reported a better stability when using needles of different lengths in the form of a ring arrangement. Additionally, it was stated that the stable voltage required for spinning in the case of using needles with different lengths is lower than the one needed for the ring arrangement [113]. The characteristics of jets in a multi-jet electrospinning procedure were examined by using simulated data [112]. The mutual Coulombic interactions affected the path followed by each electrified jet in this process. According to Dosunmu et al. [114], a porous tube is more efficient than a single-needle system. A cylindrical needle with a porous material has been employed. The electrospinning solution has been pushed through the material into the electric field. The resulting fibers showed a comparable fiber size and size distribution; however, the production rate has been greatly improved.

Although the outcome of these methods seems to be promising, there are some drawbacks involved, which led to other studies [115,116]. An important obstacle is the possibility of clogging in multi-needle systems. It has also been stated that capillary spinning (usage of needles for electrospinning purposes) does not have a very high efficiency for the synthesis of nanofibers. Hence, Miloh et al. [115] recommended the use of needleless and free surface electrospinning or accumulation of numerous jettings powered by electricity through the application of high electric fields on planar and cylindrical surfaces. The practical and theoretical studies with the aim of improving the rate of fibre production at an industrial level has taken place by making use of Newtonian and viscoelastic polymeric liquids used in free surface electrospinning [117]. Yarin et al. claimed that large-scale production of nanofibers could be done by making use of the magnetic and electric fields that act on a magnetic fluid and

the layer of polymer solution without using any needles. Nanospider[TM] [118] is a device that produces nanofibers effectively by making use of a rotating-cylinder solution-feeding system [119]. This device was studied by Jirsak et al. [119] and further improved by Wang et al. [120], where the cylinder in the Nanospider[TM] was replaced with an electrospinning disc, which consisted of a disc that would perform rotary motion.

The collector plates in a majority of electrospinning systems are made of conductive materials such as copper and aluminium. They are grounded, yielding a built-in potential difference between the two electrodes. Less fibres are produced when the material used for the collector is an insulator because the charges on the electrospinning jet cumulate on the collector plate [121].

2.6.3. Tip-to-Collector Distance

Altering the electrode gap can change the resultant electric field between the needle tip and the target collector, and the consequent travel time of the nanofiber. The distance between the two electrodes can be decreased, which in turn strengthens the electric field and increases the acceleration of the jet. The time of evaporation is thus decreased. Reducing the distance between the needle tip and target will allow the fibers to form an interconnected fiber mesh because of the excess amount of solvents.

However, beaded fiber and jet instability can occur due to strengthening of the electric field and short travel distances [27,100,110]. Increasing the distance between the needle tip and the collector can help decrease the average diameter of the fibers since there is also an increase in the flying time, which gives sufficient time for the jet to elongate and become thinner [97,102,95,122,123,105]. Increasing the distance between the two electrodes can result in narrow size distribution of the nanofibers. It was also noticed that when decreasing the intensity of the electric field, the average diameter of the fiber increased. Zhao et al. [102] noticed that if the distance between the needle tip and the target is longer than 250 mm, then the ethylcyanoethyl-cellulose/tetrahydrofuran solutions could not be electrospun with high voltages [102,108]. On the other hand, Zhang et al. [103] could not see any change of morphology while changing the tip-to-collector distance.

2.6.4. Flow Rate

The amount of solution needed for electrospinning depends on the liquid flow rate. A minimum solution flow rate for a specific voltage and electrode gap is needed to maintain a stable Taylor cone [97,23,124]. The external Taylor cone could disappear at a low flow rate. Instead, a jet bursts out from the liquid surface. On the other hand, if the electrospinning rate is less than the solution flow rate, the solution droplets will fall from the needle tip because there is not enough time for electrospinning to take place. It was noticed that an increase in the flow rate increased the diameter of the fiber and the size of the bead [100,107,125-127,124]. It was also noticed by Biber et al. [21] that the average diameter of the fibers decreased when the flow rate of the solution increased. In addition, the increased flow rate allowed for a wider size distribution of the nanofibers. It was reported by Zong et al. [107] that different shapes of fibers can be acquired by changing the solution flow rates for a given electric field. They also reported that lower solution flow rates (20 µl/min) created thinner fibers with spindle-like beads, and contrarily, higher solution flow rates (75 µl/min) led to thicker fibers with large beads [107]. For industrial applications, a compromise must be found between the increased diameter due to the higher volume flow rate and increased production rate. It takes longer to dry the fibers when more solution is drawn from the needle tip, which results in the fibers clumping together. Yuan et al. [123] conducted experimental studies using bisphenol-A polysulfone with solution flow rates of 0.0066 ml/min and 0.011 ml/min. They determined that the lower feed rate is needed to acquire thinner and bead free fibers because there is more time for the solvent to evaporate [123].

2.6.5. Needle Diameter

There are limited studies on the effects of the needle diameter on the electrospinning process. The problem of needle clogging and beading in the collected nanofibers due to low exposure of the solution to the atmosphere can be solved by using a thinner needle [99,97]. Smaller needle diameter may also contribute to a minor increase in the heat of fusion and melting temperature [128]. These parameters describe the energy needed for polymers to form crystalline structures. An increase of heat of fusion or melting temperature of polymers reduces the degree of crystallinity in the polymer, which changes optical and mechanical properties of the polymer.

Higher crystallinity results in a harder and more thermally stable, but also more brittle material, whereas the amorphous regions provide certain elasticity and impact resistance. Chen-Ming et al. [128] found a reduction of the degree of crystallinity of polycaprolactone from 60% before electrospinning to around 30% after electrospinning [128]. Reduction in the needle diameter could increase the jet flying time of the solution between the needle and the collector plate because the surface tension of the droplet is increased while there is a decrease in jet acceleration. However, when the needle orifice is smaller than 0.5 mm, it became quite challenging to electrospin the solution due to greater surface tension [102]. Nair et al. [129] noticed that the rate of electrospinning increased dramatically by using the needles with larger inner diameter. More homogeneous fibers can be produced using larger needles [21,129]. Macossay et al. [130] have electrospun polymethymethacrylate using needles of different sizes. They reported that there was no correlation between the average fiber diameter and the needle diameter.

2.6.6. Intrinsic Properties of the Polymer Solution

It has been found in the literature that the electrospinning process and the resultant fiber morphology are affected by the properties of the polymer solution. The chemical compositions of the polymer and the solvent affect the properties of the polymer solution [16]. The factors include the molecular weight and its distribution, concentration, surface tension, viscosity, permittivity and conductivity. They are briefly summarized as follows.

2.6.6.1. Viscosity

Molecular weight and concentration of the polymer affect the viscosity of the solution, and consequently, the diameter and morphology of the fiber. The larger the molecular weight of the polymer, the greater viscosity of the polymer-solvent mixture. Likewise, there is an increase in the viscosity of the polymer-solvent mixture with increasing concentration of polymer in the solution [124].

It has been noticed that the viscosity of a solution and the polymer chain entanglements have a direct relationship with each other [97]. The polymer chain entanglements increase along with the viscosity of the solution. Polymer chain entanglements have an important effect on the jet

when it breaks up into small droplets and when the resultant electrospun fibers contain beads [131]. A low chain entanglement lowers stability of the jet, leading to splitting of the jet, while an increase of the entanglement stabilizes the jet by preventing the jet from breaking up. For fibers to be formed during the electrospinning process, a minimum amount of polymer chain entanglement, i.e. concentration, is needed. In contrast, the pumping of the solution by using a syringe pump becomes challenging when the viscosity is high, and the solution may dry out at the tip of the needle before electrospinning starts [132,107,126].

In viscous solutions, it is less likely to form beaded fibers. The shape of the beads ranges from spherical to elliptical when the viscosity of the solution changes from low to high values. Thicker fibers and smaller deposition areas can be achieved by increasing the viscosity. Variations that happen in fiber morphology when the viscosity is changed are listed in Ramakrishna's research [97]. In this, the viscosity and entanglement were directly linked to the molecular weight of the applied polymer. As a conclusion, the polymer concentration alone could not give a clear indicator on the electrospun fiber size. Low concentrations could produce fine, bead free fibers, since the increased entanglement on hence increased viscosity were sufficient. The minimum concentration (and therefore viscosity) to successfully electrospin polylactic acid fibers dissolved in DCM has been found to be 1.0 wt% with a molecular weight of 300,000 g/mol. On the contrary, with lower molecular weight (100,000 g/mol), the minimum percentage has been found to be 9 wt%. For both molecular weights, beads have been found at lower concentrations. With increasing polymer concentration and thus viscosity, the produced fiber diameter increased, until the specific mass of the jet becomes too large to allow for an effective elongation of the jet [97]. Considering that the production of nanofibers is usually conducted with a specific available polymer with a specific molecular mass, the findings of Ramakrishna regarding concentration and molecular weight can be directly translated into solution viscosity. Any given electrospinning solution has a certain range of viscosity, inside which uniform electrospinning is possible. Outside of this range, beading occurs.

2.6.6.2. Surface Tension

The charges on the polymer solution must be high enough to overcome the surface tension of the solution while electrospinning. The polymer is stretched when the electrospun jet is

24

accelerated from the tip of the needle to the target, and the jet breaks up into droplets due to surface area of the solution which results in electrospraying [133]. Also, beaded fibers due to surface tension are created if there is a smaller concentration of polymer molecules [104,81,134,107]. Fong et al. [134] found a reduction of the surface tension from 76 to 50.5 mN/m improved the quality of the produced fibers, while the electric field strength has been reduced from 0.7 to 0.5 kV/cm. Due to the lower surface tension, the initial jet was larger, which led to a more stable spinning process. It can be concluded that due to a lower surface tension in the spinning solution, the electrospinning jet can also be started at a lower electric field strength.

The surface tension of a solution depends on the type and constitution of the solvent. Various solvents may have different impacts on the surface tension [97,98,107,126]. When a surfactant is added to the polymer solution, the surface tension can also be modified. Usually, when all other variables are constant, surface tension sets the upper and lower boundaries of the electrospinning process.

2.6.6.3. Conductivity

The solution is stretched and forms nanofibers by repulsion of charges at the surface of the electrospinning jet. A dramatic decrease in the diameter of the electrospun nanofibers is noticed when the electrical conductivity of the solution increases, mainly because the jet holds more charges. Adding a small amount of salt or polyelectrolyte to the polymer solution can help prevent the creation of beaded fibers as the electrical forces of the greater charge held by the electrospinning jet causing it to elongate, lead to the creation of uniform fibers. Zhang et al. [103] found that an increase of conductivity of a PVA solution from 1.53 to 10.5 mS/cm lead to a decrease of the fiber size from 214 to 159 nm [103]. Likewise, the formation of the fiber, if the solution has zero conductivity, is also not possible [110,124].

It was noticed by Kim et al. [135] that the fiber diameter decreased when there was an increase in the conductivity of a poly (2-acrylamido-2-methyl-1-propane sulfonic acid) solution. Usually, electrospun nanofibers with the smallest fiber diameter can be obtained when the solution with the greatest conductivity is used. Kim et al. [135] increased the salt concentration of sodium chloride and calcium chloride in their solution from 0.0001 to 0.1 mol%. While the

other electrospinning parameters remained unchanged, the average fiber diameter decreased from 70 to 35 nm. However, it could be seen that the viscosity also dropped from 160 cPs at 0.0001 mol% to 122 cPs at 0.01 mol%. With 0.1 mol% of salt, viscosity increased again to 128 cPs. The number of beads observed in this study followed the same trend as the viscosity; having the highest number with the highest viscosity, dropping while increasing the salt content at the local minimum of 0.01 mol% and increasing after again. The higher the polymer solution conductivity, the lower the onset voltage to enable electrospinning [122]. Choi et al. [136] found that a conductivity increase of their poly (3-hydroxybutyrate-*co*-3-hydroxyvalerate) solution from 0.5 to 10 mS/cm decreased the electrospun fiber size by almost 1 μm, while the viscosity and surface tension were almost unchanged [136]. Moreover, a greater bending instability and a larger deposition area of collected fibers resulted due to a higher solution conductivity, i.e., a higher charge concentration [136]. Other researchers have confirmed the trend of finer fibers with increased conductivity or higher salt concentrations [105], but also an increase with a larger salt content [82]. The size of the ions in the solution has a great impact on the electrospun fiber diameter along with the amount of charges carried by the jet. Ions that possessed a smaller atomic radius had a higher charge density and in turn, under an external electric field, had a higher mobility [107,136]. In Moghe et al. [137], an innovative method on producing bead free ultra-fine electrospun fibers with narrow fiber diameter distribution from Poly (3-caprolactone) has been developed. The authors have created high quality fibers by increasing the conductivity of the polymer solution by making use of a new solvent system that utilized an acid base reaction to create weak salt complexes. But, Stanger et al. [24] discovered that a decrease in the mass deposition rate and initial jet diameter during electrospinning was due to an increase in charge density. Also, a theory was given forth, where they correlated the reduction of the diameter of the curvature of Taylor cone with the increase in charge density and as a consequence, a reduction of total electrostatic forces because of an effective area which is comparatively smaller [24]. Likewise, other researchers have also given reports about the varied behavior of the Taylor cone to point out the resemblance to the Taylor's survey of ionic liquids [138,86,139]. These papers also confirmed the challenge of altering one parameter, without changing the others. Garoz et al. [138] found an interaction between surface tension and conductivity, where the best results have been achieved with a surface tension of 50 dyn/cm and a conductivity greater than 2 S/m. De la Mora [139] states that a Taylor cone (and therefore

electrospinning) requires a minimum conductivity of 10^{-4} S/m, however it also states that these values do not apply to liquids with low viscosity such as water. The research also confirms that a variety of parameters impacts the electrospinning process, due to their interactions.

Biodegradable polymers have started to be more and more utilized in the fields of food, medical and pharmaceuticals [97]. That is why, many researchers have tried to electrospin natural polymers such as cellulose acetate, chitin, chitosan, alginate, collagen, gelatin, and silk [107,97]. A carrier synthetic polymer is used mostly to electrospin natural biopolymers, due to their substantial polyelectrolyte behavior [97,89,136,140,88]. Likewise, conductive polymers have been electrospun to create semiconductor devices such as Schottky nanodiodes. For instance, Pinto et al .[141] tested electrospinning polyaniline, which is a conductive polymer; however, they have only managed to electrospin polyaniline by creating a polymer blend and combining it with polyethylene oxide (PEO) [142,141].

2.6.6.4. Permittivity

The permittivity of a solvent has a major effect on the fiber morphology. To the best knowledge of the author, however, there are not many publications on these effects. Theron et al. [143] reported a process by which the permittivity of an electrospinning solution could be calculated by measuring the complex impedance of a small cylindrical volume of the fluid [143]. A decrease in the bead formation and diameter of the resultant electrospun fibers can be achieved by utilizing a solution which has a greater permittivity. Increasing permittivity can help increase the bending instability and lengthen the path of the electrospinning jet, which in turn results in a decrease in the fiber diameter and greater deposition area. An increase in the permittivity of polymer solution can be achieved through the use of solvents such as N,N-Dimethylformamide (DMF) [144,145]. Son et al. [144] documented a decrease from 2 to 0.4 μm of their produced polyethylene oxide PEO fibers with the an increase of the dielectric constant from 5 to 80, by altering the solvent from chloroform to DMF or water. This phenomenon has been explained by the polarity of the charges in a jet. However, the altered solvents also had an impact on the other solution parameters, so an interaction between the permittivity and viscosity or surface tension of the solutions cannot be excluded.

2.7. Electrospinning of Non-Polymers

The electrospinning process of non-polymer materials relies on a polymer as a precursor. In addition, salts are dissolved to act as a metal source to the polymer and the solvent. The added salt mainly impacts the solution specific properties, such as conductivity (salts typically increase the conductivity of a liquid) and viscosity (the salt ions bind otherwise free solvent molecules, which attach to the molecule through their bipolarity). After electrospinning, the polymer in the membrane can be removed by calcination if the calcination temperature is set above melting point of the carrier polymer and the temperature increase of the heating process is slow, to allow the metal to crystallize and form grains, which follow the "template" of the polymer fibers. With higher temperatures, the salts decompose to oxides [146] and the binding forces between grains increase due to sintering effects [147,148,106]. A summary on the production methods of ceramic nanofibers can be found in Ramaseshan et al.'s work [149], showing a summary on materials, which have been electrospun and which solvents and carrier polymers have been used.

Especially catalytic metal-based fibers have found intensive research over the last years. Since the electrospinning process is considered to be identical to pure polymers, the focus of most research is focused on the production of stable fibers. An interesting ceramic is cerium oxide (ceria), which has shown great catalytic potential, because of its ability to preserve and release oxygen [150]. Liu et al. [151] produced ceria-silver carbon fiber hybrids. The electrospinning solution was created by dissolving Ag(NO3) and Ce(NO3) in DMF with polyacrylonitrand PVP as carrier polymers. The calcination process has been conducted in two steps, first drying the fibrous mats in air at 220 °C and then carbonizing the leftover polymer in an inert atmosphere at 550 °C. The results of this process were mechanically very rigid fibers with a tensile strength of 29.59 KPa. Amuse ceria's catalytic properties, Li et al. [93] produced CeO_2-ZnO fibers for photocatalytic purposes in water treatment. In this research, PVP has been used as polymer using zinc acetate and cerium nitrate precursor. In this case, the utilized solvent was a mixture of 2:1 ethanol and water. After calcining at 600 °C, fibers shrank from 227 nm after electrospinning to 46 nm. Another combination of polymer and solvent has been used by Kanzler et al. [152] to produce $ZrCeO_2$ fibers. The research group used hydrated CeCl3 and

dissolved it together with PVP in a DMF-ethanol mixture. The calcination process has been conducted in two steps. The fiber mats were dried first at 127 °C and lastly calcined in air at 700 °C with a heating rate of 3.8 °C/min. Kanzler et al. found their method suitable for other ceramics like TiO_2 and RuO_2 as well. PVA has been employed as carrier polymer in Yang et al.'s [95] research used PVA as carrier polymer and water as a solvent in order to produce ceria fibers. In this case, hydrated $CeNO_3$ has been used as a metal source. Yang et al. also applied a two-step thermal treatment of the fibrous material. The samples have been dried at 90 °C in a vacuum and then calcined for 6 hours at 500 °C. The research group found that all organic materials from solvent and polymer were no longer detectable [95]. The final fiber size after calcination has been found to be 50-100 nm.

For other materials than ceria, similarities can be found in the production of ceramic nanofibrous materials. Shao et al. [92] used $ZrCl_3$ as a metal source to produce ZrO_2 fibers in a range of 50-200 nm. As for some of the ceria samples, PVA has been used as a polymer and the thermal treatment consisted of two steps, with drying at 70 °C first and calcination at a higher temperature of 800 °C. Shao et al. also utilized a comparable method to produce pure iron nanofibers. In this case, hydrate iron nitrate has been dissolved in a mixture of PVA and water to be electrospun [153]. The calcination process was again a two-stepped process, however in this case drying at relatively low temperatures was not necessary, but after the initial calcination at 550 °C, the samples have been treated at 750 °C in a hydrogen atmosphere to reduce the iron oxide to pure iron. The resulting fibers had an average diameter of 180 nm.

George and Anandhan's [91] research on ceramic NiO fibers focused on the impact on the calcination temperature on the grain structure of the resulting ceramic fibers. As stated in other research, the organic components tend to evaporate at lower temperatures [95] and the high calcination temperatures are needed to let the metal (oxides) form grains and bonding structures between the grains [149]. In their research, George and Anandhan formed NiO fibers from nickel acetate tetrahydrate and SAN for diesel catalytic purposes, using DMF as a solvent. The electrospun samples have been calcined at 500, 600, or 700 °C and the grain morphology has been analyzed. The characteristic difference between the different calcination temperatures was the fiber diameter. Samples calcined at 500 °C showed an average fiber diameter of 135 nm, while the samples calcined at 800 °C were 88 nm (on average) in diameter. Opposing to the

fiber diameter, the diameter increased with an increase of the calcination temperature, which impacts the mechanical properties of the samples. However, a test of the mechanical strength of the samples has not been conducted.

Certain aspects are reoccurring in the literature of ceramic nanofibers. Often, metal nitrates are utilized as a precursor for the ceramic. The selected solvents are often water, water-alcohol, or pure alcohol mixtures, with ethanol and DMF being the most used. Finally, the thermal treatment often consists of a two-step process, with a drying step at temperatures below the melting point of the polymer and in the second step temperatures of 500 °C or higher to remove the polymer and form a stable grain structure. The purpose of the drying step is not elaborated on.

Research on electrospinning metal-based or ceramic nanofibers focuses on the production steps needed in order to achieve fine or functional nanofibers. This includes properties of the calcined product, its catalytic properties, and the crystal structure of the fibers. However, research has not focused on the impact of electrospinning parameters on the final product is rarely discussed. Especially the impact of solvent composition or ratio of polymer to metal and the general electrospinning setup is rarely discussed, which is surprising, since the addition of salts impacts electrospinning mixture properties like conductivity or viscosity.

2.8. Parametric Studies

The effects of the different parameters have been studied for a long time. Most studies look at the effects by altering one parameter at a time [112,154,104,17,105,106,126,124]. This approach is suitable to improve an existing production process; however, it cannot show the interactions with other parameters involved in electrospinning.

A few researchers attempted to analyse and quantify the effects of an individual parameter [28,17,29,30] Tong and Wang [30] reported the impact of polymer concentration, applied voltage, needle diameter, feed rate, salt amount, collector rotation speed (this study used a drum collector), and tip-to-collector distance on the fiber diameter. Cui et al. [28] discussed the impact of voltage, concentration, molecular weight, feed rate, needle diameter on average fiber size

and beading of the produced fibers. However, these studies also do not discuss the interactions among the parameters.

Heikkilä and Harlin [17] conduted an orthogonal experimental design in their parametric study on the electrospinning of the polymer polyamide. It was found that the largest relative impact on the fiber size is the concentration, followed by salt content and electric field strength. It was concluded that there was no universal law governing the electrospinning process due to its complex nature.

Costolo et al. [29] applied a neural network to describe the average fiber diameter of polyacrylonitrile as a function of the input parameters concentration, viscosity, conductivity, surface tension, humidity, temperature, flow rate, voltage, distance, field strength and resulting diameter. They found that the flow rate had the largest impact on the fiber size, followed by room temperature and viscosity. Contrary to Heikkilä and Harlin, Costolo et al. found the field strength to have a negligble effect. However, Costolo et al. also observed a lack of trends, which makes it difficult to determine the linear correlations between parameters in order to predict the outcome of the electrospinning process. Furthermore, the used input parameters show redundancies regarding the used parameters, like voltage, distance and electric field strength, which are investigated independently, while the electric field strength is a function of voltage and distance.

The knowledge transfer between research groups is challenging since different groups document different setups and compositions for their produced nanofibrous polymer, with a wide range of fiber size. For PVA, Lee Choi et al. [27] reported their work with voltages ranging from 5 to 30 kV, distances from 5 to 15 cm, and concentrations in the range of 5 to 15%. The resulting fibers ranged from 240 to 340 nm. Givehchi et al. [26] reported voltages between 10 and 15 kV and distances in the range of 10 to 15 cm. The measured fibers were as fine as 150 nm. Koski et al. [155] documented a single voltage of 30 kV with a distance of 10.2 cm to a plate collector. Their fiber size ranged from 250 nm to 2 μm. These are examples for PVA, which is representative of other polymers. The collector shape also has an impact on the electric field, which cannot be addressed with existing models. The calculation of the field strength in current research is based on the calculation for a homogenous field between two plates, with

E=U/d. However, the description of an electric field between a needle or a needle and a drum collector is a more involved calculation. Küchler [156] dedicated an entire book focusing on the calculation of more complicated field arrangements. The same is true for changes in solution properties like the molecular weight mentioned previously. The molecular weight has been attributed to parameters like viscosity and surface tension, however, there has been no method proposed, which can predict the viscosity of solutions based on the molecular polymer weight.

2.9. Modelling of Electrospinning

A few researchers addressed the challenge of predicting the fiber size by electrospinning. Zhmayev et al. [157] introduced a model for melt electrospinning in the stable jet region for thin filaments. This model does not consider the entire electrospinning process. Angammana [158] uses common dimensionless numbers like the Reynolds or Peclet numbers to predict electrospinning parameters through a viscoelastic electrospinning model. Theron et al. [112] and Kowalewski et al. [140] modelled the jet path from needle to collector. However, they do not address the shape or size of the fibers. A pure mathematical approach has been taken by Xu [159], however this model lacks ways for practical application of this knowledge. A set of equations describing electric field, current, magnetic field, and forces on the jet has been derived from physical laws, which are linked to the electrospinning process. A validation of the developed equations with experimental data has not been conducted. Additionally, these equations rely on vector calculations, which is not solving the problem of electric field strength not being well described in electrospinning.

Overall, the modelling attempts rely on measured data from a specific research setup and use a selection of a variety of parameters involved in electrospinning. A prediction of fiber size for a different setup has not been possible with these studies.

2.10. Conclusions/Knowledge Gap

This chapter discussed the source of nanoparticles and their impact on society, which can be both, beneficial and harmful. Nanoparticles find purposeful applications in a variety of

technologies but can also form as by-products of engineering processes. To mitigate these effects, nanofibrous materials have been employed as filters. Electrospinning is a commonly used-technique to produce these materials, which have been used and investigated for many decades. The production parameters of electrospinning range over three general types, including setup parameters like voltage and distance, solution parameters like viscosity and surface tension, and finally environmental parameters such as temperature and humidity.

Electrospinning has been intensely investigated. The literature provides information on the impact of all the parameters on the electrospinning quality and the fiber diameter of the spun fibers. There is an abundance of studies discussing the qualitative effect of single electrospinning parameters on the fiber diameter. The boundaries of electrospinning parameters voltage, distance and overall concentration have been determined for several polymers. However, these results are often contradicting (see flow rate, or voltage), likely because they use different experimental setups and methods. Additionally, only very few groups discussed the interaction of parameters between each other. Also, modelling attempts have been conducted, but it has been not possible so far to predict the fiber diameter, and the modelling effects have been purely focused on the flight path of the fibers. No model has been developed yet to predict the electrospinning outcome (fiber diameter) based on controllable parameters. There is also no characteristic number, which indicates if a proposed electrospinning setup and solution composition lead to successful electrospinning, without failures like dripping or clogging. The available research regarding metal-based fibers is even further limited. For these materials, most research focuses on the thermal treatment of the electrospun fibers. However, parametric studies discussing the impact of electrospinning settings on the electrospinning product are limited.

Finally, the knowledge transfer and the prediction of electrospinnability based on literature is challenging. At this point, it is not possible to predict, for a selected solution and setup, whether it will yield fibers. The literature on materials is partially covering a wide range of settings and solution compositions, which work only in specific setups. This makes the replication on other setups very challenging.

Chapter 3 Experimental and Methodology

3.1. Introduction

This chapter discusses the tools, setups and methodologies used in this thesis research. The experimental tools are explained in the first section of this chapter, and the second section focuses on data collection and analyses. The experimental section revolves around the production of nanofibrous materials through electrospinning and characterization of the produced samples. In addition, the solutions were analysed for their distinct properties in terms of surface tension, viscosity and conductivity. Furthermore, dimensional analysis is introduced. In this research, the Pi-theorem is applied, which allows the use of dimensionless parameters that can be used to scale up in the future.

3.2. Experimental

3.2.1. Electrospinning Fibers

Polyvinyl alcohol (PVA), Polyvinylpyrrolidone (PVP) and Cellulose acetate (CA) were used for this thesis work. All three polymers were purchased from Sigma Aldrich USA with a purity of 99.8%. PVA solutions were prepared by diluting the polymer with distilled water. The polymer concentrations were in the range of 7.5 - 12.5 wt%. The PVA-mixtures were stirred at 120 °C on a magnetic heating plate for 4 hours until the PVA dissolved completely into the solution. As a typical practice in this field of research, complete dissolution was confirmed through visual inspection, when the solvent turned into a clear liquid. Similar methods for preparation of the solvent have been reported to work well for producing CA nanofibers in the literature [160,161].

The CA solutions were prepared by diluting CA of various concentrations with a mixture of 2:1 (wt.%) ratio of N,N-dimethylacetamide (Sigma Aldrich USA, 99.8%) (DMAc) and acetone (Sigma Aldrich USA, 99.7%). The resultant mixtures were stirred at 35 °C on a magnetic stirring heating plate for approximately 2 hours to completely dissolve CA into the solvent

mixture. The polymer molecules were assumed to be adequately dissolved in the solvent for the electrospinning process. Three different CA concentrations, specifically 10 wt.%, 15 wt.% and 20 wt.%, were considered in this research.

It is necessary to use an organic precursor carrying the metal to electrospin non-organic fibers. The PVP solutions were used as the precursors for the electrospinning of metal-based fibers. The metals used in this work are ceria and alumina. Alumina nitrate nonahydrate and Ceria nitrate nonahydrate were used as precursor for metal oxides. The organic compound must be removed after the electrospinning process, typically by calcination. The calcination process also reduces the metal nitrate into oxides (see section 3.2.2). For this work, PVP was mixed with metal nitrate with a ratio of 2:1 w:w. The PVP mixtures were first dissolved into a 2:1 v:v solution of ethanol and water and then stirred at room temperature for 8 hours. The final concentrations of the PVP and metal nitrate mixture were 10 wt.% and 16 wt.%.

A schematic of the setup can be found in Figure 3-1. The prepared solution was then placed in a 5 mL syringe, which was connected to a capillary tip (gauges 22-18, metal hub blunt point, Hamilton, Canada); this solution was pressed through the tube and capillary using a syringe pump (KDS scientific Model 100) at a constant feed rate in the order of 0.3 to 1 mL/h. The capillary needle was connected to a high voltage supply (Gamma Series ES max voltage +30 kV). The voltage varied from 8 to 12 kV ± 0.1 kV with a positive polarity and the distance between needle and collector varied from 10 to 15 cm ± 0.1 cm. The nanofiber samples were deposited onto a stainless-steel screen with a wire diameter of 140 μm and opening size of 368 μm. The screens were placed on an aluminum foil that covered the grounded collector.
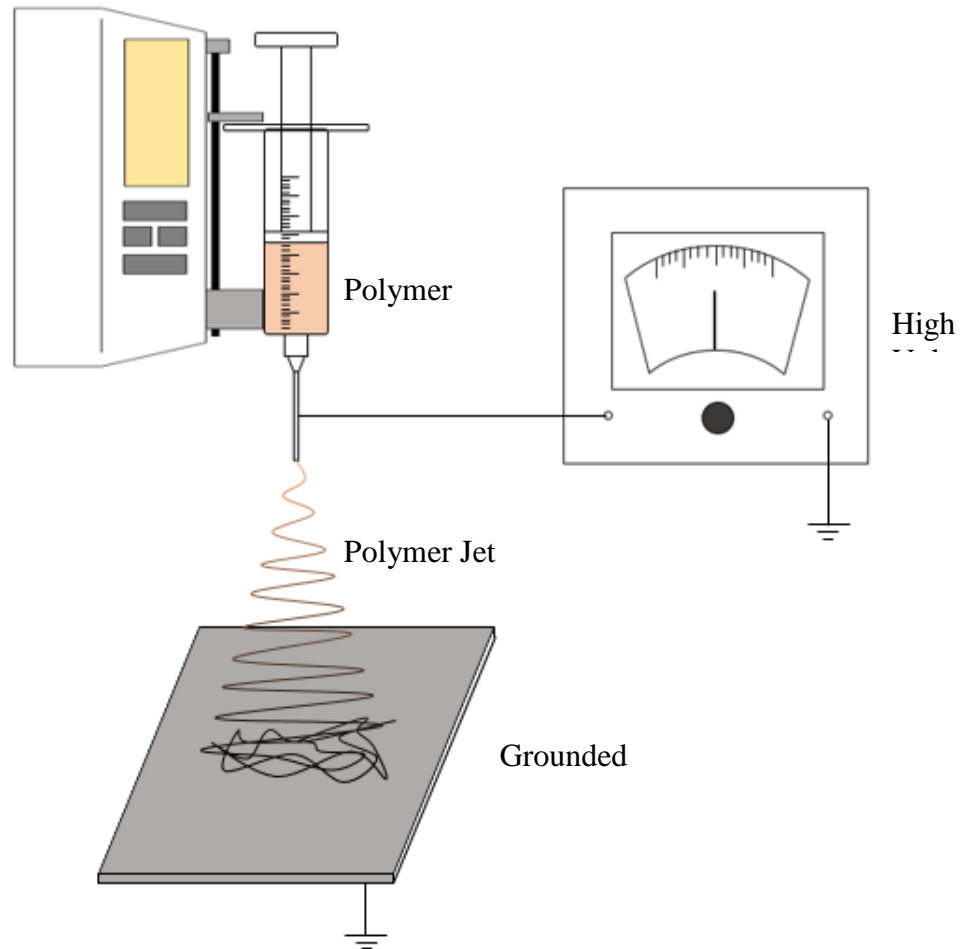
Polymer

High

Polymer Jet

Grounded

Figure 3-1. Schematic diagram of the electrospinning setup

3.2.2. Thermal Treatment and Calcination of the Metal-based Fibers

The metal-based filter samples contain polymers (e.g. PVP) after electrospinning. Since metal fibers aim at high temperature applications, the organic materials cannot withstand such temperatures and must be removed through calcination. In this study, the samples were treated in air and oxidized at temperatures of up to 1100 °C (Thermo Fisher Scientific, 1100 °C Box Furnace, BF51800 Series, Canada). The exact calcination temperature profile can be found in Figure 3-2. The samples were heated up to 550 °C from room temperature within 5 hours. The temperature was held at 550 °C for another 5 hours and then gradually cooled down back to room temperature to avoid thermal shock on the ceramics.
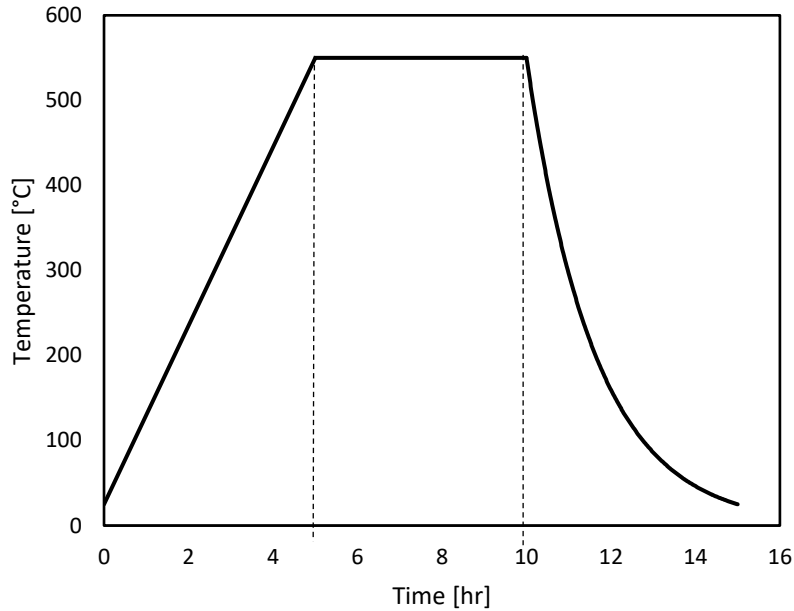
Figure 3-2 Calcination temperature profile

The calcination aims to remove the residual solution and polymer that are captured between and around the polymer chains and after the drying step. PVP starts to decompose at temperatures above 150 °C [162]. Only the metal nitrate is left for calcination at this temperature. The mechanical properties of a salt are not suited to form fibers, so it is necessary to convert the salts into ceramics. The metal salts decompose to the metal oxide, oxygen and nitrogen oxide according to [146]:

$$MNO_3 \rightarrow MO_2 + NO_2 + O_2 \tag{3-1}$$

where M stands for the metal. Depending on the metal ion, the temperature at which the nitrate (MNO_3) decomposes lies between 480 and 1100 °C. The nitrates used in this research are $Ce(NO_3)_3$, which decomposes at 570 K$\pm$30 K, and $Al(NO_3)_3$, which decomposes at 440 K$\pm$25 K. [146] Figure 3-3 shows the progression of aluminum oxide configurations depending on the sintering temperature. Ceria transforms between two stable valence states, Ce(IV) and Ce(III) are present in crystalline structures. Depending on the presence of either an

37

oxidising or reducing atmosphere, ceria switches between the III and IV configurations, where Ce(IV) is present in oxidizing atmospheres [163].
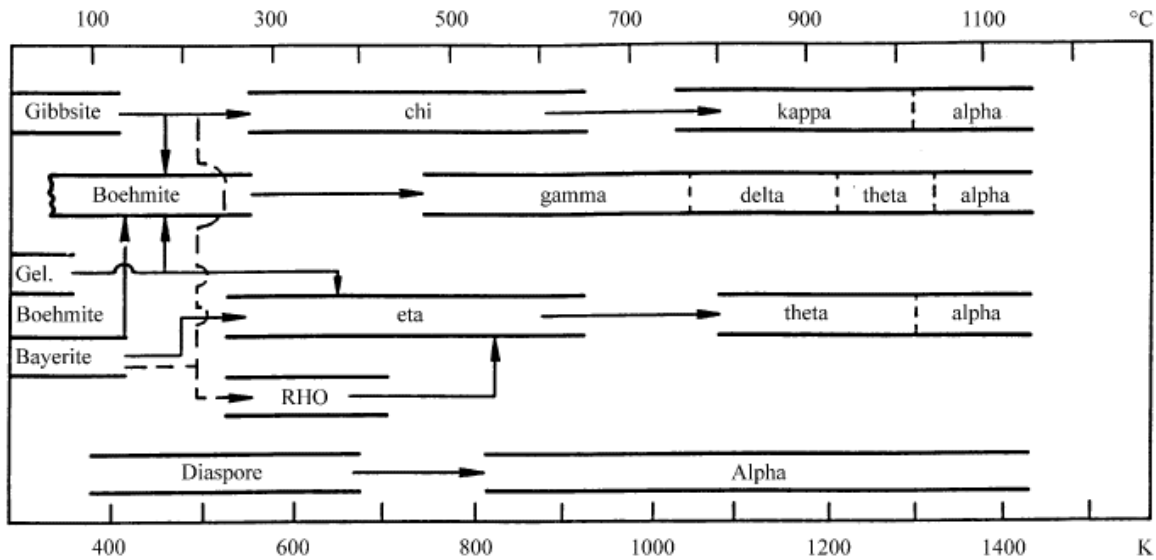
Figure 3-3 Thermal transformation of aluminum [167]

3.2.3. Fiber Sample Characterization

The sample filters were characterized using a field emission scanning electron microscopy (FE-SEM). Samples were coated with gold particles for 120 s prior to imaging. The SEM images were then quantitatively analyzed using an automated method developed in house to determine the distribution of nanofiber diameters. An image analysis algorithm was developed based on fiber individualization using MATLAB. It consists of 5 steps including pre-treatment, local thresholding, smoothing, edge detection and skeletonization [164]. Figure 3-4 demonstrates the processing of a nanofiber SEM image with high magnification using the automated method. The process has been described in detail in Givehchi et al. [70] and consist of the following five steps:

1. The original image (Figure 3-4 (a)) was pretreated by median filtering, image intensity adjustment and histogram equalization to reduce noise and increase contrast to ensure the most accurate results Figure 3-4 (b)).

2. Instead of taking the threshold of a whole image, a local thresholding method using Sauvola [165] binarization was utilized to transform the image into a binary one, i.e. black and white (Figure 3-4 (c)).

3. Undesirable noise was further reduced using repeatedly morphological opening and closing Figure 3-4 (d)).

4. Fiber boundaries were detected using canny edge detection, as shown in Figure 3-4 (e). Dilation was used to seal the openings in order to accurately detect edges. Subsequent thinning fixed the edge profile, so that they were no longer inaccurately thickened.

5. In the final stage of image processing, the fiber centerlines were defined using a skeletonization process. A pruning process was then used to delete sporadic branches (Figure 3-4 (f)).
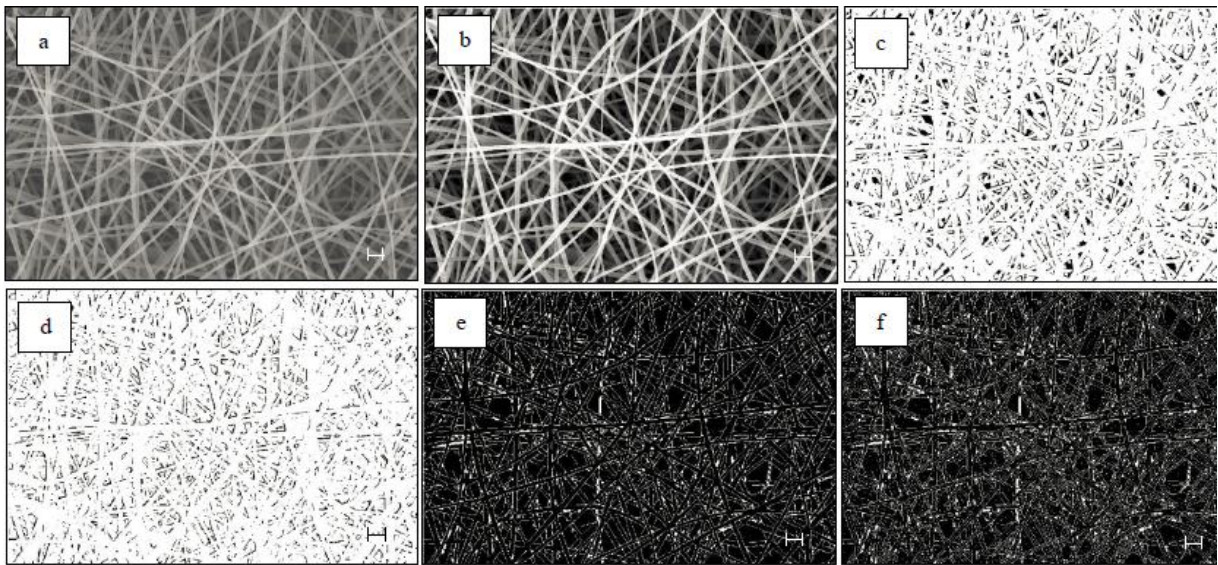
Figure 3-4 Original SEM image, scale: 1000 nm, b) filtering: median, image histogram equalization, c) local threshold, d) smoothing and noise reduction, e) edge detection, and f) skeletonization [74]

Figure 3-5 shows two SEM images for an electrospun nanofibrous filter at two different magnifications, 20.00 kX and 5.00 kX, with the fiber size distribution determined by the

automated method. As shown in Figure 3-5, fiber size distributions for the selected images had different mean fiber diameters and standard deviations. These two images were captured from various places of the sample at two different magnifications.

For more reliable statistical data, the fiber size distribution was calculated considering several images with different magnifications as shown in Figure 3-6. The average fiber diameter and standard deviation in the new size distribution were more like the low-magnification image, because the low-magnification images contain a larger area of the sample and the results, therefore, are more realistic. However, the high-magnification images also must be utilized to determine the low fiber size diameters.
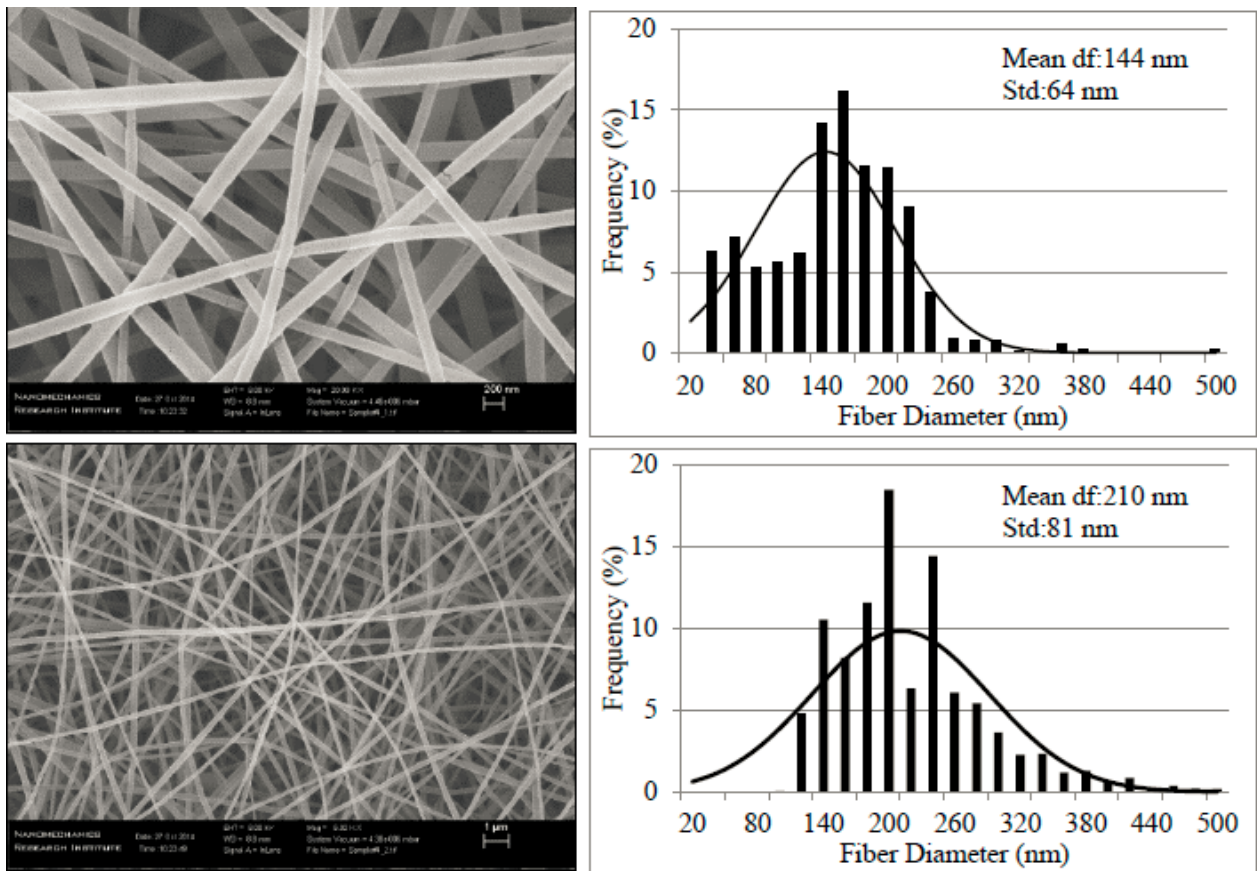
Figure 3-5 SEM images of electrospun nanofibrous filters at two different magnifications (20.00 kX and 5.00 kX), and their corresponding fiber distributions [74]
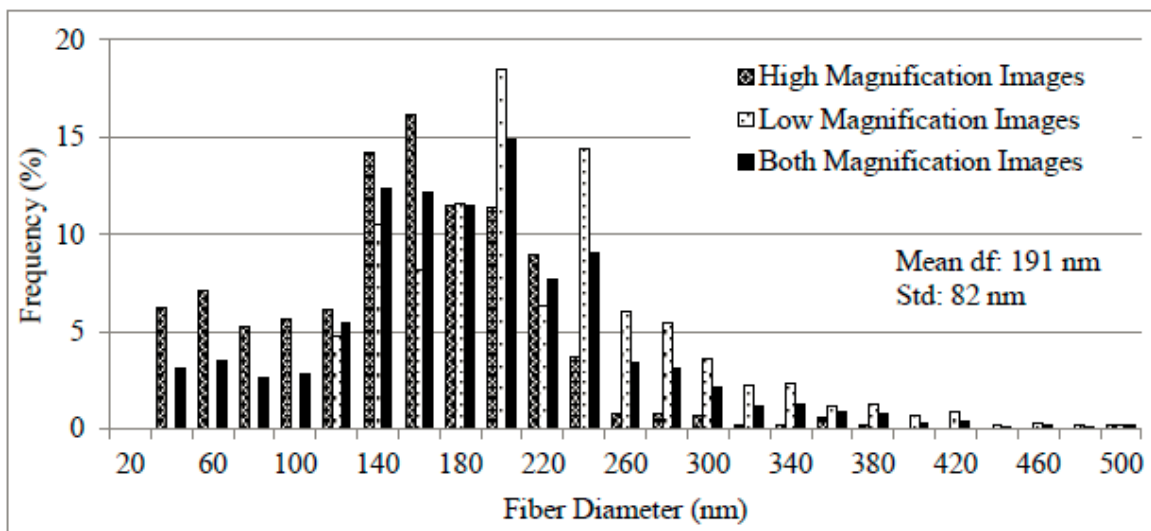
Figure 3-6 Fiber size distribution for two images at different magnifications [74]

To characterize the distribution of fiber sizes, an analysis of the statistical distribution of the created fibers has been conducted. Table 3-1 shows the distribution of ceria fibers, prepared with an Ethanol/Water ratio of 1:1. This distribution can be seen exemplary for all other samples. Trying to fit this data into common statistical distributions showed that the electrospinning process is most accurately described with a Log-Normal-Distribution. Table 3-1 shows the deviation of the data set from different distribution types.

Table 3-1 Distribution characteristics for the fiber size

Distribution	R^2 for electrospun fibers[1]	R^2 for calcined fibers
Normal	0.7888	0.7957
Weibull	0.7591	0.6637
Log-Normal	0.9239	0.8494
Exponential	0.2024	-2.277

---

[1] An error = 1 equals perfect fitting. The closest result to 1 represents the best description.

3.2.4. Filtration Test

The filter testing apparatus was the same as the one that was reported in our previous studies [26,166]. This setup is shown in Figure 3-7. The testing setup is comparable to those used by Chattopadhyay et al. [167] and Matulevicius et al. [71]. A constant output atomizer (TSI model 3076) was used to generate aerosol particles from a solution composed of 0.1 g/L sodium chloride (NaCl) in distilled water. In this case, compressed air was used to form a high-velocity jet that atomizes the solution into polydispersed NaCl aerosol particles. The aerosol particles were then passed through a diffusion drier (TSI Model 362) to remove water vapor from the generated aerosol.
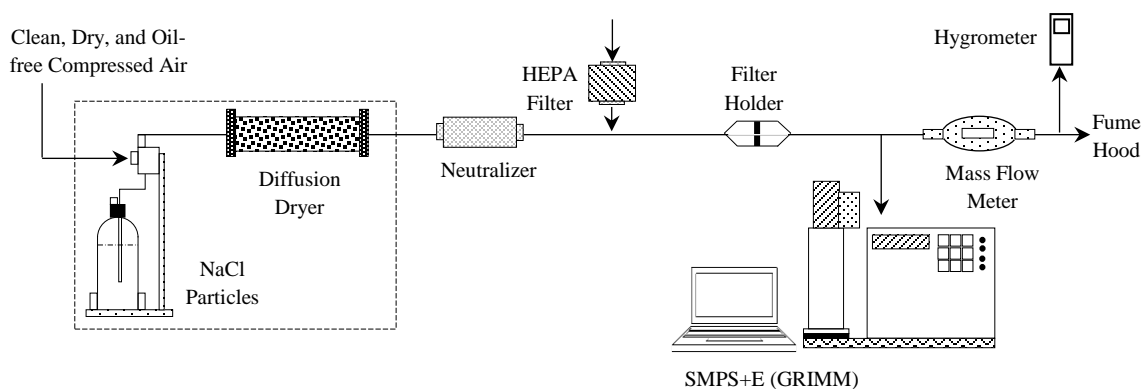
Figure 3-7 Schematic diagram of the filtration setup [26]

The concentrations of NaCl nanoparticles were measured using a scanning mobility particle sizer (SMPS) (SMPS+E, GRIMM model 5.705). The employed SMPS measures the particle number concentration distribution in the air stream. The SMPS consists of a differential mobility analyzer to classify polydispersed particles into particle size categories based on their electrical mobility and a Faraday cup electrometer to measure the number of charged particles. The range of detectable particles is 0.8 to 1100 nm according to the supplier. The functionality and accuracy of the SMPS have been thoroughly tested by Givehchi [70]. The size distribution of the used NaCl nanoparticles in the aerosol is shown in Figure 3-8. The mean diameter of the particles was 28 nm with a standard deviation of 7.2 nm.
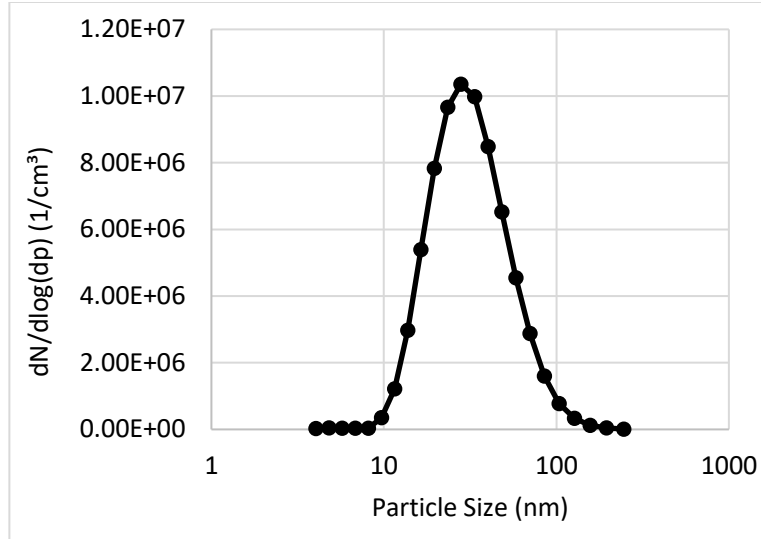
Figure 3-8 Particle size distribution of the NaCl particles

The aerosol particles were then passed through the filter medium at an air flow rate of 1.5 L/min. The filter medium was placed on a filter holder (BGI Inc., Waltham, MA). The filter sample and the filter holder have a diameter of 25 mm. With a flow rate of 1.5 L/min, the face velocity on the filter is 5.1 cm/s. The pressure-drop across the filter medium (ΔP) was monitored and recorded using a differential pressure gauge (Omegadyne, Model DPG409). Each test was repeated 5 times. All tests were conducted at room temperature, atmospheric pressure and relative humidity of 20 to about 50%.

The fractional filtration efficiency, η, was calculated using the concentrations of particles measured with and without the presence of the nanofibrous filter [26] (see Eq. (3-2)).

$$\eta = 1 - \frac{C_{w/o}}{C_w} \tag{3-2}$$

where $C_{w/o}$ and C_w are the concentrations of nanoparticles without and with the filter sample, respectively. Since they have the same unit, Eq. (3-2) is dimensionless. In this thesis, filter quality factor has been used to compare the filtration performances of the filter samples. It is a

standard parameter in filtration research [127,168]. The filter quality factor (Q_F) can be calculated using Eq. (3-3)

$$Q_F = -\frac{\ln(1-\eta)}{\Delta P} \tag{3-3}$$

where Q_F is the quality factor, and ΔP the pressure drop across the filter sample. Since the particle filtration efficiency depends on the particle size, Q_F is also size dependent. To simplify the calculation, in this paper, total efficiency is used by the summation of all particle sizes tested, averaging the particle distribution over all particle sizes.

3.2.5. Density Determination

The density of the electrospinning solution is a crucial parameter. In some research, it is linked to the electrospinning process [169]. It impacts the viscosity and surface tension of the liquids. Furthermore, it is necessary to know the density of the solution to calculate other parameters like kinematic viscosity or surface tension. All values used for the density in this research for all materials (solids and solvents) have been obtained from literature. The values used in this research can be found in Table 3-2.

Table 3-2 Densities used in this research

Material	Density [g/cm³]	Reference
PVA	1.30	[170]
PVP	1.69	[162]
Ethanol	0.789	[171]
Water	0.998	[172]
Al(NO3)3·9H2O	1.401	[173]
Ce(NO3)3 6H2O.	1.9	[174]

3.2.6. Viscosity Measurement

Viscosity is related to the resistance of a fluid to shearing flows. In electrospinning, the viscosity is an indicator for the deposited fiber diameter. A highly viscous fluid resists the whipping of

the jet more, therefore, it has a shorter travel distance and with that, a lower travel time. Low travel times are usually attributed to high fiber diameters.

In this study, a falling ball/sphere viscometer (UZ-08702-10 Gilmont Falling Ball Viscometer) was used to determine the viscosity of the samples. Stokes' law is the basis of the falling sphere viscometer, in which the fluid is stationary in a vertical glass tube. A sphere of known size and density can descend through the liquid. If correctly selected, it reaches terminal velocity, which can be measured by the time it takes to pass two marks on the tube. A sketch of the force balance can be seen in Figure 3-9.

The dynamic viscosity of the fluid, μ, is [175]

$$\mu = K(\rho_{Ball} - \rho_{Liquid})t \tag{3-4}$$

where K is the viscometer constant, ρ_{Ball} is the density of the ball (2.53 glass; 8.02 steel) [g/mL], ρ_{Liquid} is the density of the testing liquid (g/mL), and t is the time of descent (min). K is determined from [175]

$$K = \frac{\rho_{Liquid}}{(\rho_{Ball} - \rho_{Liquid})\, t} \tag{3-5}$$

The constant K has been found to be 15.3 for glass and 8.5 for stainless steel. With these values the dynamic viscosity of water has been found to be 1.0008 ± 0.0284 mm²/s (at 22°C) and ethanol 0.9956 ± 0.0239 mm²/s (at 23°C). The research proceeded using the stainless-steel ball for the electrospinning solutions. The literature values for water are 0.9795 mm²/s (at 22 °C) [176] for water and 0.983 mm²/s (at 30 °C) [177], showing a high accuracy of the setup.
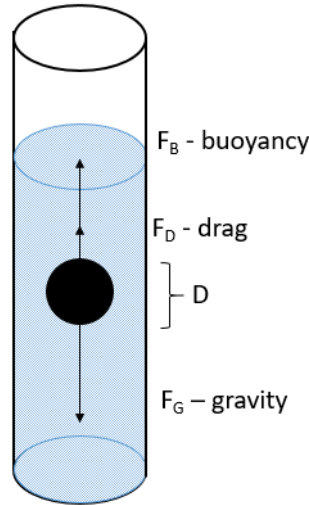
Figure 3-9 Force balance viscosity measurement

3.2.7. Conductivity Measurement

Electrical conductivity or specific conductance is the reciprocal of electrical resistivity and it indicates a material's ability to conduct electric current. It is commonly represented by the Greek letter σ (sigma), but κ (kappa) (especially in electrical engineering) or γ (gamma) is occasionally used too. Its SI unit is Siemens per metre (S/m). The electric conductivity of the electrospinning solutions in this paper was measured with a Conductivity / TDS Meter Pen (Traceable ®). Figure 3-10 shows its principle of operation. In order to measure the conductivity of a liquid, a conductivity meter measures the resistance a liquid providing an electric current. For distilled water, the conductivity has been found to be 7.6 ± 0.3 μS/m and for ethanol 2 μS/m.
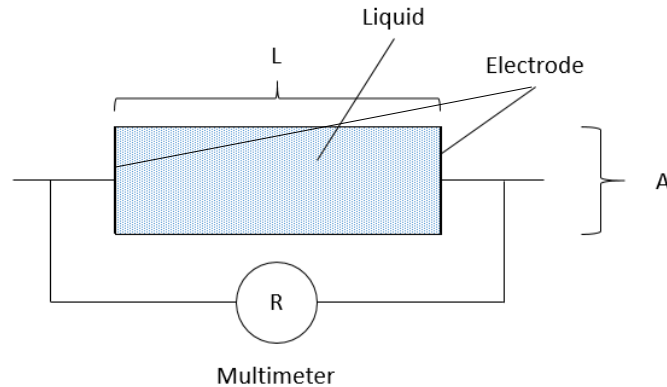
Figure 3-100 Conceptual principle of operation for conductivity measurement

3.2.8. Surface Tension Measurement

Surface tension of the solution impacts the force needed to form the Taylor-cone and the jet from the nozzle. Therefore, the surface tension directly counteracts the electric field strength. A simple way to measure the surface tension of a fluid is the droplet method. A key aspect of this method is the capture of droplets, which form at the tip of a small capillary. Knowing the weight of the droplet (density of fluid before weighting the collected mass), and the inner and outer diameter of the capillary, it is possible to calculate the gravitational force needed to overcome the surface tension. The surface tension can be calculated using [178]

$$\gamma = \frac{m\ g}{2\pi\ r\ F}$$ (3-6)

where m is the mass of a single droplet, g, the gravitational acceleration, r, the inner (or outer diameter) of the capillary, and F, the correction factor to account for the imperfect sphere shape of the droplets. A detailed discussion of the capillary droplet method can be found in reference [178]. The correction factor F in Eq (3-6) can be calculated as follows [179]:

$$F = 1.000 - 0.9121\left(\frac{r}{V^{\frac{1}{3}}}\right)^{1} - 2.109\left(\frac{r}{V^{\frac{1}{3}}}\right)^{2} + 13.38\left(\frac{r}{V^{\frac{1}{3}}}\right)^{3} - 27.29\left(\frac{r}{V^{\frac{1}{3}}}\right)^{4}$$
$$+ 27.53\left(\frac{r}{V^{\frac{1}{3}}}\right)^{5} - 13.58\left(\frac{r}{V^{\frac{1}{3}}}\right)^{6} + 2.593\left(\frac{r}{V^{\frac{1}{3}}}\right)^{7}$$

(3-7)

where r is the needle diameter and V is the droplet volume. The needle radius is a known parameter. To determine the volume of the droplets, the weight of a single droplet is determined, when the density of the solution is known. To determine the weight of the droplet, the solution was brought into the electrospinning setup without applying a voltage. The solution was then slowly pushed through the needle to allow a slow formation of droplets at the needle tip, which eventually dropped into a vessel. The vessel's initial weight has been determined before testing with a precision balance (A&D ® Weighing lab balance HR120; max 120 g d=0.1mg). Thirty droplets have been captured in the vessel. The weight of the vessel with the captured droplets has been determined using the same precision balance. Knowing the weight of the 30 droplets, it is possible to calculate the average weight of one droplet and therefore the volume needed in Eq (3-7). The flow rate was adjusted to a rate, at which the time between droplets was greater than 30 s to avoid hydrodynamic effects [178]. For distilled water, the determined surface tension with this setup has been determined to be 0.072 ± 0.0032 N/m. This value is close to the literature value of 0.0728 N/m of water [180], validating the accuracy of the setup.

3.3. Data Analysis

3.3.1. Introduction

This section aims to introduce the analytical tools used in this research to analyze the data generated in this research. A factorial design plan is used to develop an experimental plan, which can quantify the effects of different parameters on the fiber size. The second part of this section is introducing the Pi-theorem, which is used to determine to detect physical interactions of the electrospinning conditions on the fiber size and the electrospinnability. The results of the

48

factorial design plan are used for the selection of parameters for the creation of dimension matrix involved in the Pi-theorem.

3.3.2. Factorial Design

Factorial design is widely used in experimental studies involving several factors where it is necessary to study the interactive effects of the factors on a response. The following assumptions are made in factorial design: [181]

1. The factors are fixed,

2. The order of experiments is random and,

3. The normality assumptions are satisfied.

The factorial experimental design used in this work, following a two parameter setup [181], is shown in Table 3-3. The factors of the electrospinning process that can be controlled directly are electric field (by changing the voltage at a constant distance), flow rate, needle diameter, and solution concentration (wt% dissolved material in solvent). These values are changed between a high and a low level, depending on the desired metal-based fiber. The indirectly controlled values are temperature and humidity, which impact the evaporation rate of the jet. These values are recorded before every run, independent of the high/low settings of the directly controlled values; however, a direct control of the environmental settings is not possible due to the HVAC settings of the research building. Through experimental design, it is possible to calculate the impact of certain parameters.

Table 3-3 Factorial Design Plan

Run Number	Electric Field A	Needle Diameter B	Flow Rate C	Solution Concentration D	Run Label
1	-	-	-	-	(1)
2	+	-	-	-	a
3	-	+	-	-	b
4	+	+	-	-	ab
5	-	-	+	-	c
6	+	-	+	-	ac
7	-	+	+	-	bc
8	+	+	+	-	abc
9	-	-	-	+	d
10	+	-	-	+	ad
11	-	+	-	+	bd
12	+	+	-	+	abd
13	-	-	+	+	cd
14	+	-	+	+	acd
15	-	+	+	+	bcd
16	+	+	+	+	abcd

Given the measured fiber diameters, one can determine the effects of high levels of the directly controlled parameters on the fiber size. The main effect Φ of a factor A (here Electric field) on the fiber size is described in [181] (pg. 228f) as the difference between the eight runs, where A is at the high level and the eight runs where A is at the low level:

$$
\begin{aligned}
\Phi_A &= \bar{y}_{A^+} - \bar{y}_{A^-} \\
&= \frac{d_a + d_{ab} + d_{ac} + d_{abc} + d_{ad} + d_{abd} + d_{acd} + d_{abcd}}{8n} \\
&\quad - \frac{d_{(1)} + d_b + d_c + d_{bc} + d_d + d_{bd} + d_{cd} + d_{bcd}}{8n}
\end{aligned}
\tag{3-8}
$$

where n stands for the number of repetitions of each setting. Since each run is repeated once, n=1 in this work due to the high costs associated with SEM analysis. Therefore, equation (3-8) can be rewritten as

$$\Phi_A = \frac{1}{8}[d_a + d_{ab} + d_{ac} + d_{abc} + d_{ad} + d_{abd} + d_{acd} + d_{abcd} - d_{(1)} - d_b - d_c$$
$$- d_{bc} - d_d - d_{bd} - d_{cd} - d_{bcd}]$$

(3-9)

The values for B, C and D are calculated accordingly. The value calculated in the square brackets is also known as contrast.

$$\Phi_B = \frac{1}{8}[d_b + d_{ab} + d_{bc} + d_{abc} + d_{bd} + d_{abd} + d_{acd} + d_{abcd} - d_{(1)} - d_a - d_c$$
$$- d_{ac} - d_d - d_{ad} - d_{cd} - d_{acd}]$$

(3-10)

$$\Phi_C = \frac{1}{8}[d_c + d_{cb} + d_{ac} + d_{abc} + d_{cd} + d_{bcd} + d_{acd} + d_{abcd} - d_{(1)} - d_b - d_a$$
$$- d_{ab} - d_d - d_{bd} - d_{ad} - d_{abd}]$$

(3-11)

$$\Phi_D = \frac{1}{8}[d_d + d_{ad} + d_{bd} + d_{abd} + d_{cd} + d_{acd} + d_{bcd} + d_{abcd} - d_{(1)} - d_a - d_b$$
$$- d_{ab} - d_c - d_{ac} - d_{bc} - d_{abc}]$$

(3-12)

The effect of the two-factor interaction between A and B can be computed as the difference between the average "A" effects at the high and low levels of B. One-half of this difference is called AB interaction.

$$\Phi_{AB} = \frac{1}{8}[d_{ab} + d_{abc} + d_{abd} + d_{abcd} + d_{(1)} + d_c + d_d + d_{cd} - d_a - d_b - d_{ac}$$
$$- d_{bc} - d_{ad} - d_{bd} - d_{acd} - d_{bcd}]$$

(3-13)

A similar logic applies to the interactions AC, AD, BC, BD, and CD.

$$\Phi_{AC} = \frac{1}{8}\big[d_{(1)} + d_{ac} + d_{abc} + d_{acd} + d_{abcd} + d_b + d_d + d_{bd} - d_a - d_{ab} - d_c$$
$$- d_{bc} - d_{ad} - d_{abd} - d_{cd} - d_{bcd}\big] \tag{3-14}$$

$$\Phi_{AD} = \frac{1}{8}\big[d_{(1)} + d_b + d_c + d_{bc} + d_{ad} + d_{abd} + d_{acd} + d_{abcd} - d_a - d_{ab} - d_{ac}$$
$$- d_{abc} - d_d - d_{bd} - d_{cd} - d_{bcd}\big] \tag{3-15}$$

$$\Phi_{BC} = \frac{1}{8}\big[d_{(1)} + d_a + d_{bc} + d_{abc} + d_d + d_{ad} + d_{bcd} + d_{abcd} - d_b - d_{ab} - d_c$$
$$- d_{ac} - d_{bd} - d_{abd} - d_{cd} - d_{acd}\big] \tag{3-16}$$

$$\Phi_{BD} = \frac{1}{8}\big[d_{(1)} + d_a + d_c + d_{ac} + d_{bd} + d_{abd} + d_{bcd} + d_{abcd} - d_b - d_{ab} - d_{ab}$$
$$- d_{bc} - d_{abc} - d_d - d_{cd} - d_{acd}\big] \tag{3-17}$$

$$\Phi_{CD} = \frac{1}{8}\big[d_{(1)} + d_a + d_b + d_{ab} + d_{cd} + d_{acd} + d_{bcd} + d_{abcd} - d_c - d_{ac} - d_{bc}$$
$$- d_{abc} - d_d - d_{ad} - d_{bd} - d_{abd}\big] \tag{3-18}$$

Following the process described in Montgomery [181] (p.248), the equations for the interactions between three parameters and all four parameters can be calculated as following:

$$\Phi_{ABC} = \frac{1}{8}\big[-d_{(1)} + d_a + d_b - d_{ab} + d_c - d_{ac} - d_{bc} + d_{abc} - d_d + d_{ad} + d_{bd}$$
$$- d_{abd} + d_{cd} - d_{acd} - d_{bcd} + d_{abcd}\big] \tag{3-19}$$

$$\Phi_{ABD} = \frac{1}{8}\big[-d_{(1)} + d_a + d_b - d_{ab} - d_c - d_{ac} - d_{bc} - d_{abc} + d_d + d_{ad} + d_{bd}$$
$$+ d_{abd} + d_{cd} - d_{acd} - d_{bcd} + d_{abcd}\big] \tag{3-20}$$

$$\Phi_{ACD} = \frac{1}{8}\big[-d_{(1)} + d_a - d_b - d_{ab} + d_c - d_{ac} - d_{bc} - d_{abc} + d_d + d_{ad} + d_{bd}$$
$$- d_{abd} + d_{cd} + d_{acd} - d_{bcd} + d_{abcd}\big] \tag{3-21}$$

$$\Phi_{BCD} = \frac{1}{8}\big[-d_{(1)} - d_a + d_b - d_{ab} + d_c - d_{ac} - d_{bc} - d_{abc} + d_d + d_{ad} + d_{bd}$$
$$- d_{abd} + d_{cd} - d_{acd} + d_{bcd} + d_{abcd}\big] \tag{3-22}$$

$$\Phi_{ABCD} = \frac{1}{8}\big[d_{(1)} - d_a - d_b + d_{ab} - d_c + d_{ac} + d_{bc} - d_{abc} - d_d + d_{ad} + d_{bd}$$
$$- d_{abd} + d_{cd} - d_{acd} - d_{bcd} + d_{abcd}\big] \tag{3-23}$$

The values for the calculated effects can be either negative or positive. To make the values comparable, the sum of squares of the contrast for each label combination is calculated using

$$\sum_{i=1}^{n}(y_i - \bar{y})^2 \tag{3-24}$$

For the two substances ceria and alumina, the min-max values are displayed in Table 3-4. All experiments were conducted with a constant needle-to-plate distance of 15 cm. Pretests with alumina and ceria have been conducted, recording at which point electrospinning was not possible for longer than one minute. Criteria was either clogging, indicating a too high solution concentration or voltage, and dripping of the solution. In between the range of parameters presented in Table 3-4, electrospinning would take place.

Table 3-4 Min-Max values for parameter study

Parameter	Min	Max
Solution Concentration	10% (mass)	16% (mass)
Voltage	10 kV	16 kV
Flow Rate	0.3 mL/hr	0.5 mL/hr
Needle Gauge	20 (0.603 mm)	18 (0.838 mm)

3.3.3. Pi-Theorem

Dimensional analysis is a method to check the correlations between physical parameters using their dimensions. The dimension of a physical parameter is a combination of the basic physical dimensions (usually mass, length, time, electric charge, and temperature). Dimensional analysis is necessary because a physical law must be independent of the units used to measure the physical variables to be general for all cases. [182]

Dimensional analysis is routinely used to check the plausibility of derived equations and computations as well as forming reasonable hypotheses about complex physical situations that can be tested by via experimentation or by more developed theories of the phenomena, which allow categorizing the types of physical quantities. In this case, units are based on their relations or dependence on other units or dimensions, if any.

Dimensional analysis is a method, which infers information about a phenomenon by the assumption that it can be described by a dimensionless equation of variables. The usage of dimensional analysis is based on the hypothesis that certain variables are describing the problem independently and all other variables are either redundant or irrelevant. Therefore, the initial step in dimensional analysis requires an in-depth discussion of the natural phenomena being investigated.

For dimensional analysis, the Buckingham π (Pi) theorem is a key theorem. It is the formalization of Rayleigh's dimensional analysis. In 1941, Buckingham framed a theorem, which assumes that the number of Pi quantities left after performing a dimensional analysis

equals the difference between the number of quantities/parameters entering the problem and the maximum number of these that are dimensionally independent. The maximum number of dimensionally independent quantities will always be equal or less than the number of fundamental dimensions needed to write all dimensional equations. In summary, the theorem states that a number n of physical parameters are expressible by k independent fundamental physical quantities. With that, the original expression equals an equation involving p=n-k dimensionless parameters (degrees of freedom), based on the original parameters. This provides a method for computing sets of dimensionless parameters from the given variables, even if the form of the equation is still unknown. However, the choice of dimensionless parameters is not unique: Buckingham's theorem only provides a way of generating sets of dimensionless parameters and will not choose the most "physically meaningful."[182]

The math of the Pi-theorem is about the physical quantities $R_1, \dots, R_n$. These are measured in a consistent system of units, such as the SI system, in which the basic units are meter, kilogram, second, ampere, and kelvin (m, kg, s, A, K). As it will turn out, the existence of consistent systems of measurement has nontrivial consequences.

Assuming the fundamental units of a system of units are $F_1, \dots, F_m$, so that we can write:

$$R_j = v(R_j)[R_j] = \rho_j[R_j] \tag{3-25}$$

Where $\rho_j = v(R_j)$ is a number, and $[R_j]$ the dimension of R_j. We can write $[R_j]$ in terms of the fundamental units as a product of powers:

$$[R_j] = \prod_{i=1}^{m} F_i^{z_{ij}} \ (j = 1, \dots, n) \tag{3-26}$$

Where a_{ij} is the position of the unit exponent in the dimension matrix in equation (3-27). It is also important for the fundamental dimensions to be independent in the sense that

$$\prod_{i=1}^{m} F_i^{z_x} = 1 \rightarrow x_1 = \dots = x_m = 0.$$

55

The dimension matrix Z of $R_1, \dots, R_n$ is defined by.

$$Z = \begin{bmatrix} z_{11} & \cdots & z_{1n} \\ \vdots & \ddots & \vdots \\ z_{m1} & \cdots & z_{mn} \end{bmatrix} \tag{3-27}$$

The dimensionless combinations of variables R_j are combinations of powers $R_1{}^{\lambda_1} \dots R_n{}^{\lambda_n}$. The units of this combination can be calculated as:

$$\left[R_1{}^{\lambda_1} \dots R_n{}^{\lambda_n} \right] = \prod_{i=m}^{m} F_i{}^{z_{i1}\lambda_1 + \dots + z_{in}\lambda_n} \tag{3-28}$$

This combination is dimensionless, if its unit is 1. This is true, if $Z\lambda = 0$, where $\lambda = (\lambda_1, \dots, \lambda_n)^T$. Therefore, there is a 1-1 correspondence between the null space $N(Z)$ and the set of dimensionless combinations of these variables. Since $Z\lambda = 0$ it can be implied that $\prod_{j=1}^{n} x_i{}^{z_{ij}\lambda_f} = 1$. If a basis for N(Z) has been chosen together with the corresponding dimensionless combinations $\pi_1, \dots, \pi_{n-r}$ (with r the rank of Z), any dimensionless combination can be written as a product $\pi_1{}^{c_1} \dots \pi_{n-r}{}^{c_{n-r}}$ with exponents uniquely given. The exponents are coefficients of a part of N(Z) in the chosen basis. This is called the maximal set of independent dimensionless combinations.

Any physically meaningful relation $\Phi(R_1, \dots, R_n) = 0$, with $R_j \neq 0$, is equivalent to a relation of the form $\Psi(\pi_1, \dots, \pi_{n-r}) = 0$ involving a maximal set of dimensionless combinations [183]. For a detailed proof of the theorem, Hanche-Olsen [183] discussed the analysis in more detail.

In this research, the Pi-theorem is used to create dimensionless groups from the large number of electrospinning parameters in order to simplify the determination of correlations between electrospinning parameters and measured fiber size. The development of Pi-theorem tables from the electrospinning parameters fiber size, needle diameter, distance, concentration, voltage, surface tension, viscosity, permittivity, conductivity (elect.), temperature, and humidity is presented in Chapter 7. The resulting dimensionless equations then were rearranged resulting

in equations for the fiber diameter as a function of the dimensionless groups. To calculate the value of these dimensionless groups, experimental data from the production of ceria and alumina fibers will be employed. The two metal-based solutions are expected to have slightly different parameters, but significantly different fiber diameters, while using the same electrospinning setup.

The excel solver application is utilized to minimize the sum of squares resulting from the difference between calculated and measured fiber size for each sample. To be able to accurately calculate the dimensionless groups, the solution properties viscosity, surface tension and conductivity of the considered solutions have been determined. The determination of correlations between the known settings, dimensionless groups and the measured fiber diameters is done by determining factors for each group, once for all fibers and for each fiber material. This allows the determination of whether possibly found correlations are solution specific or have general validity. Additionally, to potential correlations between dimensionless groups and fiber diameter, it is possible to identify characteristic numbers describing the electrospinning process. Comparable to the Reynolds number in fluids, a characteristic number for electrospinning could describe a range, within which electrospinning is possible.

3.4. Conclusion

Experimental and analytical methods have been described, which are used to produce and characterize nanofibers as well as the electrospinning process involved. The electrospinning setup used in this research has been described, as well as the solutions used. These solutions are analyzed for their respective viscosities, surface tensions and conductivities using a variety of testing methods. The described methods are utilized in the following chapters, conducting parametric studies on several materials leading up to the attempt to describe a model of the electrospinning process with dimensionless groups.

Chapter 4 Cellulose Acetate Based Nanofibers by Electrospinning and Their Filtration Efficiencies[2]

4.1. Introduction

Reported in this chapter are the effects of the tip-to-collector distance, voltage, deposition time, and solution concentration on the fiber size distribution and filter quality factor of electrospun cellulose acetate (CA) based nanofibers. The CA solutions were prepared by diluting various concentrations of CA in a 2:1 (w:w) ratio of N,N-dimethylacetamide (concentration 10 wt.% to 20 wt.%). The electrospinning voltages ranged from 8 to 12 kV with needle-to-collector distances from 10 to 15 cm and deposition times of up to 30 minutes. The produced nanofibrous filter samples were then analyzed in terms of fiber size distribution and filter quality factor, for which the efficiency was determined using NaCl particles ranging from 4 to 240 nm in diameter. The maximum filtration efficiency measured was 99.8% based on average efficiency for filter samples obtained with an overall deposition time of 30 minutes. The maximum filter quality factor was 0.14 Pa^{-1} for a CA concentration of 20 wt.% and a tip-to-collector distance of 15 cm. The average fiber diameters of the fibers were between 175 and 890 nm, and CA concentrations below 15% led to the formation of beads.

4.2. Methodology

Table 4-1 displays the used CA concentrations and the electrospinning settings used to produce the nanofibers with the solution. The sample name resembles the applied settings, with the first number being the concentration of CA in the solution, the second number the duration of the electrospinning process in minutes, the third number represents the applied voltage in kV and

---

the last number the distance between needle and collector in cm. The range of parameters is taken from literature experience, where the impact of concentration, voltage and distance has been investigated [167,71]. The literature shows a minimum concentration of CA of around 10%, and used voltages as low as 8 kV at a distance of 10 cm. To study the impact of the single parameters, those reported values have been increased to 20%; 12 kV and 15 cm. The deposition time has been altered to analyse its impact on the filtration performance, an impact on the fiber size is not expected.

As described in chapter 3.2.3, the fabricated nanofibrous filter samples were first analyzed by scanning electron microscopy (SEM) (Zeiss Gemini Model Leo 1550) to observe their morphology. Then fiber size distribution was analysed using a MATLAB code. More details can be found in Givehchi et al. [70]. Finally, those same samples were tested in terms of filtration efficiency.

Table **4-1**. Electrospinning parameters for the nanofiber samples

Sample name	CA concentration (wt.%)	Deposition time (min)	Applied voltage (kV)	Tip-to-collector distance (cm)
CA10_5_8_10	10	5	8	10
CA10_5_8_12.5	10	5	8	12.5
CA10_5_8_15	10	5	8	15
CA10_15_8_10	10	15	8	10
*CA15_5_8_10	15	5	8	10
*CA15_5_8_12.5	15	5	8	12.5
*CA15_5_8_15	15	5	8	15
*CA15_5_10_10	15	5	10	10
*CA15_5_12_10	15	5	12	10
CA15_15_8_10	15	15	8	10
CA15_15_10_10	15	15	10	10
CA15_15_12_10	15	15	12	10
CA15_30_8_10	15	30	8	10
CA15_30_10_10	15	30	10	10
*CA20_5_8_10	20	5	8	10
*CA20_5_8_12.5	20	5	8	12.5
CA20_5_8_15	20	5	8	15
*CA20_5_10_10	20	5	10	10
CA20_5_12_10	20	5	12	10
CA20_15_8_10	20	15	8	10
CA20_30_8_10	20	30	8	10

* Samples with an asterisk are also displayed in Figure 4-1

4.3. Results and Discussion

Figure 4-1 shows the fiber size distributions of the samples indicated with an asterisk in Table 4-1. These distributions represent the variety of fiber size distributions observed for all tested samples. The SEM images used to generate these distributions can be found in Appendix A.2.

It is noticeable that the distributions have a skewed log-normal shape, and depending on the production parameters, the standard deviations and means of the samples differ strongly from sample to sample. The effects of the single parameters voltage, tip-to-collector distance and concentration, on the fiber distribution are discussed in the following sections.

(a)

CA15_5_8_10

Mean d_f: 145 nm

Std: 82.8 nm

(b)

CA15_5_8_12.5

Mean d_f: 254.6 nm

Std: 238.6 nm

(c)

CA15_5_8_15

Mean d_f: 72.7 nm
Std: 176.6 nm

(d)

CA15_5_10_10

Mean d_f: 283.7 nm
Std: 254.7 nm

(e)

CA15_5_12_10

Mean d_f: 252.5 nm
Std: 252.2 nm

62

CA20_5_8_10

Mean d_f: 252.5 nm
Std: 245.4 nm

(f)

CA20_5_8_12.5

Meand d_f: 319.4 nm
Std: 491.4 nm

(g)

CA20_5_10_10

Mean d_f: 723.3 nm
Std: 751.2 nm

(h)
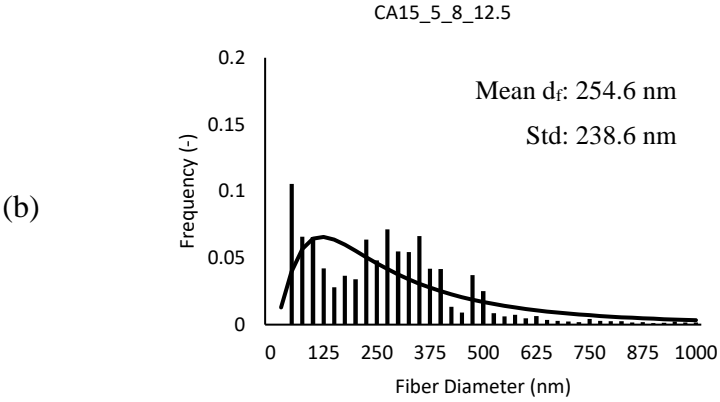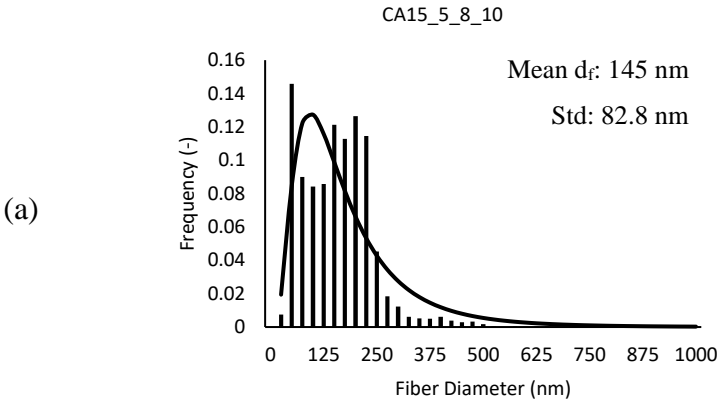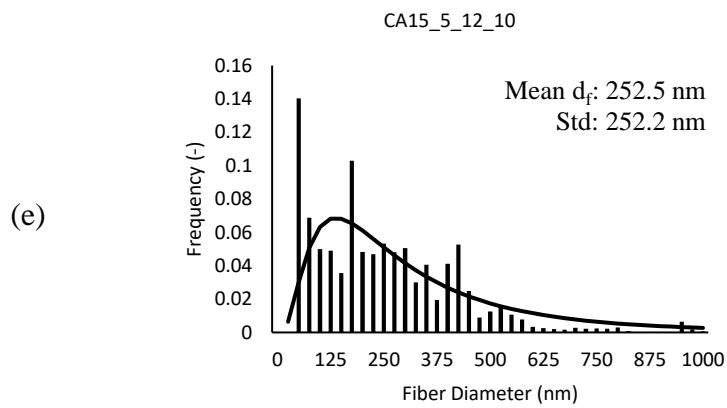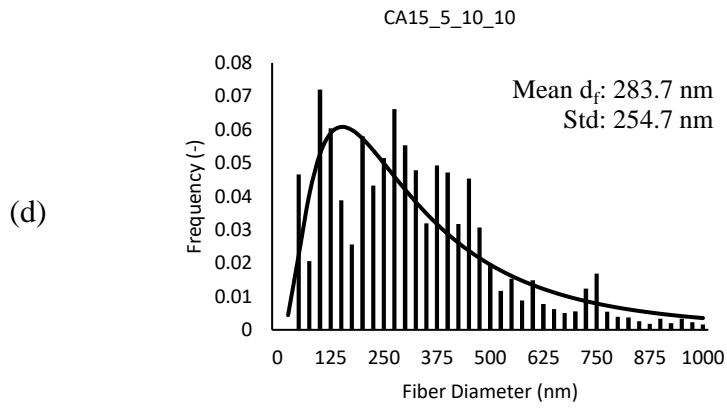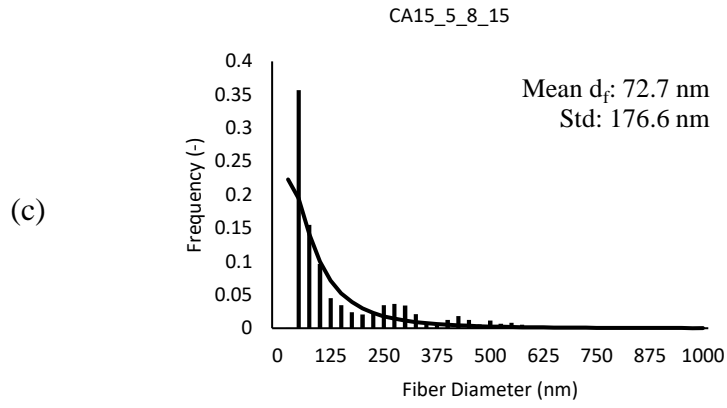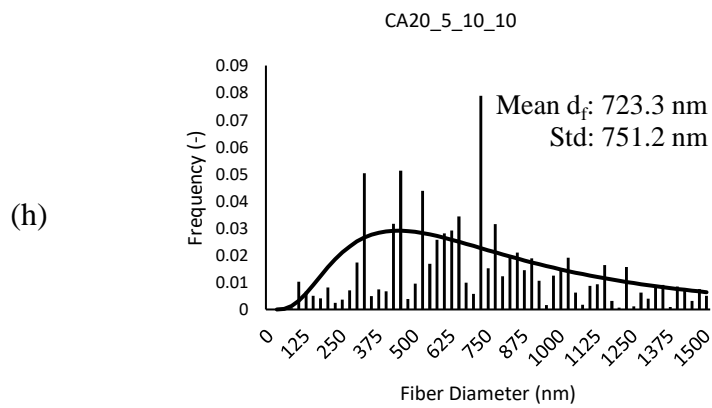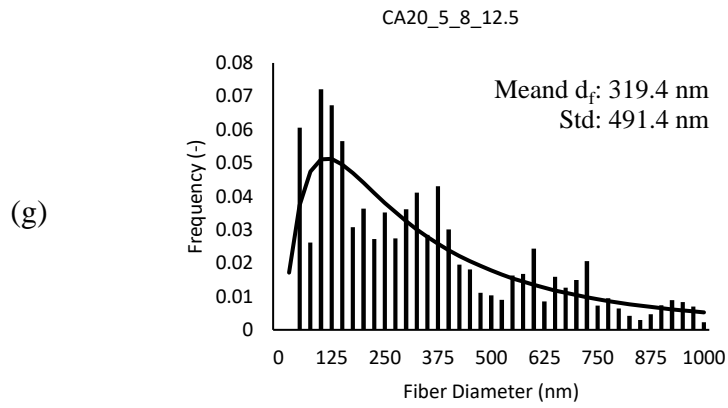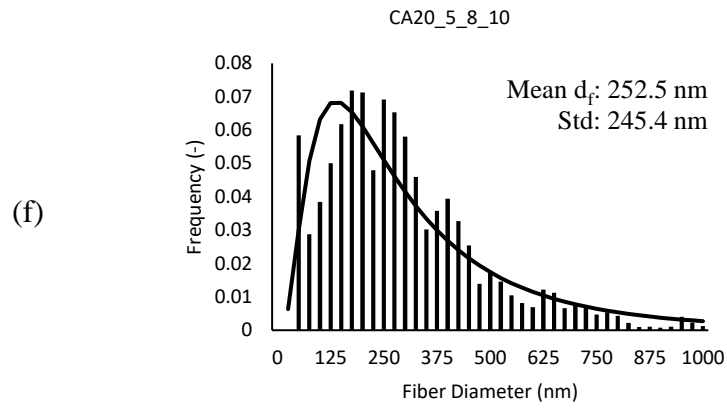
Figure 4-1 (a) – (h) Determined CA fiber size distributions

63

4.3.1. Effects of CA Concentration on Sizes and Morphology of the Nanofibers

The SEM image in Figure 4-2a is for a sample with 10 wt.% CA. It clearly shows beading of the polymer. Droplet formation was observed when the polymer concentration was below the critical chain entanglement concentration, c_e.[131]. Such defects were not observed when it was above this critical concentration. Similar findings were reported by other researchers [167]. The magnitude of c_e is dependent on solvent-polymer interactions [161]. Bead-free nanofibers are expected at high CA concentrations, *i.e.* over 15 wt.%. Higher Dimethylacetamide (DMAc) content in the solvent leads to strong hydrogen-bonding interactions between the solvent and CA molecules. For the 2:1 DMAc/acetone formulation, the evaporation of the solvent is expected to be slower, resulting in a wet jet landing on the collector. The solution minimizes the surface area, resulting in spherical beads.

Note that, in an earlier study [161] using a 2:1 DMAc/acetone solvent solution, the beading phenomenon was observed at concentrations as high as 20 wt.%. Bead-free nanofibers were only obtained at a CA concentration of 25 wt.%.[161] In the current work, the absence of droplets in the 15 wt.% micrographs indicates that the critical chain entanglement concentration for the 2:1 DMAc/acetone solvent mixture is somewhere between 10 wt.% and 15 wt.% of CA. This also indicates that other factors may have played an important role in bead formation. It is likely that relative humidity or temperature of the air have an impact, since both parameters can influence the conductivity or the surface tension of the solution. Based on the qualitative observations above, only 15 wt.% and 20 wt.% samples were analyzed from now on for fiber diameter, filtration efficiency and filtration quality.

A higher CA solution ultimately leads to a higher viscosity of the solution, and consequently a greater resistance of the liquid being precipitated by the electric field. This great resistance leads to lower bending instabilities and ultimately thicker nanofibers. Similar trends were observed by other researchers with CA nanofibers [185,186,161,160]. The increase in fiber size is also common for high polymer concentrations [167]. In this study, the concentration of 15% CA resulted in a mean fiber diameter of 302 ± 127 nm, whereas the mean fiber diameter corresponding to 20% CA was 669 ± 341 nm.
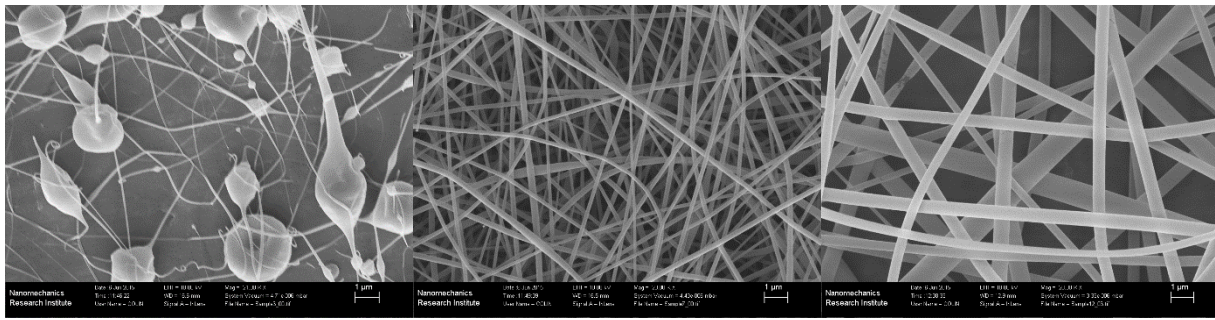
<div align="center">(a)   (b)   (c)</div>

Figure 4-2. SEM images of the nanofibers produced with different CA concentrations (a, CA10_5_8_10; b, CA15_5_8_10; c, CA20_5_8_10)

4.3.2. Effects of Tip-to-Collector Distance on Fiber Size Distribution

Tip-to-collector distance can impact the quality of the fibers; beads can be observed if the tip-to-collector distance is either too short or too long [22]. Tip-to-collector distances of 10 cm, 12.5 cm and 15 cm were considered for the following study because preliminary tests show that no beading was observed for these three tip-to-collector distances.

As seen in Table 4-2, for the concentration of 15 wt.% CA, there is a general trend of increase in fiber diameter with increasing tip-to-collector distance up to 12.5 cm, after which it drops again. For the concentration of 20 wt.% CA, the average fiber diameter increased from 327 ± 245 nm to 466 ± 262 nm when the tip-to-collector distance changed from 10 cm to 12 cm. A further increase of 2.5 cm in the tip-to-collector distance resulted in an increase in fiber diameter to 836 ± 690 nm. Other researchers reported that a larger tip-to-collector distance results in thinner nanofibers [97,102,95,122,123,105]. A larger distance provides longer time for the solvent to evaporate. Therefore, the jet undergoes increased elongation due to greater bending instabilities in the system. Hence, thinner fibers can be obtained.

The increased range of fiber diameters could also be attributed to a decrease of bending instability. The continuous whipping alters the traveling distance of the fibers, which has a direct impact on the final fiber size. The increased distance at constant applied voltage decreases the

electric field strength, which can lead to a decrease in the whipping motion of the jet. The traveled distance of the jet is shorter as direct consequence of the reduced whipping, resulting in larger fibers on the collector. However, a similar study showed that the size and morphology of the fibers were not significantly influenced by the deposition range between 5 cm and 15 cm [186]. Similarly, there was a minimal impact of the tip-to-collector distance from 15 cm to 30 cm on the corresponding SEM images [186]. It would be desirable to have some data at a shorter distance, but no fibers could be formed or collected at the distance of 10 cm. An advanced experimental setup shall be developed for nanofiber fabrication at short distances. It is worth noting that it is normal to have a wide range of fiber size. The fiber sizes depend not only on the operating condition (voltage, distance, and concentration), but also on the experimental setup itself. Chattopadhyay et al. [167] used a drum collector, and Christoforou et al. [186], a horizontal setup with a plate sized 24x24 cm. They all demonstrated that collector size directly impacts the strength of the electric field, and final fiber morphology.

Table 4-2. Fiber size distributions at different concentrations and tip-to-collector distances

CA Concentration	Sample Name	Tip to Collector Distance (cm)	Average Nanofiber Diameter (nm)
15 wt%	CA15_5_8_10	10	145 ± 82
	CA15_5_8_12.5	12.5	284 ± 238
	CA15_5_8_15	15	151 ± 176
20 wt%	CA20_5_8_10	10	305 ± 245
	CA20_5_8_12.5	12.5	459 ± 491
	CA20_5_8_15	15	799 ± 1000

4.3.3. Effects of Applied Voltage on Fiber Size

Samples were produced at different applied voltages with two CA concentrations of 15 wt.% and 20 wt.% CA, but with the same deposition time of 5 minutes, and the same tip-to-collector distance of 10 cm. These two groups of samples were used to study the effects of applied voltages (8, 10 and 12 kV) on the fiber diameter.

The experimental results are summarized in Table 4-3. For both CA solutions, an increasing trend is observed for the average fiber diameter with applied voltage. The sharp increase in the

average fiber diameter can be seen when the voltage was increased from 8 kV to 10 kV for both CA concentrations. For the concentration of 20 wt.%, the average fiber diameter increases by over 600 nm when the voltage increased from 8 kV to 10 kV. When the applied voltage increased from 10 kV to 12 kV, the average fiber diameter decreased by 100 nm. A similar trend was also observed for the concentration of 15 wt.%.

The effects of applied voltage on the fiber diameter were not conclusive based on earlier studies [167,186]. In a separate study on CA nanofibers, other researchers found an inverse effect of applied voltage on the mean fiber diameter [22]. This was attributed to stronger electrostatic force at a higher voltage, which caused the fibers to stretch more and become thinner. Another study showed that voltage had a negligible effect on the diameter of CA nanofibers [122]. Increasing applied electric field resulted in a slight decrease in mean fiber diameter for ethylcellulose nanofibers. However, an increase in fiber diameter may also be attributed to a stronger electric field, which can result in solution being ejected more quickly from the capillary tip.

Table 4-3. Fiber diameters at different concentrations and applied voltages

CA Concentration	Sample name	Voltage (kV)	Average nanofiber diameter (nm)
	CA15_5_8_10	8	145 ± 82
15 wt.%	CA15_5_10_10	10	330 ± 255
	CA15_5_12_10	12	308 ± 252
	CA20_5_8_10	8	305 ± 245
20 wt.%	CA20_5_10_10	10	971 ± 751
	CA20_5_12_10	12	879 ± 783

Table 4-4 shows the results of similar studies in literature. It can be seen that the variance of the produced fibers strongly depended on the operating parameters. The parameters also varied between studies for different experimental setups, especially the collector shape and dimension. Furthermore, it can be seen that a higher polymer concentration leads to a greater mean fiber

diameter. The fiber sizes produced in our study herein for concentrations of 15 wt.% are comparable with those produced by other researchers.

Table 4-4. Fiber diameters and production parameters of other research

CA Conc.	Mean fiber diameter	Voltage (kV)	Distance (cm)	Reference
11%	120 ± 70 nm (beading)	75-80	20	[167]
15%	300 ± 10 nm	75-80	20	[167]
17%	500 ± 19 nm	75-80	20	[167]
15%	275 ±195 nm (different molecular weight)	8	15	[161]
15%	241 ± 111 nm	8	15	[161]
15%	287 ± 165 nm	8	15	[161]
11%	350 ± 129 nm (different solvent)	18	16	[71]
11%	363 ± 131 nm	18	16	[71]

4.4. Air Filtration Performances

4.4.1. Effects of CA Concentration on Air Filtration using the Nanofiber Samples

Figure 4-3 shows the effects of CA concentration on the filtration efficiencies and the quality factors corresponding to deposition times of 5 to 30 minutes. The tip-to-collector distance and applied voltage were kept constant at 10 cm and 8 kV, respectively. Since obvious beading of the polymer was observed for 10 wt.% CA, only samples for the concentrations of 15 wt.% and 20 wt.% are considered in this work. At all deposition times, except for 15 minutes, filtration efficiency and quality factor increased when the CA concentration increased from 15 to 20 wt.%. For example, in the case of 30 minutes deposition time, increasing the CA concentration

from 15 wt.% to 20 wt.% led to an increase in average filtration efficiency from 14.8% to 60.4%. Under the same condition, the quality factor increased from 0.0214 to 0.027 Pa^{-1}.
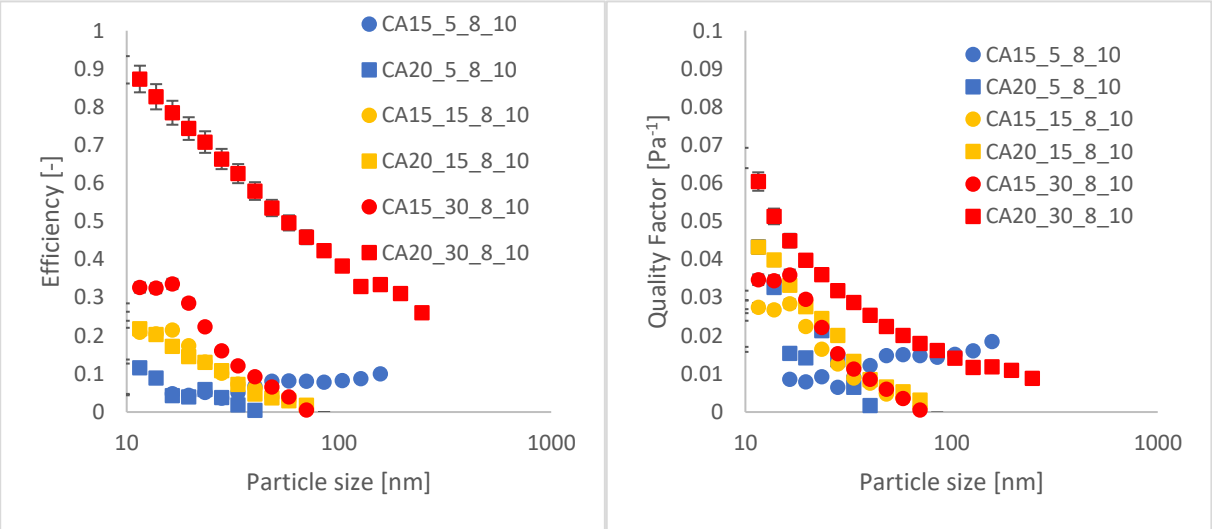
(a)   (b)

Figure 4-3. (a) Filtration efficiencies and (b) Quality factors at different CA concentrations

The higher filtration efficiency can be attributed to the increased mass deposition of fibers due to higher polymer concentration of the solution. A higher concentration of polymer in the solution leads to relatively less volatile solvent in the jet, which results in a higher polymer mass deposition rate and solidity of the produced filters. The higher filtration quality is connected to higher filtration efficiency with an equal pressure drop or less. The slipping effect of the very fine fibers enables a low pressure drop [66,67]. Slip flow occurs, when the size of the fiber approaches the mean free path of the air. As a result, the air molecules "slip" over the fiber surface, which leads to a lower pressure drop. As a result, the deposited mass does not impact the pressure drop significantly.

4.4.2. Effects of Tip-to-Collector Distance on Air Filtration Performance

Figure 4-4 shows the effects of tip-to-collector distance on the filtration efficiency and quality factor for filter samples obtained with 15 and 20 wt.% CA. The deposition time and applied voltage were kept constant at 5 minutes and 8 kV, respectively. For both CA concentrations, positive trends were observed for filtration efficiency and quality factor with increasing tip-to-collector distance. There was generally an increase in average fiber diameter with increasing tip-to-collector distance. Typically, the thinner the nanofiber, the higher the filtration efficiency. However, this was not the case in the study herein. As seen in Table 2, although the mean sizes of certain samples were relatively large, these samples have many fibers that are smaller than the mean fiber diameter. Therefore, the effects of nanosized fibers can be observed for samples with a high mean fiber size. In a separate study using PVA nanofibers [70], a similar correlation was obtained between tip-to-collector distance and both filtration efficiency and filter quality factor.
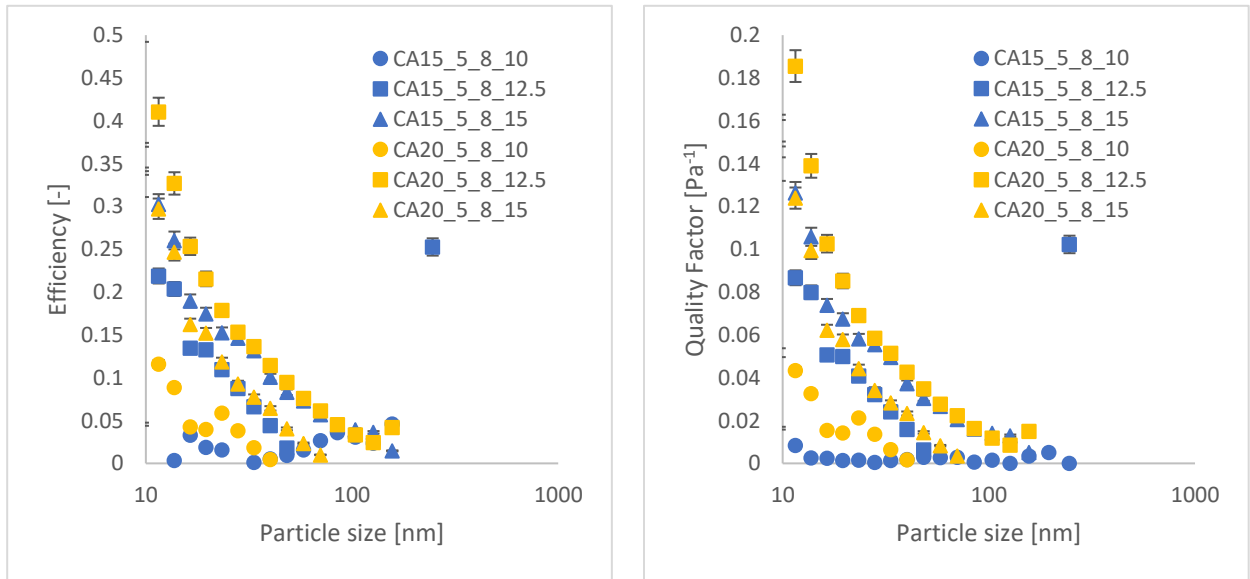
(A)   (B)

Figure 4-4. (A) Filtration efficiencies and (B) Quality factors at different tip-to-collector distances

4.4.3. Effects of Deposition Time on Air Filtration Performance of the Filter Samples

The effects of deposition time on total filtration efficiency and quality factor are shown in Figure 4-5. All data points were for 15 wt.% and 20 wt.% CA solutions with the same tip-to-collector distance of 10 cm and the same applied voltage of 8 kV. It was observed that, for both concentrations, both the filtration efficiency and the quality factor increased with deposition time. The filtration performance was relatively poor for all tested samples produced with the deposition time of 5 minutes. As shown in Figure 4-4a, the filtration efficiency was around 10% for all samples. An increase in deposition time, however, obviously promoted the filtration performance. Increasing the deposition time from 5 min to 30 min led to a jump of average filtration efficiency from 1.8% to 60.4%. As discussed above (section 4.4.1), slip flow regime was in effect when nanofiber diameter was less than 500 nm [64]. Thicker nanofibers may be one factor that led to low filtration efficiency.

It can be seen from Figure 4-5 that the filtration quality factors of samples produced with 15% CA and 20% CA concentrations are close to each other. Table 4-2 and Table 4-3 show that a lower concentration resulted in finer fibers. Thinner fibers can be deposited for a longer time than thick ones without restricting the air flow to a point that the pressure drop overcomes the gain in the filtration efficiency.
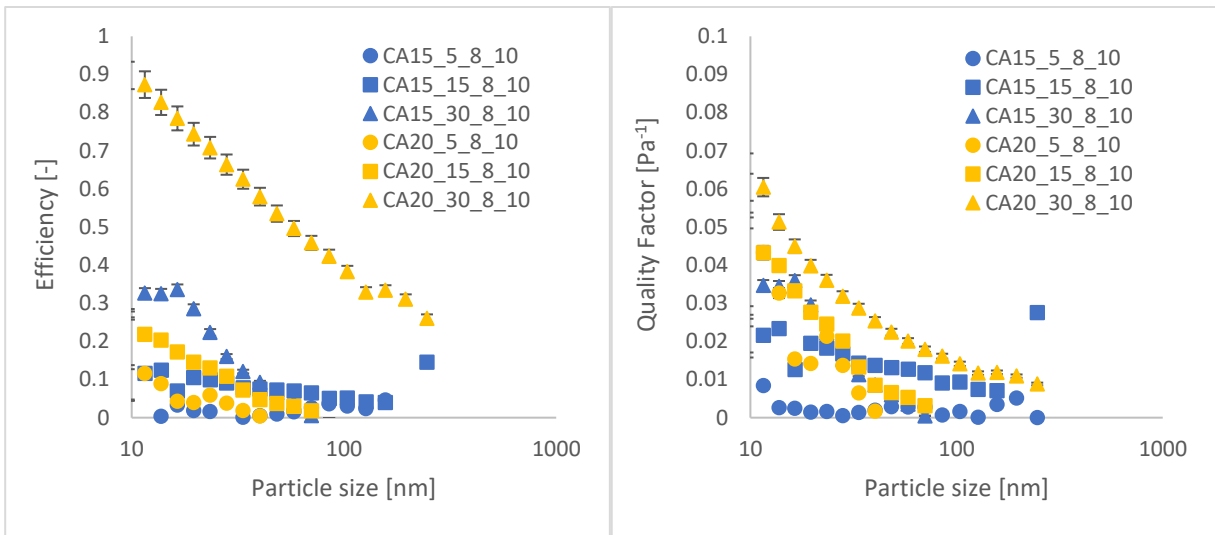
(A)   (B)

Figure 4-5. (A) Filtration efficiencies and (B) Quality factors at different deposition times

Figure 4-4 to Figure 4-6 also show the effects of deposition time on filtration performance. The circle, squares and rectangle stand for short, medium, and long deposition times, respectively. All three graphs show that a short deposition time corresponds to the lowest filtration efficiency, while a long deposition time corresponds to high filtration efficiencies. The higher filtration efficiency is attributed to the thicker filter, which resulted from a longer electrospinning time. As expected, however, the increased amount of deposited fibers leads to a higher pressure drop. Nonetheless, the overall filtration quality is still the highest for all samples made with long deposition time.

4.4.4. Effects of Applied Voltage on Air Filtration using the Nanofiber Samples

Figure 4-6 shows the effects of applied voltage on the total filtration efficiency and quality factor of the produced samples. For a given deposition time, the filtration efficiency increased with increasing applied voltage. The corresponding concentration was 15 wt.% with a tip-to-collector distance of 10 cm. The results for 20 wt.% showed promising results as well, however the production of high concentration samples over a longer time poses more challenges in regard

72

to clogging and dripping. A similar trend was also observed in terms of the filtration quality factor of the media. This trend in filtration efficiency is clearly observed for all deposition times. As the voltage increased from 8 kV to 12 kV, the filtration efficiency approached 100%. For example, for the deposition time of 15 min, the filtration efficiency for 10 kV sample was 36.7% and it was 99.3% at 12 kV. As seen in Figure 4-6, a higher applied voltage required a shorter deposition time to make a filter with a filtration efficiency greater than 99%. The local maximum filtration quality factor was 0.06 Pa^{-1}, while the maximum quality factor overall was 0.027 Pa^{-1}. Commercial filters have been found to have a quality factor as high as 0.007 Pa^{-1} [187]. Thus, the nanofibers in this study outperformed these commercial products.

Figure 4-6 illustrates the relationship between the filtration efficiency and the pressure drop. The pressure drop increased substantially enough for 10 kV, that the rise of the filtration efficiency was negligible. From the results in Table 4-3 it is clear that a higher voltage lead to a greater average fiber diameter. It also led to the increase in pressure drop. The same is true for 12 kV, which shows a sharp increase of the filtration efficiency, but relatively little increase in the filter quality factor. In contrast, the increase in the filtration efficiency of the thinner fibers for 8 kV led to an equivalent increase of the filtration quality factor. These trends suggest that the filter with thicker fibers may be more efficient in capturing nanoparticles, but they also have high solidity, which led to a high pressure drop. Furthermore, the slipping effect reduces the pressure drop for finer fibers. This finding matches the theory described in the models summarized by Hinds [80,12]. Notable differences are the samples CA15_5_12_10 and CA15_15_12_10, which show consistently high filtration efficiencies.

(a)   (b)
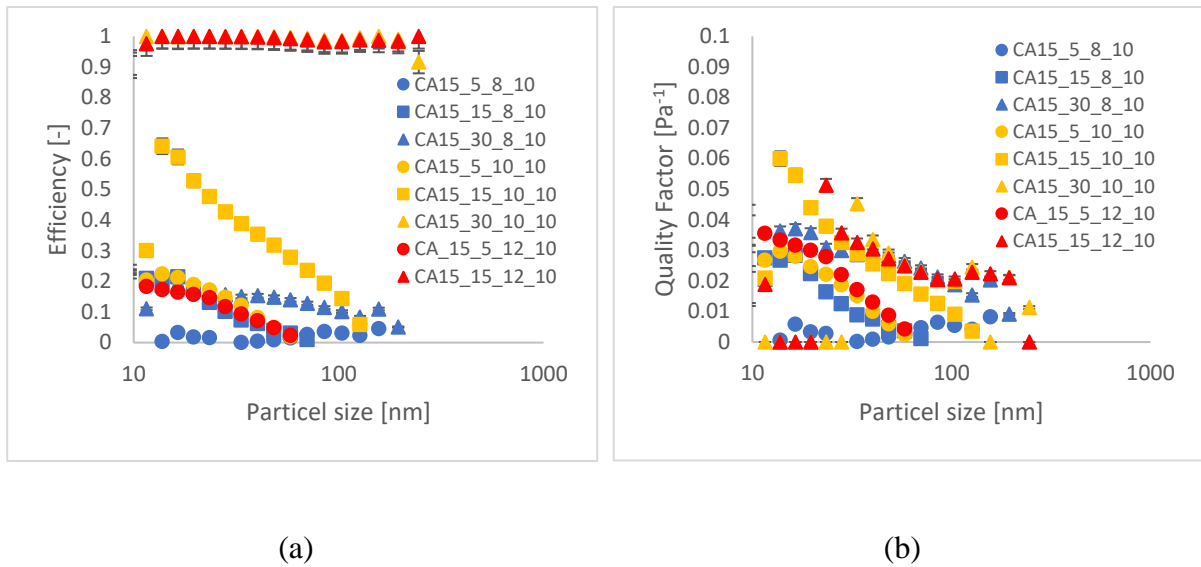
Figure 4-6 (a) Filtration efficiency and (b) Quality factor depending on applied voltage

4.5. Conclusions

The results of this research show that the applied voltage, tip-to-collector distance, CA concentration, and deposition time in electrospinning affect the sizes of the nanofibers, and consequently the filtration efficiency and filtration quality factor. With CA concentrations of less than 15%, beads were formed during the electrospinning process, regardless of other electrospinning parameters. A higher CA concentration resulted in larger fiber diameters. Furthermore, longer tip-to-collector distances and higher applied voltages also led to larger fiber diameters. The impacts of the tip-to-collector distance and voltage are comparable with respect to the increase in fiber diameter.

Finally, the larger the mean fiber diameters, the higher the resulting filtration efficiency. The increased filtration efficiency did not necessarily mean a higher filtration quality factor, especially for filters obtained with longer deposition time. The maximum filtration efficiency was 99.8% for filters made with an overall deposition time of 30 minutes. The maximum filter quality factor was 0.05 Pa^{-1} for a filter corresponding to a CA concentration of 20 wt.%, a tip-to-collector distance of 12.5 cm, a voltage of 8 kV and a deposition time of 5 minutes.

74

Summarizing this chapter, the production of pure polymer filters has been successfully conducted. The fiber mats were also applied as filter mats, as they showed great potential, especially for small particles. The setup used in this research can produce fibers as small as nanofibers.

Chapter 5 Fabrication and Evaluation of Metal Based Nanofibers Produced by Electrospinning

5.1. Introduction

Metal-based nanofibers containing aluminum nitrate or ceria nitrate were fabricated using different solution compositions to determine the optimal precursor solution for further metal-based electrospinning. It was possible to determine a solution mixture enabling the production of metal-based fibers, based on a mixture of ethanol and water with PVP as a carrier polymer. Calcination is a necessary step to remove the polymer content of these fibers and to leave the metal oxides behind, but during this process the fibers and the filter sample shrank dramatically by 25-fold in sample size. Finally, the filtration efficiency of alumina-based nanofibers was determined, and it was shown that the efficiency was higher than that of existing commercial products with 0.07 Pa^{-1}.

5.2. Preliminary Results

Following the methodology presented in Chapter 3, preliminary tests were conducted to determine the optimum precursor combination. In these preliminary tests, effects of overall solid concentration, solvent composition and dilution of the solvent with water are documented. These tests are necessary to the development of a reliable fiber production method, which can cover as wide a range as possible of production parameters. Since the literature suggests different compositions, several trials were necessary. Table 5-1 shows the two different solution compositions taken from the literature that have been tested. For both mixtures, the w:w ratio of polymer to metal was 2:1.

Table 5-1 Tested electrospinning mixtures

Mixture	Solvent	Polymer	Solid Concentration	Reference
Mixture 1	1:4 w:w Ethanol: DMF	PVP	25%	[188]
Mixture 2	2:1 v:v Ethanol : Water	PVP	16%	[93]

5.3. Effects of Solution Composition on Fiber Morphology

Figure 5-1 shows the SEM images of the samples produced from Mixture 1 following the procedure of Lee et al. [188] using a sole alcohol solution of ethanol and DMF. The fibers were too thick to be considered nanofibers (in this case approximately 1 μm). Additionally, the fibers degenerated after calcination and they did not have a true cylindrical shape anymore. Instead, they were entangled forming a flat membrane. These results could be reproduced with different voltages and DMF-to-ethanol ratios. High polymer concentration may have resulted in a high viscosity due to increased entanglement of the polymer chains in the solution [97]. The high polymer portion melts during the heating process and leads to a connection of fibers. In the literature, higher polymer concentration resulted in the formation of completely flat fiber structures [189]. It was found that the formation mechanism of the flat structures can be credited to rapid gelation on the surface of the electrospun jet followed by buckling of the jet associated with bending instability [189]. This phenomenon could be observed in this case as well.
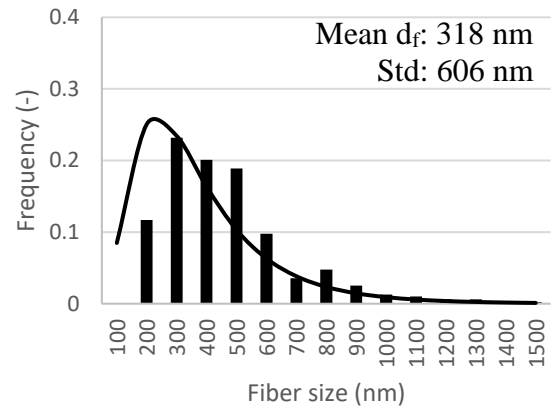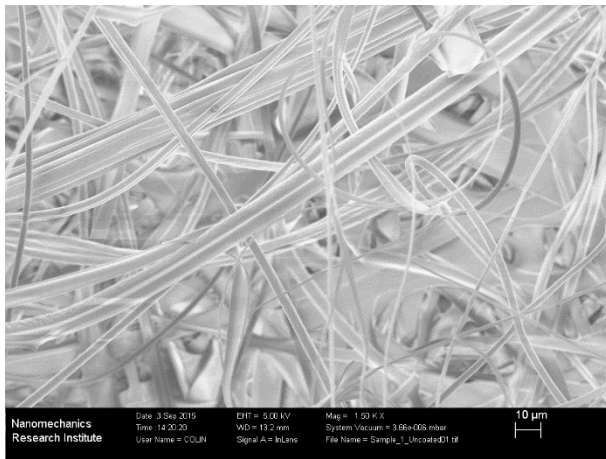
(a)
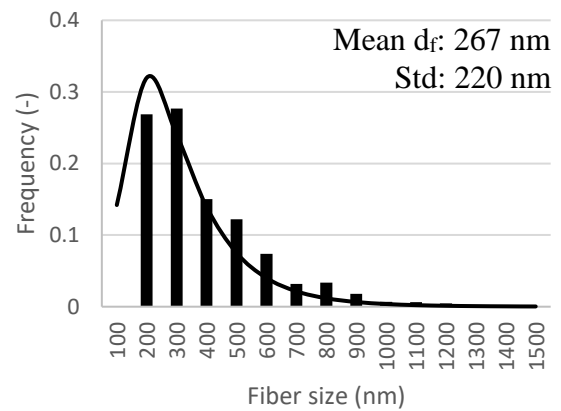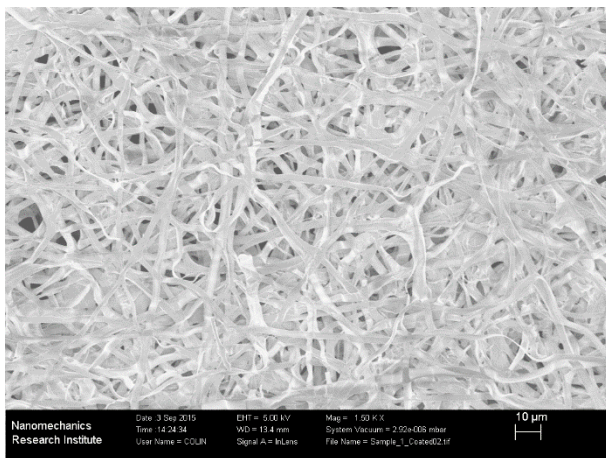
(b)

Figure 5-1 Electrospun mixture 1 (a) before and (b) after calcination using the same fabrication procedure as in Lee et al. [188]

In addition to the undesirable fiber morphology, the conducted electrospinning process with Mixture 1 has been problematic (e.g. needle clogging and dripping). Due to the high conductivity of a pure alcohol solution, the effect of surrounding electric fields had a remarkable impact. Contrary to Mixture 1, Mixture 2 has water instead of DMF as part of the solvent. As a result, the conductivity is lower, and the mass of polymer is lower, relative to the overall mass of the precursor. The fibers created with Mixture 2 show thinner fibers and production

difficulties were not encountered, unlike Mixture 1 (see Figure 5-2). The electrospinning process with the 2:1 ethanol-water mixture didn't drip, or clog, and resulted in fibers that had a small and distinct distribution, which is desirable for the production of filter media. The adjustment of solid content and solvent composition leads to better evaporation behavior during the flight phase between nozzle and collector, and these fibers became fine enough, so they did not melt to the flat structure in the calcination process.
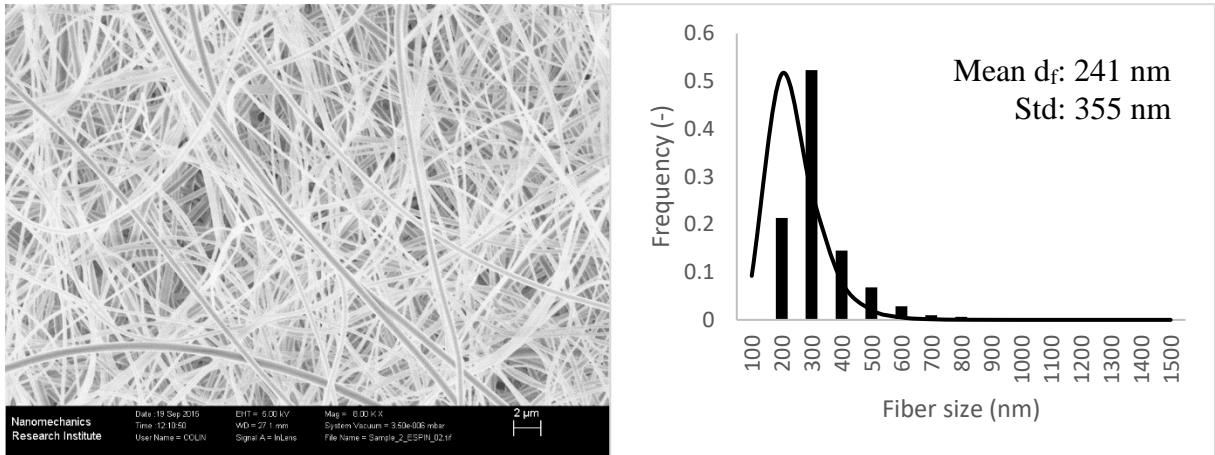
(a)
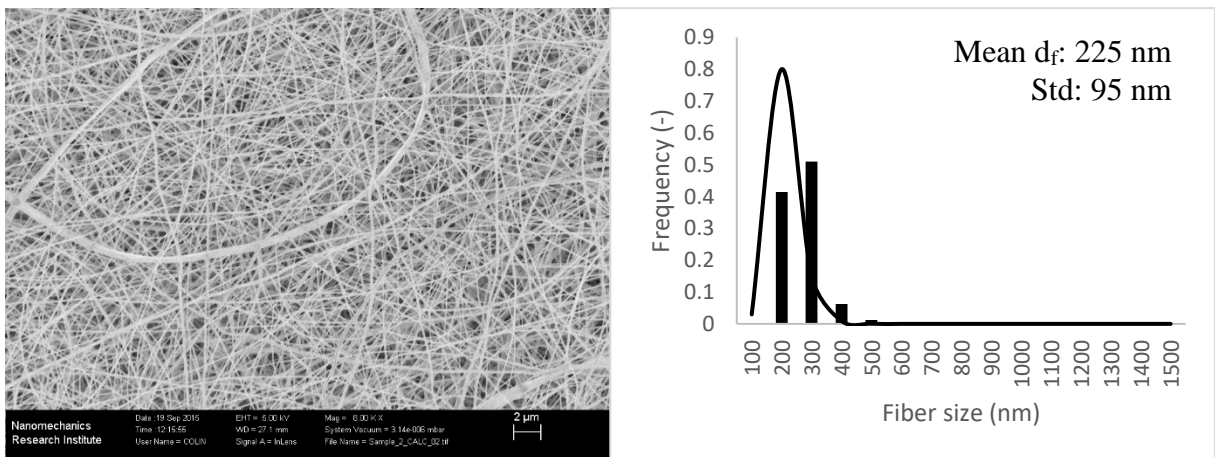
(b)

Figure 5-2 Electrospun mixture 2 (a) before and (b) after calcination

5.4. Effect of Water Concentration on Nanofiber Size

It was determined in the previous section that water as a solvent component has a beneficial impact on the electrospinning quality of PVP+Ceria combinations. It is essential to understand the influence of the ethanol/water ratio on nanofiber size. Setting the ethanol/water ratio at 2:1 with a fiber diameter of 225 nm after calcination as a baseline, the effects of ratios of 1:1, 1:2, and 3:1 were investigated. The 2:1 ratio is considered as a baseline, since the literature [93] suggests it, without elaborating on other concentrations. The overall concentration of solids was kept constant during this process.

Table 5-2 shows that the fiber diameter only changes minimally. Again, fiber sizes in all tables in this thesis are mean diameters $\pm$ standard deviations describing the distribution curve, not to be mistaken as error bars. Furthermore, the shape of the fibers with the 3:1 ethanol/water ratio shows the flat structure (Figure 5-3) again due to the high alcohol content and the altered deposition mechanics. The high ethanol content leads to a larger gel layer around the polymer, which leads to a larger amount of liquid deposited with the polymer deposited on the collector [85]. Due to the flat structure of the fibers deposited with a 3:1 ratio, the determined fiber sizes for this composition in Table 5-2 are not accurate. The program expects cylindrical fibers, and therefore the flat structures become misinterpreted. The general tendencies remain never the less.

Table 5-2 Solvent ratio and average fiber diameter of calcined ceria

Ratio Ethanol/Water	Average Fiber Diameter [nm]
3:1	575$\pm$511
2:1	225$\pm$95
1:1	202$\pm$59
1:2	209$\pm$91
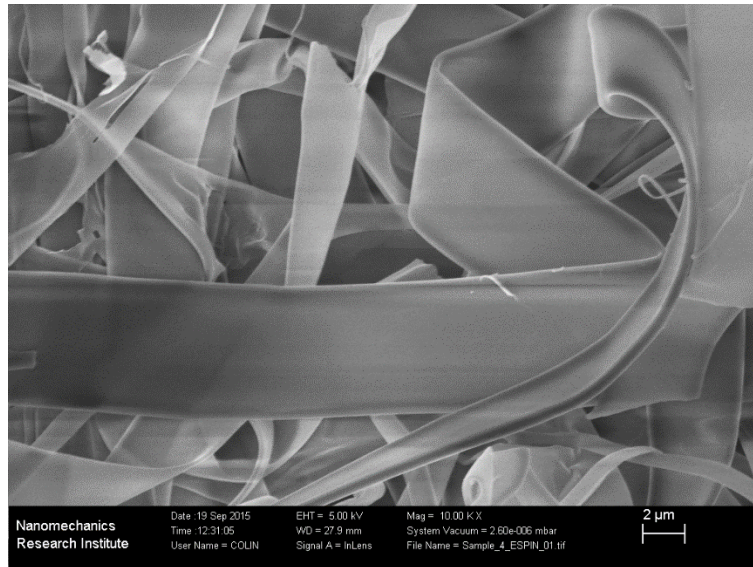
Figure 5-3 Electrospun fibers with an ethanol-water ratio of 3:1

There are a few possible reasons for the large diameters corresponding to high ethanol concentrations. First of all, with the high ethanol concentration, an increased amount of material is deposited, due to the higher gelation caused by the ethanol. The increased amount of material is also visible for identical deposition times. Samples produced with higher ethanol content lose their transparency quicker than samples with lower ethanol content. The larger amount of material deposited leads to larger polymeric fibers, which collapse during the calcination process. Furthermore, the viscosity of the ethanol rich mixture is visibly a lot higher than those of mixtures with higher water contents. This leads to a larger Taylor cone in the electrospinning process and a thicker jet since a greater electric potential is needed to deposit the fiber onto the collector. Therefore, since the voltage has been constant at 16 kV for these trial runs, the electric field could not accelerate the jet of the high ethanol concentration (3:1) at the same rate as with the lower ethanol concentrations.

On the contrary, the diameters of the mixtures with a high-water concentration only differ minimally from each other. The sizes of the fibers produced with ratios of 1:1 and 1:2 only differ by 3 % and are roughly 10 % smaller than that for the 2:1 ratio. The smaller fiber size comes with a trade-off. With higher water content, more solvent evaporates during the

81

electrospinning process, which can also be attributed to the larger gel layer formed with the gelation of the polymer. Due to the gelation, less liquid can evaporate during the deposition process. On the contrary, with higher water content, the gel layer is smaller [85], allowing more liquid to evaporate. Along with higher water ratios comes less material deposited on the collector. This becomes problematic since the deposited mass of the created fiber mats is much lower for equal deposition times, especially after removing the polymer through calcination. Since the difference between the mixtures with lower alcohol content is rather small, but the thickness of the deposited filters is higher with higher ethanol content, a mixture with 2:1 ratio is desirable. Nanofibrous materials generally benefit from the slip-flow effect, which improves for finer fibers [66]. Therefore, the fibers produced with the ratio of 2:1 are sufficiently thin and an ethanol to water ratio of 2:1 has been used for the rest of the study, showing both good sample rigidity and fine fibers.

5.5. Effect of Calcination Temperature on Ceria-based Nanofibers

Calcination is an important step in the preparation of a stable fiber, because it removes the polymer from the fiber and prepares the catalyst to withstand high temperatures. Multiple difficulties correlating to the calcination process could be observed in the previous tests.

The first observation is the shrinkage of the sample after calcination. All fresh samples were deposited on a collector with the same size of 10 x 10 cm, and they were placed as a whole piece in the oven for calcination. After calcination, the samples shrank to a size of 2 x 2 cm, which is a 25-fold reduction in surface area.

Figure 5-4 shows the effects of calcination on a sample prepared with 1:2 ratio ethanol:water. Figure 5-4 shows in (a) the samples right after electrospinning, and in (b), the same sample after calcination. It can be seen that not just the fiber diameter is reduced, but also the free space. The calcination process results in a more compact fiber mat compared to the original electrospun fiber mat.
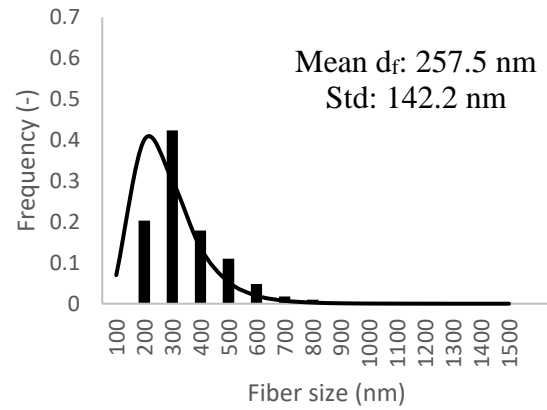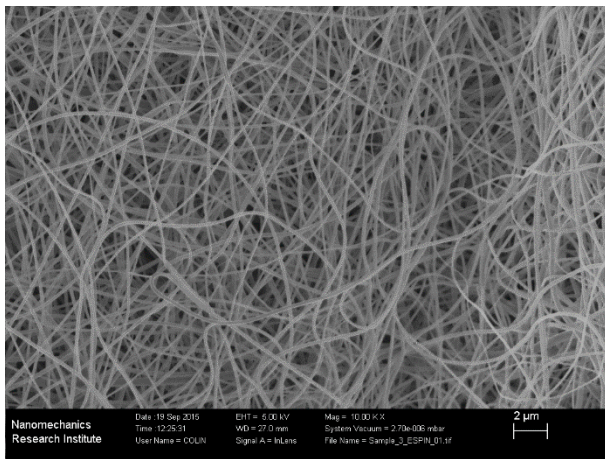
(a)
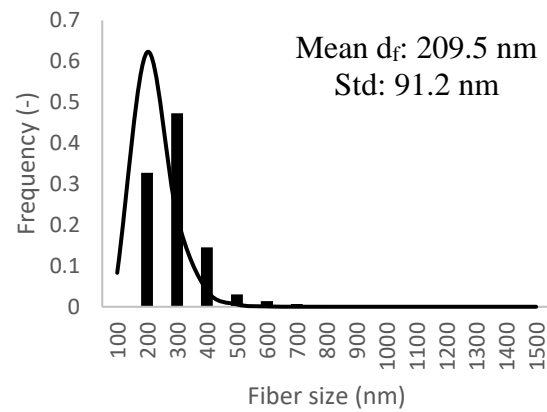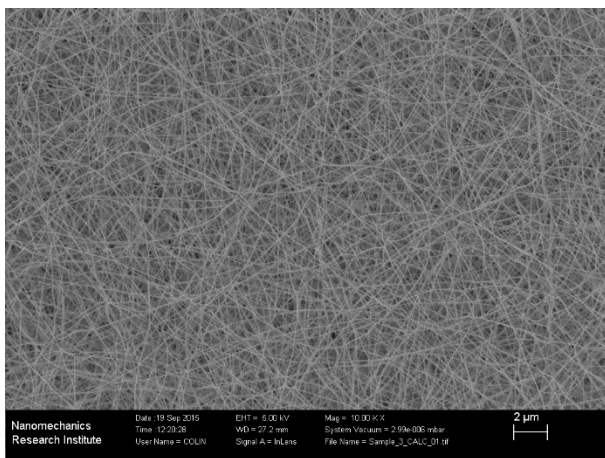
(b)

Figure 5-4 Effect of calcination on 1:2 ethanol/water ratio with fiber size distribution before (a) and after (b) calcination

The exact reduction of the fiber diameter cannot be predicted yet. The potential in reduction of the fiber diameter depends mainly on the absolute amount of polymer that is present right after the electrospinning process. For a high polymer ratio, the diameter reduction is also high. When thinner fibers are produced by electrospinning, the reduction after calcination is small.

Another difficulty is the detachment of the electrospun fibers from the metal mesh and collector it has been deposited on. Since the fibers are deposited onto a metal collector, which expands when heated, this goes in the opposite direction for the fibers, as the fibers themselves shrink under the influence of heat [190]. As a result, many electrospun fiber mats were ripped during the calcination process as the samples adhered to the collector.

The following measures were taken to mitigate the problem of ripping in the calcination process: 1) the samples were electrospun on a metal mesh, and 2) the electrospun samples were dried at 120 °C for two hours in air. The fiber mats after drying are easier to detach from the aluminum collector. This mitigated the adhering of the samples to the collector in the calcination process, allowing the sample to contract freely. The ripping of samples during the calcination process was reduced tremendously, and the final samples are more undamaged than samples that have not been dried and detached from the collector before the calcination.

For the removal of the polymer through the calcination process, the literature suggests that temperatures up to 500 °C are sufficient, as described next. Lee et al. [188] removed PVP from their ceria fibers and found 500 °C to be sufficient. Kang et al. [96] documented a process for the calcination of alumina fibers produced with a mixture of $AlCl_3$ and PVP. They documented a significant weight loss between room temperature and 250 °C due to drying and more weight loss starting at 250 °C due to the decomposition of PVP. The decomposition was completed at 450 °C [96]. Based on this literature information, it was assumed in this research that PVP is removed after calcination at 550 °C.

The absence of polymer in calcined samples was further confirmed through thermal gravimetric analysis (TGA Q500, TA instruments, 10 °C/min, 60 mL/min nitrogen, 40 mL/min air) of a calcined alumina fiber sample. Figure 5-5 shows the weight loss of the alumina sample vs. temperature. No significant weight loss has been detected over the entire temperature range, indicating that the used alumina sample had been converted without PVP left in the fibers. The relative weight loss of 3% can be attributed to evaporating moisture on the sample and the degradation of a small amount of unsaturated backbone residues [96]. The increase of the weight at temperatures over 550 °C can be attributed to phase transitions of the alumina (see Figure

3-3) [167], leading to a slight weight increase, since this sample had not been exposed to these temperatures before the thermal gravimetric analysis.
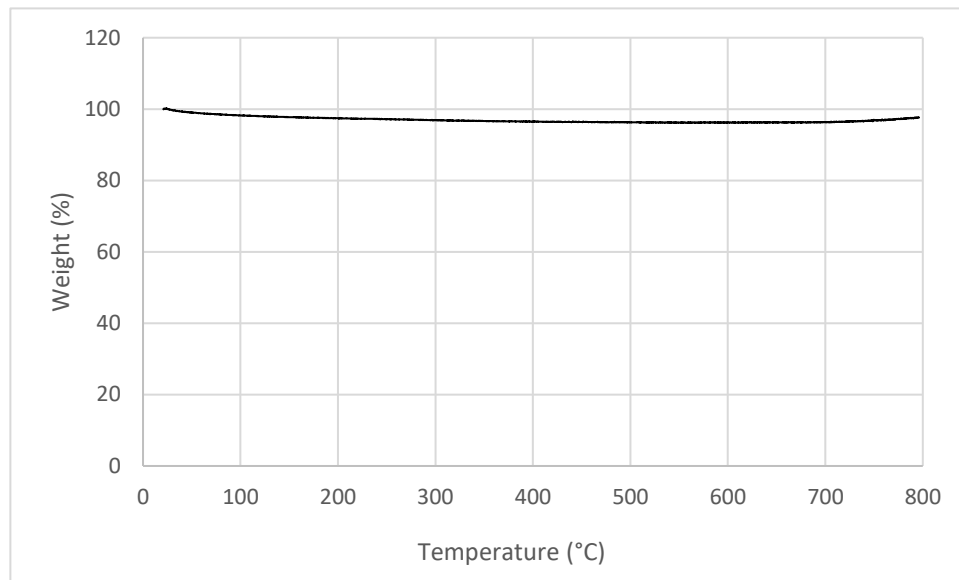
Figure 5-5 Thermal gravimetric analysis of calcined alumina samples

5.6. Produced Alumina and Ceria Fibers

Table 5-3 shows the average fiber sizes and standard deviations for the produced alumina fibers. The non-calcined alumina fibers ranged from 257 to 705 nm in mean diameter, while the calcined fibers range from 203 to 407 nm in mean diameter. Regarding the standard deviation, the largest fiber size distributions also show the greatest standard deviations. Overall, the average non-calcined fiber diameter is 385 nm and the average calcined fiber diameter is 295 nm, which implies an average shrinkage of 23% in terms of average diameter.

Table 5-3 Fiber size distribution of alumina

Label	Diameter before calcination [nm]	Calcination Diameter [nm]
1	386 ± 335	273 ± 194
a	276 ± 165	257 ± 173
b	227 ± 135	203 ± 135
ab	284 ± 269	269 ± 203
c	375 ± 348	328 ± 431
ac	328 ± 298	257 ± 160
bc	257 ± 151	203 ± 114
abc	291 ± 296	257 ± 213
d	530 ± 1044	404 ± 678
ad	407 ± 368	328 ± 484
bd	287 ± 227	227 ± 130
abd	512 ± 375	363 ± 303
cd	386 ± 251	257 ± 242
acd	705 ± 566	407 ± 281
bcd	328 ± 325	284 ± 183
abcd	584 ± 414	404 ± 285

Table 5-4 shows the results for the determined fiber size distributions of ceria. The non-calcined fiber sizes ranged from 275 to 2197 nm. Major entanglement of the spun fibers could be observed, especially for "bcd" and "abcd", which explains the increase in mean fiber diameter. For sample "1", after calcination the sample completely lost its fiber structure and therefore, it was not possible to determine a fiber size distribution for this sample. For the other samples, the calcined fiber diameters lie between 203 to 481 nm. Overall, the average non-calcined fiber diameter of 678 nm was reduced through the calcination by 53% to 315 nm.

Table 5-4 Fiber size distribution of ceria

Label	Diameter before calcination [nm]	Calcination Diameter [nm]
1	419 ± 506	N/A
a	346 ± 246	257 ± 296
b	385 ± 357	266 ± 481
ab	489 ± 402	227 ± 194
c	454 ± 420	257 ± 221
ac	442 ± 593	224 ± 260
bc	275 ± 315	254 ± 352
abc	454 ± 446	295 ± 417
d	386 ± 510	276 ± 177
ad	490 ± 479	265 ± 186
bd	762 ± 700	257 ± 196
abd	900 ± 788	375 ± 310
cd	590 ± 777	463 ± 743
acd	786 ± 627	481 ± 517
bcd	1480 ± 1907	374 ± 518
abcd	2197 ± 1532	455 ± 424

Overall, it could be observed that the fiber diameters shrank through the calcination process. As can be seen in the compared SEM images (see Appendix A – SEM Images) the solidity (fraction of filter volume made up of fibers) does not change, but the filter material shrinks. Furthermore, the ceria filters shrank more than the alumina samples. The reduction of 53% in diameter for ceria can be converted to a volumetric loss of 79% (the reduction of 23% diameter for alumina equals 42% volumetrically). The volume of a single fiber can be calculated as a cylinder:

$$V = \pi \left(\frac{d}{2}\right)^2 h \tag{5-1}$$

with V being the fiber volume, d the fiber diameter and h the length of the fiber. The change in volumetric change is an estimate based on the assumption that the fiber length does not change. The reduction of the volume in % is calculated as:

$$\Delta V = \frac{d_{calcined}^{\ 2}}{d_{non-calcined}^{\ 2}} \cdot 100\%$$

Ceria has a greater density (7.22 g/cm³) than alumina (3.95 g/cm³). Since the weight percentage in precursor mixtures is identical in the sense of metal nitrate weight to polymer weight, it can explain the greater reduction in fiber volume of ceria over alumina. The same weight ratio for metal/polymer has been employed for the precursor of the ceria and alumina solutions. Since ceria has a higher density, the relative volume of ceria in the solution is lower than in the case of alumina. Therefore, a greater reduction in the case of ceria can be expected after the removal of the polymer compared to alumina.

The fiber size distributions deviated strongly between different samples for both materials. Larger mean diameters of fibers tend to be associated with a wider spread of the fiber sizes. The fine fibers are more uniform with a narrow distribution (see Figure 5-6).

(a)

Ce "acd" Calcined

(b)
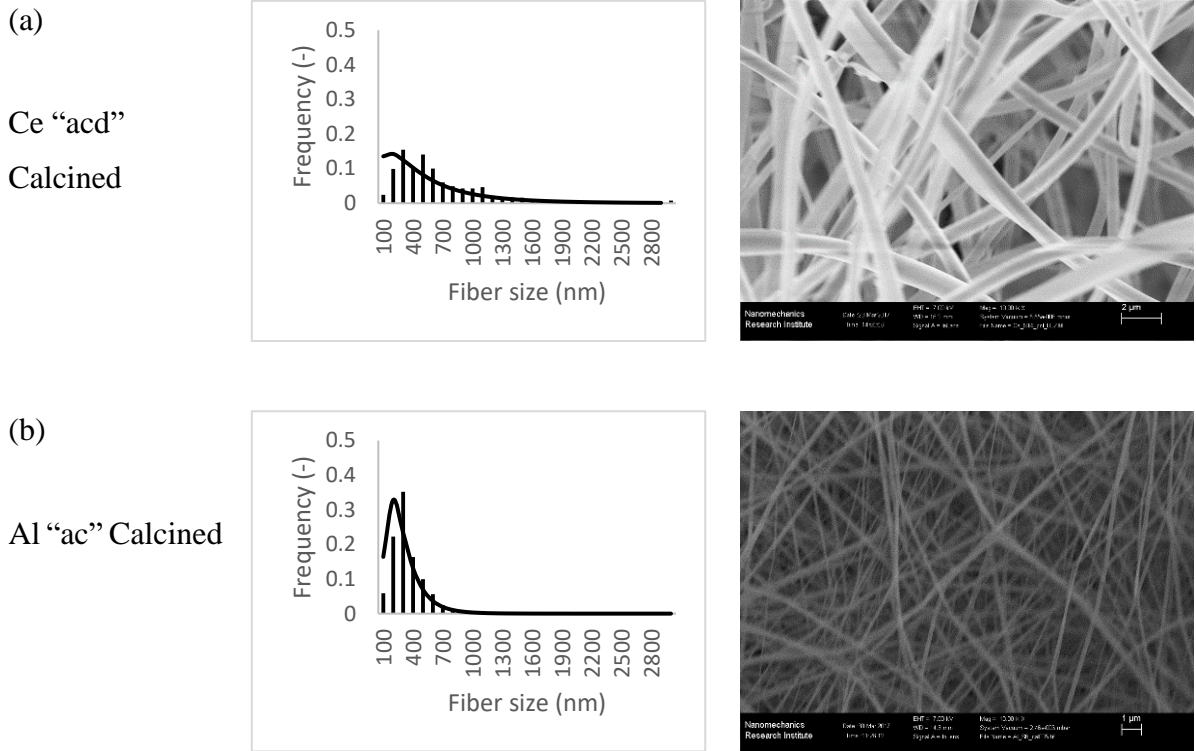
Al "ac" Calcined

Figure 5-6 Example for (a) wide fiber size distribution (Ce acd) and (b) narrow fiber size distribution (Al ac)

Table 5-5 shows the averaged fiber diameters calculated using the two different materials in their two states non-calcined and calcined. Independent of non-calcined or calcined, the finest fiber diameter was determined for low voltage (thus low electric field) and concentration, but large needle diameter and flow rate (label "bc"). The diameters were 266 and 228 nm on average for non-calcined and calcined fibers. The experiments with all 4 factors high ("abcd"), led to the largest average diameters (1390 nm after electrospinning and 429 nm after calcination)

Table 5-5 Average fiber sizes for ceria and alumina in both calcination states

	Average Non-calcined Diameter [nm]	Average Calcined Diameter [nm]	Overall Average Diameter [nm]
1	402.5	273	359.3
a	311	257	284
b	306	234.5	270.25
ab	386.5	248	317.25
c	414.5	292.5	353.5
ac	385	240.5	312.75
bc	266	228.5	247.25
abc	372.5	276	324.25
d	458	340	399
ad	448.5	296.5	372.5
bd	524.5	242	383.25
abd	706	369	537.5
cd	488	360	424
acd	745.5	444	594.75
bcd	904	329	616.5
abcd	1390.5	429.5	910

5.7. Repeatability of the Electrospinning Process

To ensure the repeatability of the produced fibrous samples, three alumina fiber samples have been produced under the same conditions. The applied settings represent average settings with a solution concentration of 13%, applied voltage of 13 kV, and a flow rate of 0.4 mL/hr. The used needle gauge was 20 and the tip-to-collector distance 15 cm.

Figure 5-7 displays the fiber size distributions of the three runs and their average. It indicates a good repeatability of the electrospinning process. The electrospun fibers have been characterized for their fiber diameter. The mean of the three samples was 506 nm with a mean standard deviation of 401 nm. However, the determination of the repeatability has only been conducted for this sample only, all other samples presented in this work have been conducted only once. Therefore, the accuracy of theses samples has to be assumed based on the results of the 13% alumina sample.
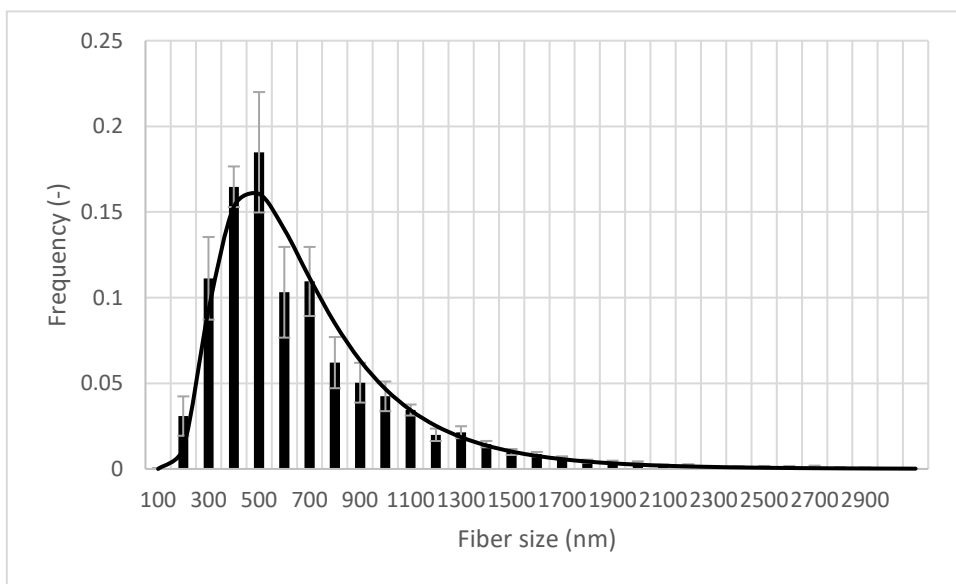
Figure 5-7 Fiber size distribution of 13% alumina replicas

5.8. Alumina Production on a different Collector

To compare the filtration behavior of the produced metal filters with the previously discussed CA fibers, a larger filter sample had to be produced. As the alumina fibers were on average finer than the ceria fibers, an alumina filter has been produced for this test. Finer fibers are preferred in filtration technology due to the possible use of slip-flow. However, due to the shrinkage of the samples, the initially used 10 x 10 cm plate collector was not large enough to produce a calcined sample that is large enough for test in the existing filtration setup. The filtration setup requires round samples of at least 2.5 cm diameter. The samples produced with the plate

collector are squares of 2 x 2 cm, and therefore too small to be tested. To produce a large sample, a drum collector (RC-5000 collector, Tong-Li-Tech, China) (30 cm length, 10 cm diameter, 10 rpm) was used. Average settings have been employed, to receive an average representation of all fibers. In this case, an overall solid concentration of 13 % was selected, along with an applied voltage of 12.5 kV, a needle gauge of 20, and a flow rate of 0.4 mL/hr. The calcination process was conducted in the same manner in air as described in the Chapter 3.

Figure 5-8 displays the shrinkage of the produced alumina sample after calcination at 550 °C. The filter size after electrospinning was around 20 cm x 15 cm; it shrank to approximately 5.4 cm x 3.2 cm or so after calcination, which was large enough to be tested in the filtration setup.
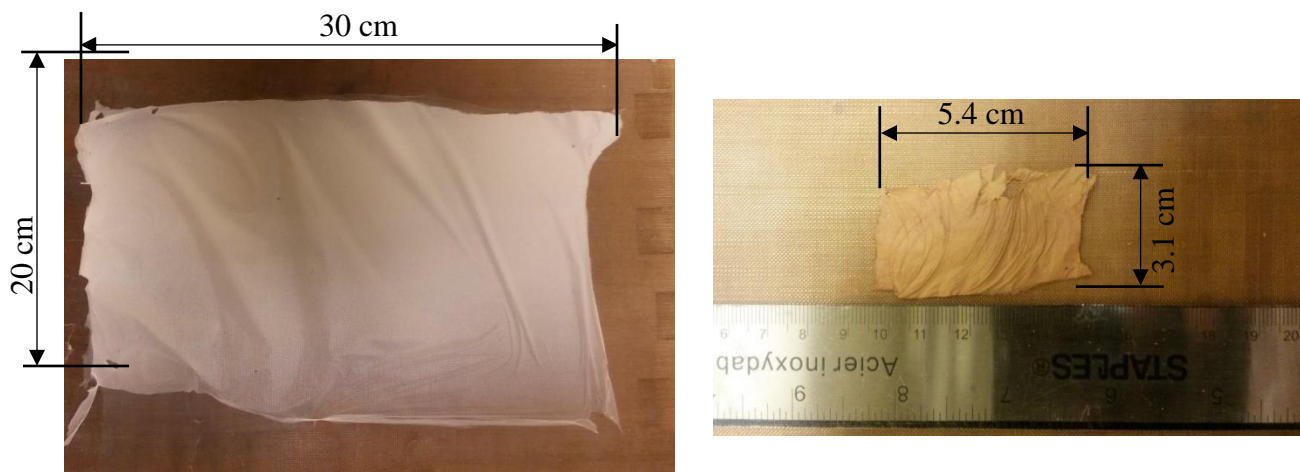
Figure 5-8 Shrinkage of a large alumina fiber sample after calcination

As seen in Figure 5-9, the calcined alumina fibers had a mean diameter of 475 nm with a standard deviation of 395 nm. They are larger than the alumina fibers produced on the 10 x 10 cm plate. The largest fibers produced on the plate collector where 404 nm on average. The different electric fields created with the different collector shapes most likely impacted the electrospinning process. Figure 5-10 shows calculated electric field strengths for the plated and drum collectors using an applied voltage (U) of 20 kV and a needle-collector distance (s) of 10 cm. For the calculation, the collectors have been broken down into multiple small collectors acting as homogenous fields with the needle tip. The electric field strength can be calculated as:

$$E = \frac{U}{s} \tag{5-3}$$

The changing variable of the calculation are the distances of the needle tip to the different points of the collector, the exact calculated values for distance and field strength can be found in Appendix B. Local distance and electric field strength between needle and collector. The maximum voltage for both collectors was 2000 V/cm. A homogenous field would yield an electric field strength of 2000 V/cm everywhere on the collector, which is not the case for the two calculated collectors. The average electric field for the plate collector is 1833 V/cm (8.35% less than homogenous field) with a local minimum of 1632 V/cm (18.4% less than homogenous field) and needle to drum average field of 1642 V/cm (17.9% less than homogenous field) and a minimum of 1240 kV/cm (which is 38% less than the homogenous field).
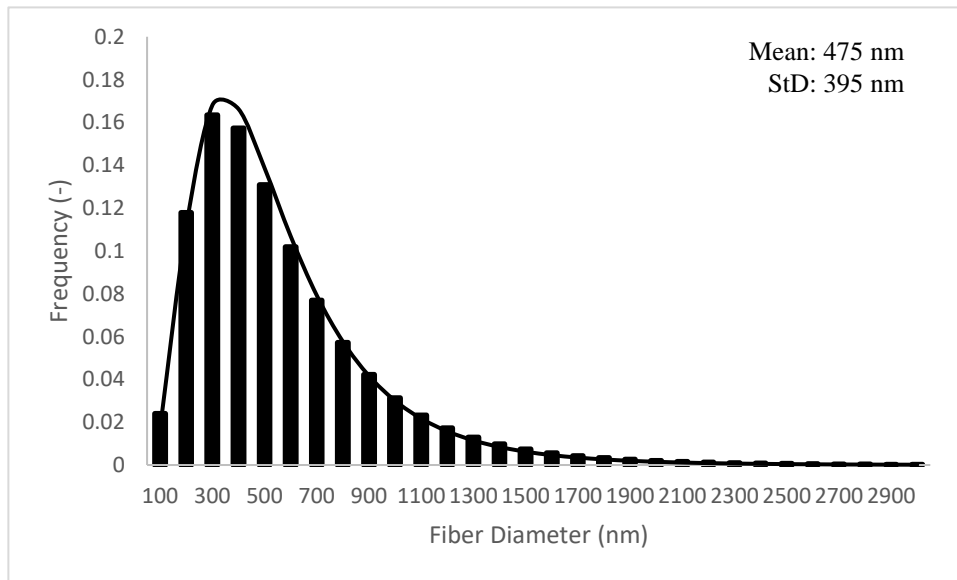
Figure 5-9 Size distribution of calcined alumina fibers produced on drum collector

$$(a) \qquad\qquad (b)$$
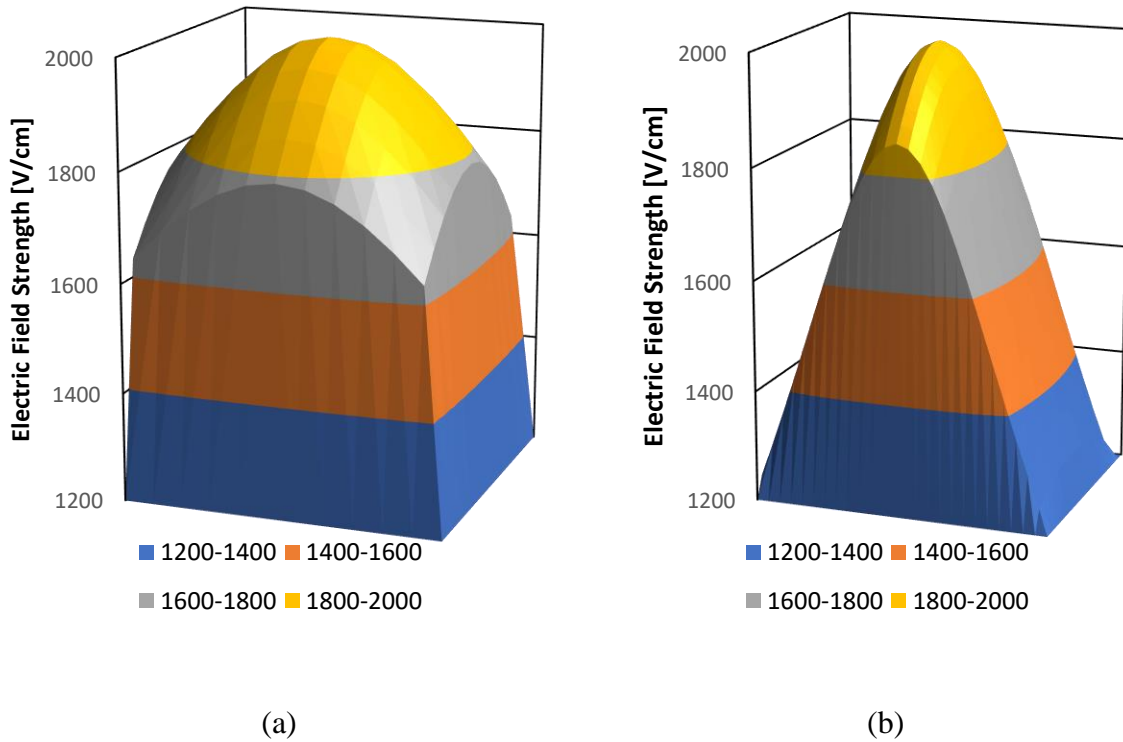
Figure 5-10 Electric fields between needle and (a) plate collector (b) drum collector

The clear differences in the shape of the electric fields are due to the different dimensions of the compared collectors. The plate collector is smaller in the horizontal dimension (10 x 10cm) than the drum collector with 30 x 10 cm. Additionally, the drum collector has a vertical dimension, which further increases the distance of collector sections from the needle and therefore reduces the electric field strength. As stated in section 2.6. , the calculation of the electric field strength for electrospinning applications is based on the homogenous field strength between two parallel plates, whereas in lab or industrial applications it is usually a needle to plate or needle to drum scenario (see Figure 5-11).

(a)   (b)
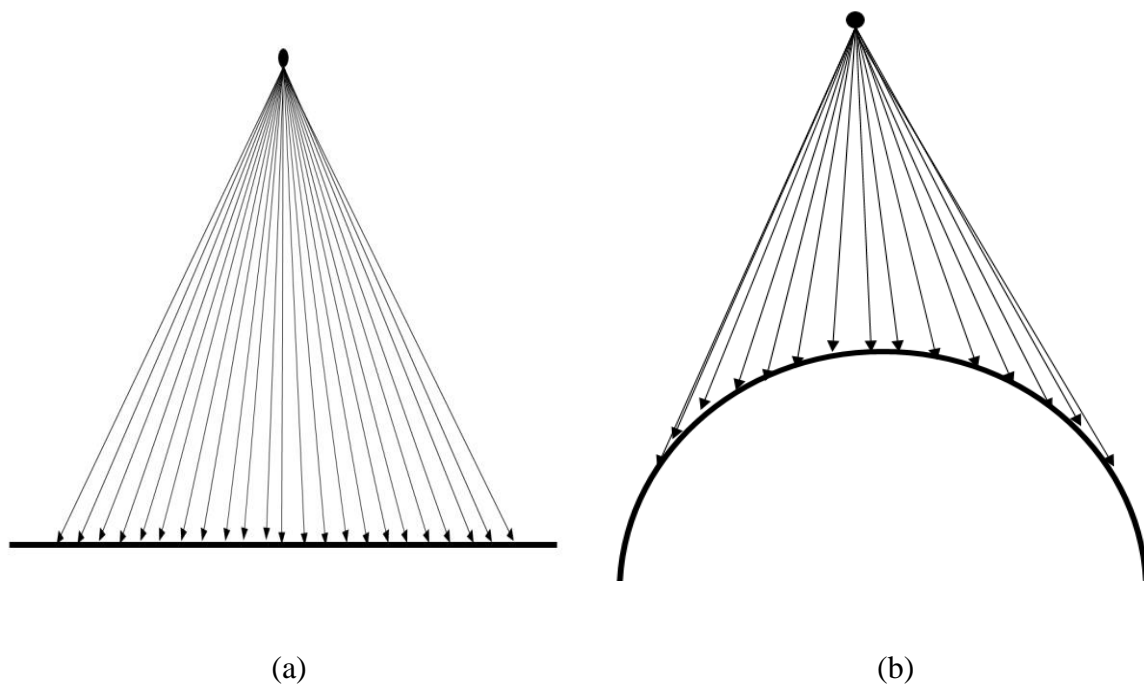
Figure 5-11 Electric field lines between needle and (a) plate and (b) drum collector

Due to the change in collector, the deposition of the electrospun material changed as well. While on the plate collector, the deposition took place on almost its entire surface, the deposition on the drum collector took place in stripes with an approximate 5 cm width. This indicates that the jet moves differently throughout the two different electric fields. Reneker et al. [89] observed different jet-whipping behaviour in different field strengths as well. However, the difference between their modeled whipping behaviours and the experimentally observed behaviour increased dramatically with the flight time of the jet. For simplicity, this research will continue treating the electric field as a homogenous field, since an accurate correction factor has not been described in the literature. The electric field calculations conducted in this chapter are estimates and as stated, the deposition of the fibers did not take place on the entire collector, which further complicates the estimation of the exact impact of the electric field on the fiber deposition behavior.

5.9. Filtration Efficiency of Alumina Filter

The alumina filter sample produced on the drum collector has been tested in the same setup as the CA filters in Chapter 4. The pressure drop has been recorded as 123 Pa. Figure 5-12 shows the filtration efficiency vs. the particle size, with an average filtration efficiency of 45.7%, and a maximum efficiency of around 70% for particles as small as 9 nm in diameter. The quality factor ranges from a maximum of 0.024 Pa^{-1} to a minimum of 0.01 Pa^{-1}, with an average of 0.0126 Pa^{-1}. These values are not as good as for the previously produced CA fibers with an optimal value of 0.05 Pa^{-1}. However, it is still greater than those of commercial facemask filters of polypropylene, which have been found to be 0.007 Pa^{-1} with a fiber diameter of approx.10 μm [187]. It is possible to increase the filtration performance with further research regarding optimal settings for the electrospinning of the desired PVP-salt combination. Due to the change in deposited fiber size on the drum collector, a prediction based on the results of section 5.6. is not possible. The production process of large filter samples is also very time intensive, due to the low output of our electrospinning setup.
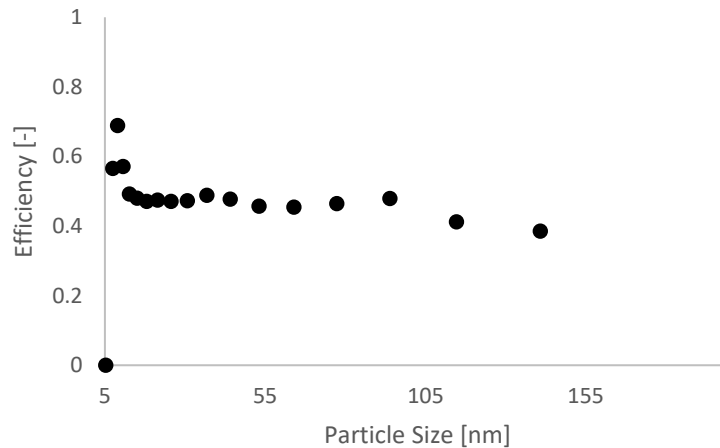
Figure 5-12 Filtration efficiency alumina filter
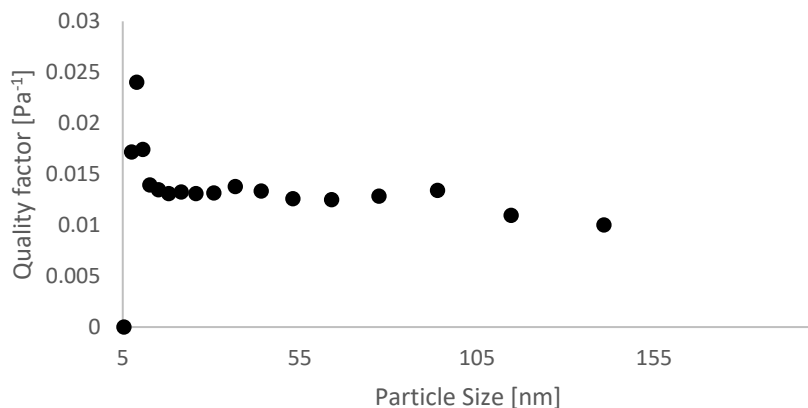
Figure 5-13 Quality factor alumina filter

5.10. Conclusion

In this chapter, filter materials based on alumina and ceria have been produced. To electrospin these materials, a mixture of PVP and nitrate, containing the desired metal, was dissolved in a mixture of ethanol and water (2:1 v:v ratio). Other mixtures with higher alcohol concentrations have not shown to be capable of nanofibrous fiber production. The metal-based fibers were deposited onto a metal mesh and dried at 120 °C for detachment. The fibers were then calcined to remove the polymer content. A calcination atmosphere of air yielded the best results, while reducing and inert atmospheres yielded carbonized fibers, which could not be used as filter material.

Alumina and ceria fibers with average diameters ranging from 200 to 400 nm (after calcination) have been produced on a 10 x 10 cm plate collector. These filter samples shrank to a size that was not possible to test the filtration performance. Therefore, a larger drum collector has been used to produce larger samples of alumina fibers to verify the filtration performance of the metal-based filters. Resulting from the increased collection area and changed collector shape, the produced alumina fibers were significantly larger. The setup with a plate collector produced a range of different fiber sizes based on different concentrations, metal nitrates, voltages, flow rates and needle diameter, which can be used for a parametric study. Furthermore, it can be concluded that the finest fibers are produced for low concentration of ethanol and applied voltage, while the largest fibers are produced with a high concentration of ethanol.

Based on our one test, the filtration performance of alumina nanofibers is comparable to those of other nanomaterials, like the produced CA fibers with a quality factor of up to 0.027 Pa^{-1}. In this test, the quality factor has been determined to be 0.0125 Pa^{-1}, which is much higher than the filtration quality of other commercial materials.

Chapter 6 Parametric Study on Electrospinning of Metal-Based Fibers

6.1. Introduction

The ceria and alumina metal-based fibers introduced in Chapter 5 have been analysed using the factorial design method introduced in Chapter 3. Results show that the concentration of dissolved material in the solution has more influence on the fiber size than voltage, needle diameter and flow rate of the electrospinning solution. These three parameters have a comparable effect on the fiber size, considering the possible interactions of parameters. Furthermore, the calcination state of the fibers does not impact the documented contribution of parameters on the fiber size. The results of this work are comparable to other parametric studies conducted on pure polymer materials.

6.2. Solution Properties

According to the methods introduced in Chapter 3, the surface tension, viscosity and conductivity of the used alumina and ceria solutions have been measured (Table 6-1). The increase in solution concentration mainly led to an increase in the viscosity (increase by a factor of 3) and surface tension (increase by 50%), while the conductivity only increased by approximately 18%. The effect of viscosity and surface tension increases due to higher polymer content has also been measured in other parametric studies [17,29,28], while Heikkilä et al. [17] used the salt potassium formate to increase the conductivity of their electrospinning solution. The values measured in this work show that the impact of an increased solution concentration mainly impacts the electrospinning solution properties surface tension and viscosity, therefore the findings of this parametric study are comparable to other parametric studies, although the metal content in this work is higher.

Table 6-1 Solution properties of ceria and alumina solutions

Solution	Density [g/mL]	Surface Tension [N/m]	Viscosity [mm²/s]	Conductivity [mS/m]
Alumina (10 wt%)	882.7	0.0342	44.52	4.6
Alumina (16 wt%)	896.5	0.0416	169.72	5.4
Ceria (10 wt%)	886.4	0.0362	72.93	2.7
Ceria (16 wt%)	902.5	0.0450	173.1	3.3

6.3. Contribution of Parameters on Fiber Size

The electrospun alumina and ceria samples were characterized to determine the effects of the applied voltage (A), needle diameter (B), flow rate (C) and solution concentration (D) on the nanofiber size. The experimental design plan introduced in Chapter 3 has been utilized to quantify the effects of each parameter and their interactions on the fiber size. The effects of a parameter were quantified using equations (3-1) to (3-23) in Chapter 3. These effects are represented by the values of the corresponding dimensionless parameters. A positive number indicates an increasing effect on the fiber size. The contribution T of a parameter combination was calculated using Eq. (6-1),

$$\mathrm{T}(x_i) = \frac{|\Phi(x_i)|}{\sum_{x=1}^{ABCD}|\Phi(x_i)|} 100\%$$

(6-1)

with Φ as the effect of a parameter combination and 1 to ABCD the run labels.

Table 6-2 and Table 6-3 show the ranking of the parameter combinations according to their contributions to the fiber size in decreasing order. These tables are separated into two parts, where the half on the left show the effects and contributions of the non-calcined fibers, and where the right half of the table shows the effects and contributions of the respective calcined fibers. In this chapter, whenever an effect or contribution is calculated or discussed, it is referring to the effect or contribution of a parameter or parameter combinations on the fiber size, unless stated otherwise.

Both Table 6-2 and Table 6-3 show that the contributions of a single parameter to the fiber size is the most dominant factor. For both ceria and alumina-based nanofibers, it is one single parameter that dominates the contribution to the fiber size. Independent of the metal element (Ceria or Alumina) or state (before or after calcination), the contribution of the solution concentration lies between 31 and 40%, while it also presents effects when concentration is combined with other parameters. Other parameters with a significant effect are the electric field (A) and flow rate (C), however they are smaller compared to the effect of the solution concentration.

Besides the solution concentration, most other parameters seem to be almost equal in their effect on the fiber size, ranging from 0 to 10% effect. Assuming even a small error due to the partially wide fiber size distributions, the order of the other parameters and their interactions become almost interchangeable for individual parameters with a rank of 7 or higher for alumina or above the rank of 5 for ceria.

Table 6-2 Parameter effect for alumina fibers with (A) Voltage (B) Needle Diameter (C) Flow Rate (D) Solution Concentration

	Non-Calcined Alumina			Calcined Alumina		
Rank	Parameter	Φ	T [%]	Parameter	Φ	T [%]
1	D	164.4	40.3	D	78.4	34.3
2	AD	92.9	12.9	AB	48.6	13.2
3	B	-77.9	9.0	A	45.4	11.5
4	A	76.4	8.7	B	-37.6	7.9
5	AB	66.6	6.6	AD	37.1	7.7
6	AC	64.1	6.1	ABCD	-35.6	7.1
7	ABC	-62.1	5.8	ACD	34.6	6.7
8	ACD	54.1	4.4	BCD	29.1	4.7
9	C	43.1	2.8	ABC	-24.9	3.5
10	ABCD	-40.6	2.5	AC	17.9	1.8
11	CD	23.6	0.8	BC	12.4	0.9
12	BC	-5.6	0.05	C	9.1	0.5
13	ABD	4.6	0.03	BD	8.1	0.4
14	BCD	-4.6	0.03	ABD	-3.1	0.05
15	BD	-1.4	0.003	CD	-1.6	0.01

Table 6-3 Parameter effect for ceria fibers with (A) Voltage (B) Needle Diameter (C) Flow Rate (D) Solution Concentration

	Non-Calcined Ceria			Calcined Ceria		
Rank	Parameter	Φ	T [%]	Parameter	Φ	T [%]
1	D	540.9	31.1	D	145.8	41.3
2	BD	393.1	16.4	C	110	23.5
3	B	378.6	15.2	ABCD	-54.5	5.8
4	CD	316.1	10.6	A	54	5.7
5	C	312.6	10.4	ABD	51.8	5.2
6	BCD	223.9	5.3	BC	-46.8	4.2
7	A	169.1	3.0	BD	-41	3.3
8	BC	154.9	2.5	CD	40	3.1
9	AD	119.6	1.5	ABC	38	2.8
10	AB	115.4	1.4	B	35	2.4
11	AC	100.9	1.1	AC	-27.3	1.4
12	ACD	66.9	0.5	ACD	25.3	1.2
13	ABC	62.6	0.4	BCD	-4.8	0.04
14	ABCD	59.1	0.4	AB	-3.8	0.03
15	ABD	23.4	0.06	AD	-2.5	0.01

For further analysis, the average contributions for alumina and ceria have been investigated. The contributions of each parameter have been averaged over both materials in both states. Parameter D, solution concentration, remains the most influential with a contribution of 36.7% (see

Table **6-4**). The other individual parameters are close together with 9.3% (flow rate), 8.6% (needle diameter), and 7.2% (voltage). The parameter combination with the highest effect is the combination AD (high voltage and solution concentration) with 5.5%, while the least impactful combination of parameters is the combination "ABD".

Table 6-4 Average contribution of non-calcined and calcined alumina and ceria fibers depending on production with (A) Voltage (B) Needle Diameter (C) Flow Rate (D) Solution Concentration

Parameter	T [%]
A	7.22
B	8.64
C	9.28
D	36.73
AB	5.31
AC	2.61
AD	5.52
BC	1.92
BD	5.01
CD	3.64
ABC	3.11
ABD	1.34
ACD	3.19
BCD	2.53
ABCD	3.92

To quantify the overall effect of a single parameter on the fiber size, the sum of contributions of each combination involving a given parameter was generated. The sum of contributions involving all eight possible combinations of the parameter A is 32.2, 31.8 for B, 30.2 for C and 61.9 for D for a total of 156.1 (see

Table **6-5**). The ratio of the sum of contributions per parameter to the total contributions yields the overall effect of the single parameter on fiber size. Considering all possible combinations, the solution concentration remains the most dominant parameter with approximately 40% contribution to fiber size. The other three parameters are almost identical, with 20% contribution each.

Table 6-5 Ranked contribution by parameter with (A) Voltage (B) Needle Diameter (C) Flow Rate (D) Solution Concentration

Parameter	T [%]	T(A)	T (B)	T(C)	T(D)
D	36.73				36.73
C	9.28			9.28	
B	8.64		8.64		
A	7.22	7.22			
AD	5.52	5.52			5.52
AB	5.31	5.31	5.31		
BD	5.01		5.01		5.01
ABCD	3.92	3.92	3.92	3.92	3.92
CD	3.64			3.64	3.64
ACD	3.19	3.19		3.19	3.19
ABC	3.11	3.11	3.11	3.11	
AC	2.61	2.61		2.61	
BCD	2.53		2.53	2.53	2.53
BC	1.92		1.92	1.92	
ABD	1.34	1.34	1.34		1.34
Σ	100.00	**32.23**	**31.79**	**30.22**	**61.90**
	Weighted T	**20.6%**	**20.4%**	**19.4%**	**39.7%**

6.4. Effect of Solution Concentration

The solution concentration (parameter D) has been found to be the most impactful parameter in this parametric study. The solution concentration contributes to around 36%, and considering interactions and weighting, it reaches a 40% overall contribution (see

Table **6-5**). In all possible combinations, an increase of the concentration results in an increase of the fiber size.

The dominant effects of solution concentration on the fiber size can be attributed to the solution composition and its impact on electrospinning. Factors like surface tension and viscosity change with the solution concentration. These parameters increase with increasing concentration, which are linked to an increase in fiber size in the literature [124]. In contrast, an increase of concentration of dissolved material leads to an increase of dissolved metals in the solution, which leads to an increase in conductivity of the solution. An increased electric conductivity has been documented to lead to finer fibers [103]. The finer diameters obtained with a lower solution concentration are related to a higher mobility of the polymer chains, which also allows stronger instabilities in the jet during electrospinning [191]. This enables a longer stretching of the polymer jet, ultimately leading to the production of finer fibers [191]. A higher polymer content leads to a stable jet, since entanglement of the polymer is increased, strongly hindering the wiping motion of the jet, which leads to thicker fibers [191]. The same effects as described in the literature can be observed in this research.

As stated above, the solution concentration impacts different solution parameters, namely viscosity, density, surface tension and electric conductivity. This means that a change of the concentration of dissolved material may change at least four more electrospinning parameters. In contrast, the parameters voltage, needle diameter and flow rate do not impact any other parameters that have a documented impact on the electrospinning process. The investigated processing parameters are strictly independent of one other and other electrospinning parameters. A further investigation of the effect of the individual solution parameters on the

fiber size is therefore necessary. However, it can be stated that solution composition is the most relevant aspect of the electrospinning process, which has also been confirmed in Cui et al.'s work [28].

6.5. Effect of Voltage on Fiber Size

The effect of the voltage in this research has a lower impact as a single parameter than the solution concentration, with approximately 7% by itself. Considering all possible combinations involving the voltage, the value increases to 20%, which is half of the solution concentration effect. In the literature, the effect of the voltage has been found to be controversial for polymeric materials, with studies finding that an increase of the voltage leads to an increase in the fiber size [27,103] while another study found a decrease of the fiber size with an increase of the voltage [192]. In the present research, the general trend shows that an increase of the voltage increases the fiber size; however, a few parameter combinations involving the voltage led to a decrease of the fiber size, when the voltage was high. Most prominent are the combinations "ABCD" and "ABC" in alumina (see effect in Table 6-2) and "ABCD" and "AC" for calcined ceria (see Table 6-3), which shows a decrease in fiber diameter, when all four parameters solution concentration, voltage, needle diameter and flow rate are high. However, the general trend shows an increase of the fiber size with an increase of the voltage. An increase of fiber size with higher voltage has been explained with a higher mass flow of the nozzle through the increased electrostatic force, which leads to a thicker jet, causing less instabilities and bigger fibers [193], which is the case in this work. Comparing the individual parameters directly with one another, the voltage appears to have the lowest contribution to the increase in fiber size (see

Table **6-5** Parameter A), with a notable difference between ceria and alumina. For alumina, the single parameter effect was as high as 11%, while for ceria the contribution lies only at 6%. Nevertheless, through the interaction effects with the other parameters it can be considered as important for the fiber size as the flow rate and needle diameter. Considering the single parameter effect, a low impact of electric field strength on the fiber size has also been documented by Cui et al. [28]. However, in Cui et al.'s work, the flow rate has been ranked higher in its effect on the fiber size than the electric field strength, while the electric field

strength was found to be comparable to the needle diameter in their effect. The comparable effect of voltage to the needle diameter could be confirmed in this work.

6.6. Effect of Flow Rate on Fiber Size

Overall, the flow rate (parameter C) has been found to be comparable in its effect to the voltage or needle diameter. As a single parameter, its effect lies at around 9%, and all interactions combined and weighted yield an overall contribution of 20%, identical to voltage and needle diameter. It is worth noting that the single parameter effect of the flow rate is much lower in alumina fibers (around 3% Table 6-2) than in ceria fibers (around 10% Table 6-3).

A high flow rate is typically linked to thicker fibers and wider fiber distributions in the literature [194,28]. Overall, it has been found to have a marginal effect, which can be lessened even more at lower solution concentrations [104]. The feeding rate is critical for the quality of the electrospinning process. An equivalent flow rate to the produced amount of fibers leads to a stable Taylor cone, while a flow rate that is too low can cause clogging and a flow rate that is too high can cause dripping and might also cause beaded fibers [103]. A higher flow rate can increase the productivity if dripping does not occur. Flow rates can also affect the optimal setting of other parameters, for example the optimum point of voltage, which increases with a higher flow rate [195].

In this work, the flow rate has proven to be a relevant parameter for the produced fiber size. As an individual parameter, it has a higher contribution than needle diameter and voltage (

Table **6-5** Parameter C), while its interactions are shown to be less impactful than the interactions of the needle diameter, leading to an overall ranking on the same level as voltage and needle diameter. The effect of the reduced effect for reduced concentrations could also be calculated. The effect of the flow rate as a single parameter was three times higher in ceria fibers compared to the alumina fibers, which can be explained by the lower viscosity and surface tension of the alumina solution compared to the ceria solution.

107

6.7. Effect of Needle Diameter on Fiber Size

In this study, the needle diameter (parameter B) showed mixed effects on the fiber size. In alumina, the single parameter needle diameter leads to finer fibers, when the diameter has been increased. Combinations involving a higher needle diameter ("BCD", "ABCD", "BC" and "BCD") showed a decrease of fiber size for alumina fibers (see Table 6-2). However, this effect could not be observed in ceria fibers where all combinations including the needle diameter lead to an increase of the fiber diameter when the diameter has been increased (Table 6-3). The absolute effect on the needle diameter considering the interactions makes the parameter comparable to the voltage and flow rate, around 20% in total, half the effect of the concentration.

Like the other parameters, the effect of the needle diameter on the fiber size has been mixed in other research papers. An increase in the nozzle size has been found to have an increasing effect on the fiber size [194], as well as a minimal decrease [28]. The increase of fiber diameter has been attributed to a larger Taylor cone diameter in the literature, which allowed a thicker jet ultimately leading to larger fibers. Reasons for the documented decrease in fiber diameter with increase of the nozzle size have not been discussed in Cui's work [28] since the decrease was small compared to effects of other parameters. However, Cui's work indicated an interaction between the needle diameter and flow rate. This interaction could also be observed in this work. As stated, for the alumina samples, the combinations "BCD", "ABCD", "BC" and "BCD" had a decreasing effect on the fiber size, while the same combinations showed increased fiber sizes for ceria samples. What these four combinations have in common, are the parameters flow rate and needle diameter. The circumstance that cause the effects to reverse for the two different solutions stems from the fact that the effect of flow rate is much smaller on alumina samples (compare section 6.6.), however, both needle diameter and flow rate as individual parameters lead to an increase in fiber diameter. A decrease of the combinations "BCD", "ABCD", "BC" and "BCD" despite of the reverse effect of the single parameters involved indicates interactions between flow rate and needle diameter. An interaction of voltage with needle diameter and flow rate can be excluded, since the parameter "A" appears in one of these combinations.

The nozzle size has proven to have an immediate effect on the fiber size distribution [102], where an increased nozzle size leads to a wider distribution [130]. There has also been a

correlation of nozzle size and clogging and bead formation documented in the literature [99], which occurred for finer needle diameters. These effects could not be observed in this research. No beading has been observed for the produced fibers and the standard deviations were not part of the statistical analysis.

6.8. Discussion

The main finding of this parametric study is that the solution concentration has the greatest effect on the fiber diameter. This matches the results of other multi-parametric studies [17,29,28]. These studies have been conducted with only polymeric materials, however the results are comparable to this research as well, since the effects of the change in solution concentration are mostly due to the change in polymer content in the electrospinning solution. A higher salt content in the solution is usually linked to higher electric conductivities [17]. The higher conductivity could also be observed in this study (see Table 6-1), however the increase in viscosity and surface tension were more significant.

Heikkilä and Halrin [17] found that viscosity and salt content (and therefore the conductivity) of an electrospinning solution affect the fiber diameter the most. Costolo et al. [29] determined the flow rate to be the most impactful parameter, followed by parameters linked to the concentration like viscosity and surface tension. The results of the present research do not indicate the same effect of the flow rate on the fiber size as Costolo et al.'s work. Heikkilä and Harlin indicated a significant effect of the nozzle size on the fiber diameter, which could be confirmed in this work, but which is contrary to the results of Cui et al. [28], which indicated that the nozzle diameter has the lowest effect on the fiber size. The effect of the applied voltage has been contradicting in the research of Heikkilä and Harlin [17] and Costolo et al. [29]. Costolo et al. determined the voltage to be as impactful as the viscosity, which could not be seen in this research. Heikkilä [17] and Cui et al. [28] found that the applied voltage is comparable to the flow rate.

The differences in the observed effects can be explained by the different selected electrospinning solutions and different boundary conditions like voltage and distance, as well as other parameters selected for the parametric study. In this work, the solution was based on

water and ethanol, with PVP as a polymer, the voltage ranged from 10 to 16 kV, a flow rate of 0.3 to 0.5 mL/hr and needle diameters of 0.60 and 0.84 mm. Heikkilä used polyamide-6 as a polymer, while Costolo et al. considered a wide range for the voltage, ranging from 4 to 30 kV, and the flow rate of the used polymer PAN had been between 0.1 and 9.0 mL/hr. Cui et al. produced poly(DL-lactide) fibers dissolved in different mixtures of acetone and chloroform with a voltage ranging from 15 to 25 kV. A difference between the setups was also the orientation of the collector. Costolo et al. worked with a vertical setup, identical in orientation as the setup in this work. Heikkilä used a horizontal setup. A summary of the used settings in parametric studies of other research groups can be found in

Table **6-6**.

<p align="center">**Table 6-6** Settings and boundary conditions of parametric studies in the literature</p>

Parameter	Heikkilä et al. [17]	Costolo et al. [29]	Cui et al. [28]	This work
Voltage [kV]	30 – 50	4 – 30	15 – 25	10 – 16
Distance [cm]	10 – 20	5 – 11	15	15
Field – Orientation	Horizontal	Vertical	N/A	Vertical
Polymer	Polyamide-6	Polyacrylonitrile	Poly(DL-lactide)	PVP
Solvent(s)	Formic acid	Dimethylacetamide Dimethylformamide Acetone 1-methyl-2-pyrrolidinone Formic acid	Acetone Chloroform	Ethanol Water
Concentration [wt.%]	N/A	1.5 – 6.25	10 – 30	10 – 16
Needle Diameter [mm]	0.3 – 0.5	N/A	0.45 – 0.8	0.60 -0.84
Flow Rate [mL/hr]	N/A	0.1 – 9.0	1.8 – 9.0	0.3 – 0.5

The effect of the parameter selection and the selection of the range of these parameters, as well as the selected polymer, have a significant impact on the determined effect. The polymer used

in all three parametric studies have been different and therefore the solution parameters differ significantly as well, limiting the range of setup parameters like applied voltage or flow rate. Resulting from the different ranges, the determined effects will turn out to be different, depending on the used polymer, making a quantitative comparison between parametric studies challenging.

6.9. Conclusions

Two factorial experimental design has been used to study the effect of key parameters in the electrospinning process to produce alumina and ceria nanofibers. Obtained morphologies of the fibers were comparable to the morphologies reported in other electrospinning papers. The main parameter effecting the fiber size has been found to be the solution concentration. Due to the applied changes to the concentration, the viscosity and surface tension changed accordingly. This led to a higher resistance against the electrospinning process and led, therefore to larger deposited fibers. This was not offset by a higher conductivity, which is known to lead to finer fibers. The other three investigated parameters, voltage (thus electric field), needle diameter and flow rate are comparable in their effect on the electrospinning product, while the voltage is the least influential as a single parameter but shows most effect interacting with the other parameters, leading to a comparable overall contribution as flow rate and needle diameter.

Chapter 7 Pi-Theorem Analysis of the Electrospinning Process

7.1. Introduction

Electrospinning parameters have been developed into dimensional matrices using the results of the parametric study. The goal of the dimensional matrices is the development of dimensional groups or numbers describing the electrospinning process or correlating with the fiber size using the Pi-theorem. Developed dimensionless numbers are then applied using experimental data from the ceria and alumina solutions produced in the previous chapters, considering observations during the electrospinning process of these samples. No single dimensionless group has been found, which can describe the entire electrospinning process or predict electrospinnability in general. However, the dimensional group $\frac{\nu\gamma}{E^2 d_N{}^3 \kappa}$ yielded small numbers for production parameter combinations, which have been problematic in the production, indicating a potential cut-off number.

7.2. Methodology

The data generated in Chapter 5 in regard to fiber size and electrospinning settings as well as solution parameters of the used solutions for ceria and alumina are used to develop dimensionless groups. The dimensional groups have been created following the Pi-theorem introduced in Chapter 3. This chapter aims to justify the selected parameters for the dimensional table and demonstrate the derivation of dimensionless numbers from dimensional matrices.

The selection of parameters for the used parameters is explained, starting with all parameters significant for the electrospinning process. In the next steps, parameters are removed from the dimensional table, eliminating redundancies between the parameters. The final goal is the simplification of the dimensional table so that it yields one single dimensional group. The significance of the developed dimensional groups is afterwards verified with experimental data for the produced ceria and alumina fibers.

7.3. Development of Pi-Theorem tables

This section describes the process of the development of the dimensional matrixes characterizing the electrospinning process. As stated in Chapter 3, the development of a dimensional matrix to apply the Pi-theorem necessitates the selection of the appropriate parameters [182]. It is important to avoid redundancies, while still considering all parameters that have an impact on the electrospinning process. In the context of dimensional analysis, redundancies between parameters are to be avoided in a sense that all parameters are strictly independent from one another.

It starts with all electrospinning parameters and narrows them down by eliminating redundant and non-useful parameters. As seen in Chapter 3, the literature suggests that the following 13 parameters are those with the most impact on the resulting fiber size in electrospinning. The parameters voltage, needle diameter, tip-to-collector distance and electric field strength represent processing parameters. Representing the solution parameters are electric conductivity, kinematic and dynamic viscosity, surface tension and solution density. The environmental parameters humidity and temperature are also represented.

Processing Parameters:

- Needle Diameter, $d_N=[L]$

- Distance, $d_{TC}=[L]$

- Voltage, $U=[ML^2I^{-1}t^{-2}]$

- Electric Field Strength, $E=[L^1M^1t^{-3}I^{-1}]$

- Flow rate $\dot{V}=[L^3t^{-1}]$

Solution Parameters:

- Surface tension, $\gamma = [Mt^{-2}]$

- Kinematic Viscosity, $\nu = [ML^{-1}t^{-1}]$

- Dynamic viscosity, $\mu = [L^2t^{-1}]$

- Permittivity, $\varepsilon = [t^4I^2M^{-1}L^{-3}]$

- Density, $\rho = [L^{-3}M^1]$

- Conductivity (elect.), $\kappa = [t^3I^2L^{-3}M^{-1}]$

Environmental Parameters:

- Temperature, $\theta = [T]$

- Humidity, $RH = [1]$

Table 7-1 shows the 13 factors or parameters related to electrospinning in a dimensional matrix and their dimensions. The dimensions for those parameters can be expressed as a function of 5 SI base dimensions: length (L), mass (M), time (t), current (I) and temperature (T). There would be 8 dimensionless groups according to the degree of freedom to the dimensional table. The degree of freedom of a dimensional table is calculated as the difference between parameters considered and dimensions describing the phenomenon. For Table 7-1, the degree of freedom equals 13-5=8.

This is a large number of groups, which would be a slight improvement in terms of number of parameters in the analysis of electrospinning, however this table consists of many parameters that are redundant to one another or cannot be measured easily. Therefore, further simplification of the parameter selection is necessary.

Table 7-1 Dimensional table all electrospinning parameters

Dimensions	Electrospinning parameters												
	U	d_{TC}	d_N	θ	RH	κ	ν	γ	ε	ρ	$\dot{V}$	E	μ
L	2	1	1	0	0	-3	2	0	-3	-3	3	1	2
M	1	0	0	0	0	-1	0	1	-2	1	0	1	0
t	-3	0	0	0	0	3	-1	-2	4	0	-1	-3	-1
I	-1	0	0	0	0	2	0	0	2	0	0	-1	0
T	0	0	0	1	0	0	0	0	0	0	0	0	0

Measuring the permittivity is an involved process, which was not able to be conducted within the scope of this research. Permittivity is typically measured as a function of frequency and is called dielectric/ impedance spectroscopy [196].

Humidity and temperature have been dropped from the dimensional tables for the rest of the research for the following reasons; Humidity is a dimensionless parameter [M/M=1] and has therefore no impact on the outcome of the Pi-theorem. The temperature is an important parameter on the electrospinning process, impacting the evaporation rate [90]. However, it is represented in many other parameters, namely density, surface tension and viscosity of the used solvents, which makes the temperature a redundant parameter, and thus should be dropped for further discussion in the context of dimensional analysis.

The next simplification is the elimination of redundancies within the parameters. Table 7-2 consists of 7 parameters described with 4 dimensions leading to 3 degrees of freedom. The kinematic viscosity in this study is calculated through solution density and measured dynamic viscosity, which makes the usage of density and dynamic viscosity in this table redundant. Furthermore, the electric field can be dropped, since it is a function of distance and applied voltage. Applying the Pi-theorem on Table 7-2, leads to the kernel vectors in Table 7-3.

Table 7-2 Dimensional table for eliminated redundancies

	U	d_{TC}	d_N	κ	v	γ	$\dot{V}$
L	2	1	1	-3	2	0	3
M	1	0	0	-1	0	1	0
t	-3	0	0	3	-1	-2	-1
I	-1	0	0	2	0	0	0

To obtain the kernel vectors (or null space) of the dimensional table, it is necessary to treat the table as a matrix. In the first step, the dimensional matrix is converted into its reduced echelon form[3], resulting in matrix **M** equation (7-1). The detailed steps yielding **M** from Table 7-2 can be found in Appendix C – Development of Echelon Form.

$$M = \begin{bmatrix} 1 & 0 & 0 & 0 & 0 & 2 & 0 \\ 0 & 1 & 1 & 0 & 0 & 1 & 1 \\ 0 & 0 & 0 & 1 & 0 & 1 & 0 \\ 0 & 0 & 0 & 0 & 1 & -1 & 1 \end{bmatrix} \tag{7-1}$$

The matrix has 4 pivot columns[4] (columns 1, 2, 4 and 5) and 3 free columns (columns 3, 6 and 7). In the next step, the free columns are turned into a separate matrix and multiplied by -1 yielding matrix **F** equation (7-2).

$$F = \begin{bmatrix} 0 & -2 & 0 \\ -1 & -1 & -1 \\ 0 & -1 & 0 \\ 0 & 1 & -1 \end{bmatrix} \tag{7-2}$$

---

[3] Reduced echelon form of a matrix satisfies following conditions:
- The first non-zero element in each row, called the **leading entry**, is 1.
- Each leading entry is in a column to the right of the leading entry in the previous row.
- Rows with all zero elements, if any, are below rows having a non-zero element.
- The leading entry in each row is the only non-zero entry in its column.

[4] A pivot position in a matrix, A, is a position in the matrix that corresponds to a row–leading 1 in the reduced row echelon form of A.

In the next step, the identity matrix of F is added the rows of F, corresponding with the free columns in M, to yield a new matrix with identical number of rows to the number of columns in **M**, resulting in **S** (the added rows are bolded) (7-3).

$$
\mathbf{K} = \begin{bmatrix} 0 & -2 & 0 \\ -1 & -1 & -1 \\ \mathbf{1} & \mathbf{0} & \mathbf{0} \\ 0 & -1 & 0 \\ 0 & 1 & -1 \\ \mathbf{0} & \mathbf{1} & \mathbf{0} \\ \mathbf{0} & \mathbf{0} & \mathbf{1} \end{bmatrix}
\tag{7-3}
$$

Finally, the null space of the matrix **M** is defined by the scalar multiples of the three column vectors of **S** (see equation (7-3)). Every column represents a kernel vector used to create the dimensionless numbers.

Table 7-3 Kernel vectors after elimination of redundancies

$$
\begin{array}{r}
\text{Voltage (U)} \\
\text{Distance (}d_{TC}) \\
\text{Needle Diameter (}d_N) \\
\text{Elec. Cond (}\kappa) \\
\text{kin Vis (}\nu \\
\text{Sur Ten (}\gamma) \\
\text{Flow Rate (}\dot{V})
\end{array}
\begin{bmatrix} 0 \\ -1 \\ 1 \\ 0 \\ 0 \\ 0 \\ 0 \end{bmatrix}
\begin{bmatrix} -2 \\ -1 \\ 0 \\ -1 \\ 1 \\ 1 \\ 0 \end{bmatrix}
\begin{bmatrix} 0 \\ -1 \\ 0 \\ 0 \\ -1 \\ 0 \\ 1 \end{bmatrix}
$$

The Pi-groups are formed from the kernel vectors of the dimensional matrix are $\Pi_0 = \frac{d_N}{s}$, $\Pi_1 = \frac{\nu\gamma}{U^2 s \kappa}$, $\Pi_2 = \frac{V}{s \nu}$. For the kernel vectors, each vector represents the dimension of each parameter, i.e. in Table 7-3 the first kernel vector indicates the first dimensional group $\frac{d_N}{s}$. The number in each row describes the potency of the parameter in the corresponding row in M. The process is identical for every dimensional table. Table 7-4 shows a different approach to the dimensional matrix Table 7-2. Instead of using both distance and voltage in the table, both were summarized

using the electric field strength. This reduces the degree of freedom to 2, which marks a further simplification. The resulting dimensionless groups are $\Pi_0 = \frac{\nu\gamma}{E^2 dN^3 \kappa}$, $\Pi_1 = \frac{V}{dN\,\nu}$ (Table 7-5).

Table 7-4 Dimensional table for alternate eliminated redundancies

	E	dN	κ	ν	γ	$\dot{V}$
L	1	1	-3	2	0	3
M	1	0	-1	0	1	0
t	-3	0	3	-1	-2	-1
I	-1	0	2	0	0	0

Table 7-5 Kernel vectors after elimination of redundancies (alternate)

$$
\begin{array}{l}
\text{Electric Field (E)} \\
\text{Needle Diameter (d}_N) \\
\text{Elec Conductivity (}\kappa \\
\text{Kinematic Viscosity (}\nu) \\
\text{Surface Tension (}\gamma) \\
\text{Flow Rate (}\dot{V})
\end{array}
\quad
\begin{bmatrix} -2 \\ -3 \\ -1 \\ 1 \\ 1 \\ 0 \end{bmatrix}
\begin{bmatrix} 0 \\ -1 \\ 0 \\ -1 \\ 0 \\ 1 \end{bmatrix}
$$

Table 7-6 and Table 7-8 mark another step in simplifying the Pi-theorem table. The parametric study (Chapter 6) showed that both the flow rate and the needle diameter have a comparable effect and are interacting with each other. It can be concluded that the needle diameter and the flow rate are not independent in terms of electrospinning. Therefore, in Table 7-6 and Table 7-8 the Pi-tables drop either d_N (Table 7-6) or drop V (Table 7-8). This further reduction leads to a degree of freedom of 1 in the tables. This represents the furthest possible degree of simplification. The results of the Pi-theorem on these tables are a very different. For the focus on flow rate (Table 7-6), the group is $\Pi_0 = \frac{E^{\frac{2}{3}} \kappa^{\frac{1}{3}} V}{\nu^{\frac{4}{3}} \gamma^{\frac{1}{3}}}$; while for focusing on needle diameter (Table 7-8) the group is $\pi_0 = \frac{\nu\gamma}{E^2 dN^3 \kappa}$, identical to the result of Table 7-4. It can be seen that both versions for the Pi-theorem tables yield different results. The results for the focus on needle

diameter resemble the results from the previous longer tables (Table 7-4). In contrast, the focus on flow rate yields a very different style of dimensionless group. The denominator for the group created Table 7-6 (focus on flow rate) consists of viscosity and surface tension. These two values are typically considered to increase the fiber size, when they increase as discussed in the literature [103]. The numerator consists of electric field and conductivity, which are linked to finer fibers in the literature when increased [99,27,100,103]. A high flow rate is typically linked to thicker fibers and wider fiber distributions in the literature [194,28].

Table 7-6 Dimensional table including parameter study (focus V)

	E	κ	$\mathbf{\nu}$	$\mathbf{\gamma}$	$\dot{\mathrm{V}}$
L	1	-3	2	0	3
M	1	-1	0	1	0
t	-3	3	-1	-2	-1
I	-1	2	0	0	0

Table 7-7 Kernel vector incl. parameter study (focus V) results

$$
\begin{matrix}
\text{Electric Field (E)} \\
\text{Electric Conductivity } (\kappa) \\
\text{Kinematic Viscosity } (\nu) \\
\text{Surface Tension } (\gamma) \\
\text{Flow Rate } (\dot{\mathrm{V}})
\end{matrix}
\quad
\begin{bmatrix}
\frac{2}{3} \\
\frac{1}{3} \\
-\frac{4}{3} \\
-\frac{1}{3} \\
1
\end{bmatrix}
$$

Table 7-8 Table including parameter study (focus d_N)

	E	d_N	κ	ν	γ
L	1	1	-3	2	0
M	1	0	-1	0	1
t	-3	0	3	-1	-2
I	-1	0	2	0	0

Table 7-9 Kernel vector incl. parameter study (focus d_N) results

$$
\begin{array}{l}
\text{Electric Field (E)} \\
\text{Needle Diameter } (d_N) \\
\text{Electric Conductivity } (\kappa) \\
\text{kinematic Viscosity } (\nu) \\
\text{Surface Tension } (\gamma)
\end{array}
\quad
\begin{bmatrix}
-2 \\
-3 \\
-1 \\
1 \\
1
\end{bmatrix}
$$

The arrangements from both tables are promising in the sense of forming a dimensional number describing the electrospinning process. The resulting groups are consisting of factors linked to larger fibers when increased, like viscosity, or parameters linked to finer fibers when increased, like electric field strength, in either the denominator or numerator.

7.4. Characteristic Numbers Describing the Electrospinnability

In section 7.3. , the Pi-tables have been developed. This was based on the assumption that the aspect of electrospinnability is not a measurable value, but something observable. The resulting dimensionless numbers could also be applied to describe a range, within which electrospinning is possible, if there is an onset/cut-off for electrospinning, or a general trend of the fiber size. The range, within which electrospinning for the ceria and alumina solutions is possible, has been determined in this research manually (see Table 7-10). Furthermore, ceria runs with the

parameter combination "bcd" and "abcd" were problematic during the production regarding entanglement and dripping. If a dimensionless number yields a maximum or minimum for these values, it could be interpreted as a limiting dimensionless number.

Table 7-10 Determined boundary conditions for used solutions

Parameter	Min	Max
Concentration	10% (mass)	16% (mass)
Voltage	10 kV	16 kV
Flow Rate	0.3 mL/hr	0.5 mL/hr
Needle Gauge	20 (0.603 mm)	18 (0.838 mm)

As results from the Pi-table, removing the redundancies and focusing on the flow rate yielded the dimensionless group of $\frac{E^{\frac{2}{3}}\kappa^{\frac{1}{3}}V}{\nu^{\frac{4}{3}}\gamma^{\frac{1}{3}}}$. For the alternate case with the focus on needle diameter, the resulting dimensionless group is $\frac{\nu\gamma}{E^2 d_N{}^3\kappa}$. The dimensional group $\frac{V}{d_N\,\nu}$ derived from Table 7-4 does not yield significant results in the context of electrospinnability or fiber size.

Table 7-11 displays the calculated values for the three mentioned dimensionless numbers. Each material has two maxima and two minima for each characteristic number. $\frac{\nu\gamma}{E^2 d_N{}^3\kappa}$ has its maxima overlapping with values that is matching fine fibers for each material (Al and Ce "a" and "ac"), but not the finest fibers. The minima of this dimensionless group also describes relatively fine fibers ("bd and "bcd"). Together with the finding for its maxima, it can be stated that $\frac{\nu\gamma}{E^2 d_N{}^3\kappa}$ does not correlate with the produced fiber size. This might be due to an overestimation of the parameter needle diameter. The needle diameter has been found to impact the electrospinning, yielding thicker fibers for larger needles [17], however, $\frac{\nu\gamma}{E^2 d_N{}^3\kappa}$ is having a large focus on d_N, since d_N is cubed in this dimensional group. This certainly resulted in an overrepresentation of the factor d_N in $\frac{\nu\gamma}{E^2 d_N{}^3\kappa}$.

However, $\frac{\nu\gamma}{E^2 d_N{}^3\kappa}$ does yield a minimum for samples that have been problematic in the production (Ce "bcd") with 0.0015. The other problematic production configuration Ce "abcd" yield a small number of 0.0038 which is still small compared to the maximum value of 0.0241 for the ceria samples. It is possible that this dimensional number can describe the cut-off for electrospinning, however more data is needed to validate this statement.

$\frac{E^{\frac{2}{3}}\kappa^{\frac{1}{3}}V}{\nu^{\frac{4}{3}}\gamma^{\frac{1}{3}}}$ shows maxima for the "c" and "bc" runs and minima for "ad" and "abd". For both samples the run "bc" yielded fine fibers, however the run "c" resulted in medium sized fibers, indicating that the maxima of $\frac{E^{\frac{2}{3}}\kappa^{\frac{1}{3}}V}{\nu^{\frac{4}{3}}\gamma^{\frac{1}{3}}}$ does not describe the finest fibers. The minima of $\frac{E^{\frac{2}{3}}\kappa^{\frac{1}{3}}V}{\nu^{\frac{4}{3}}\gamma^{\frac{1}{3}}}$ are also falling within an intermediate size range, which has been unproblematic in the electrospinning process. What would have been expected from $\frac{E^{\frac{2}{3}}\kappa^{\frac{1}{3}}V}{\nu^{\frac{4}{3}}\gamma^{\frac{1}{3}}}$ is fine fibers for large numbers, since the denominator consists only out of viscosity and surface tension. These two parameters have been found to increase the fiber diameter drastically, when they are increased, while having a minimum value required for electrospinning [97,89]. The fact that this group did not yield a significant result regarding fine and large fibers indicates that potencies of the parameters are not suited for this problem, or that correction factors are needed.

Table 7-11 Characteristic numbers for alumina and ceria

Run label	Mean Fiber size [nm]	$\dfrac{\nu\gamma}{E^2 d_N{}^3 \kappa}$	$\dfrac{E^{\frac{2}{3}}\kappa^{\frac{1}{3}}V}{\nu^{\frac{4}{3}}\gamma^{\frac{1}{3}}}$
Al (1)	386	0.0053	0.0470
Al a	276	**0.0135**	0.0344
Al b	**227**	0.0020	0.0470
Al ab	284	0.0050	0.0344
Al c	375	0.0053	**0.0825**
Al ac	328	**0.0135**	0.0603
Al bc	257	0.0020	**0.0825**
Al abc	291	0.0050	0.0603
Al d	530	0.0013	0.0076
Al ad	407	0.0034	0.0055
Al bd	287	**0.0005**	0.0076
Al abd	512	0.0013	**0.0055**
Al cd	386	0.0013	0.0134
Al acd	**705**	0.0034	0.0098
Al bcd	328	**0.0005**	0.0134
Al abcd	584	0.0013	0.0098
Ce (1)	419	0.0094	0.0228
Ce a	346	**0.0241**	0.0167
Ce b	385	0.0035	0.0228
Ce ab	489	0.0090	0.0167
Ce c	454	0.0094	**0.0386**
Ce ac	442	**0.0241**	0.0282
Ce bc	**275**	0.0035	**0.0386**
Ce abc	454	0.0090	0.0282
Ce d	386	0.0039	0.0068
Ce ad	490	0.0101	**0.0050**
Ce bd	762	**0.0015**	0.0068
Ce abd	900	0.0038	0.0050
Ce cd	590	0.0039	0.0117
Ce acd	786	0.0101	0.0085
Ce bcd	**1480**	**0.0015**	0.0117
Ce abcd	**2197**	0.0038	0.0085

7.5. Conclusion

The Pi-theorem has been used to create a dimensionless number describing the electrospinnability of a solution in the given setup. From the dimensional analysis, two dimensionless groups could be formed, namely $\dfrac{E^{\frac{2}{3}}\kappa^{\frac{1}{3}}V}{\nu^{\frac{4}{3}}\gamma^{\frac{1}{3}}}$ and $\dfrac{\nu\gamma}{E^2 d_N{}^3 \kappa}$. Analysing these groups with experimental electrospinning and solution data shows that neither of the groups correlates with recorded fiber sizes. However, $\dfrac{\nu\gamma}{E^2 d_N{}^3 \kappa}$ showed minima for parameter combinations, which have been problematic in the electrospinning process, potentially showing a cut-off value for electrospinning.

To develop a more accurate understanding of the dimensionless numbers in context with electrospinning, more experimental data is required, which is both time intensive and expensive. Having all or different electrospinning parameters available to apply them to the Pi-theorem may lead to different characteristic numbers describing the electrospinning process. Furthermore, considering the effect of collector shape and size described in Chapter 5, a further discussion of the electric field and the impact it has on the electrospinning process is needed. This may lead to a further adjustment of the electric field strength in the calculation of the dimensionless numbers. Different parameters could also be selected for the Pi-tables, which could impact the results further.

Chapter 8 Conclusions and Recommendations

8.1. Conclusions

The primary goal of this work was the production of metal-based nanofibers and a better understanding of the electrospinning process and the effect of the parameters involved. To evaluate the electrospinning process, pure polymeric filter samples from CA have been produced, analyzing the impact of parameters by changing a single parameter at a time. To further analyze the impact on multiple parameters, a parametric study based on the nanofiber production of the metals ceria and alumina has been conducted. Finally, the collected data has been utilized to apply the Pi-theorem in order to develop characteristic numbers describing the electrospinning process.

8.1.1. Fabrication of Nanofibers and Filtration Characteristics

It was found that a successful electrospinning of CA nanofibers requires a concentration of over 15 wt% CA in the electrospinning solution, otherwise beading was observed. An increase of each of the following three factors, tip-to-collector distance, voltage and concentration of dissolved polymer, lead to an increase of fiber size. The produced fibers had diameters between 175 to 880 nm. The maximum filtration efficiency obtained was 99.8% for a CA concentration of 15 wt%, deposition time of 30 minutes, voltage of 15 kV and a tip-to-collector distance of 12 cm. The corresponding filtration quality has been found to be 0.05 Pa^{-1}, which is superior to conventional polymeric filter (typically ~0.01 Pa^{-1}).

The fabrication of ceria and alumina fibers was based on PVP as a carrier polymer and nitrates of the metals acting as a metal source. As a functional solvent-mixture, a 2:1 mixture of ethanol and water has been determined. The thermal treatment has been conducted in 2 steps, drying the fibers at 120 °C for two hours and calcining the samples at 550 °C for 5 hours. The drying step has become necessary to mitigate the ripping effect to the filters caused by adhering fibers to the collector before the calcination. The calcination process led to considerable shrinkage in the filter size, about 25-fold reduction in filter mat surface area. The produced calcined fibers

ranged from 200 to 400 nm for alumina fibers, and from 230 to 480 nm for ceria fibers. One alumina filter was tested, and the average filtration efficiency obtained was 45.7%. The corresponding filtration quality has been found to be 0.013 Pa^{-1}, which is in line with the value for conventional polymeric filters.

8.1.2. Parametric Study for metal-based Nanofiber Production

The quantitative impact of key parameters on the alumina and ceria fiber size has been studied with a factorial design plan. The investigated parameters were voltage, flow rate, needle diameter, and solution concentration. The solution concentration has been found to be the dominant factor of the electrospinning process. An increase of solution concentration led to an increase of viscosity and surface tension, which significantly increased the resulting fiber size. The parameters voltage, flow rate and needle diameter were comparable in impact on the fiber size if the interactions with the other parameters were also considered. The voltage has been found to be the least impactful as single parameter; however, considering the interactions with other parameters, it is comparable to flow rate and needle diameter. Furthermore, it was found that the parameters flow rate and needle diameter interact with each other and that the solution concentration impacts the effect of the flow rate as well. To the author's knowledge, this was the first parametric study on electrospun metal-based nanofiber, and the results (qualitative trends) match findings in the literature for electrospun polymeric nanofibers.

8.1.3. Characteristic Number for metal-based Nanofiber Production

The Pi-theorem has been used to generate dimensionless numbers describing the electrospinnability of a solution in the given setup. The generated dimensionless numbers consist of combinations of two types of parameters: 1) processing parameters, i.e., electric field strength and needle diameter, and 2) solution parameters, i.e., electric conductivity, kinematic viscosity and surface tension. Analysis of these groups, in combination with experimental electrospinning data, shows that no single group correlates well with recorded fiber sizes. However, the group $\frac{\nu\gamma}{E^2 d_N^3 \kappa}$ showed minima for parameter combinations, which have been problematic in the electrospinning process, potentially showing a cut-off value for electrospinning.

8.2. Recommendations for future Research

This section discusses potential areas of research that would extend the work started in this thesis. The focus of the recommendations is the production of metal-based fibers and how to improve the parametric study, as well as the dimensionless groups.

The first limitation of this work is the calculation of the electric field strength. Chapter 5 shows a clear difference between the fiber sizes of fibers produced on the plate collector and fibers produced on the drum collector. The difference may be a result from the collector size, which was either a 10 x 10 cm plate or 30 x 10 cm cylindrical drum collector. The shape and the rotation speed likely also impacted the fiber size and the associated distribution of the produced fibers. A study on the effect of collector shape and size on the deposited area as well as the fabricated fiber size could be conducted with a variety of collector sizes and shapes. More information on the impact of the deployed electric field depending of the collector on the fiber size could also improve the dimensionless groups. A potential correction factor for the collector could be introduced. This correction factor could be calculated as a function of size and shape of the used collector and needle arrangement and put in relation to a homogeneous field formed between two plates.

One sample of the produced metal-based fibers has been tested for filtration efficiency. The resulting filtration efficiency has been found to be comparable to other nanofibrous materials. However, only one sample has been tested, due to the great effort necessary to produce a sample large enough to be tested for its filtration characteristics. More optimal settings of the electrospinning process, which lead to a more filtration favourable fiber size distribution could be determined. An electrospinning setup with a larger output, like a multi-needle setup would increase the productivity and therefore the viability of an intensive study of the filtration characteristics of metal-based fibers.

The results of the factorial design plan yielded a dominance in effect of the solution parameter concentration on the fiber size. However, the concentration of dissolved material in the solution impacts a multitude of parameters, foremost the electric conductivity, viscosity, surface tension

and density. A follow-up experimental design plan focusing on these solution parameters would be advisable to quantify the impact of the solution parameters on the fiber size.

A limitation of this work was that the permittivity could not be measured and thus was not taken into account in the dimensional matrixes. The permittivity values show the interaction of an external field with the electric dipole moment of the sample. The integration of permittivity could lead to different selections for the dimensional matrixes as well. The permittivity can be measured following one of the following methods [196]:

- Transmission/reflection line method

- Open ended coaxial probe method

- Free space method

- Resonant method

It could be considered to develop the dimensional matrix in a different way, by allowing for other combinations of parameters. The dimensional matrix could be developed with dynamic viscosity and density of the solution, while neglecting the surface tension and kinematic viscosity for the dimensional matrix. It could also be argued for dimensional groups, which focus more on the processing parameters. The dimensional numbers derived in Chapter 7 only contain 2 processing parameters compared to 3 solution parameters, which are directly dependent on the concentration of polymer and metal in the solution. The nature of selection of parameters for the Pi-theorem is to a point arbitrary and requires careful selection. The usage of dimensionless numbers could also be expanded on the fiber size distributions, describing the uniformity of the produced fibers.

In addition to potentially different dimensionless groups, more data on the different electrospinning processes is needed. To gain a deeper understanding of the electrospinning process, an in-depth documentation of the used settings and solution parameters is needed. This includes documenting the collector size and shape, as well as documenting solution properties like viscosity, and surface tension and electric conductivity. In connection with more data on linked fiber size distributions, it would be possible to further refine the characteristic numbers

128

and correction factors describing the electrospinning process. A variety of polymers and solutions can be tested to determine the dimensional numbers of these solutions, or if there is a common number connecting different solutions in the sense of the electrospinning process. This knowledge could support the electrospinning of new combinations on new setups, minimizing the trial and error process, which is widely used in the current state of the art setups.

Letter of Copyright Permission

RE: Inquiry to use content of paper for PhD thesis

PermissionsUK <PermissionsUK@sagepub.com>

Tue 2/5/2019 12:50 PM

To:Joerg Ahne <jahne@uwaterloo.ca>;

Dear Joerg Ahne,

Thank you for your email. I am pleased to report we can grant your request without a fee as part of your thesis.

Please accept this email as permission for your request as detailed below. Permission is granted for the life of the edition on a non-exclusive basis, in the English language, throughout the world in all formats provided full citation is made to the original SAGE publication.

The permission is subject to approval from any co-authors on the original project. Please note approval excludes any graphs, photos, excerpts, etc. which required permission from a separate copyright holder at the time of publication. If your material includes anything which was not your original work, please contact the rights holder for permission to reuse those items.

If you have any questions, or if we may be of further assistance, please let us know.

Best Wishes,

Craig Myles
on behalf of SAGE Ltd. Permissions Team

SAGE Publications Ltd
1 Oliver's Yard, 55 City Road
London, EC1Y 1SP
UK
www.sagepub.co.uk
SAGE Publications Ltd, Registered in England No.1017514
Los Angeles | London | New Delhi
Singapore | Washington DC
The natural home for authors, editors & societies

Thank you for considering the environment before printing this email.

From: Joerg Ahne <jahne@uwaterloo.ca>
Sent: Monday, February 4, 2019 12:13 PM
To: permissions (US) <permissions@sagepub.com>
Subject: Inquiry to use content of paper for PhD thesis

To whom it may concern,

My name is Joerg Ahne and last year, we have published the paper "Ahne, J., Li, Q., Croiset, E., & Tan, Z. (2018). Electrospun cellulose acetate nanofibers for airborne nanoparticle filtration. *Textile Research Journal*. https://doi.org/10.1177/0040517518807440 " with you.

References

1. Kreyling WG, Semmler-Behnke M, Möller W (2006) Health implications of nanoparticles. Journal of Nanoparticle Research 8 (5):543-562

2. Oberdörster G, Stone V, Donaldson K (2007) Toxicology of nanoparticles: a historical perspective. Nanotoxicology 1 (1):2-25

3. Oberdörster G, Celein RM, Ferin J, Weiss B (1995) Association of particulate air pollution and acute mortality: involvement of ultrafine particles? Inhalation toxicology 7 (1):111-124

4. Roduner E (2006) Size matters: why nanomaterials are different. Chemical Society Reviews 35 (7):583-592

5. Castellano P, Ferrante R, Curini R, Canepari S An overview of the characterization of occupational exposure to nanoaerosols in workplaces. In: Journal of Physics: Conference Series, 2009. vol 1. IOP Publishing, p 012009

6. Marra J, Voetz M, Kiesling H-J (2010) Monitor for detecting and assessing exposure to airborne nanoparticles. Journal of Nanoparticle Research 12 (1):21-37

7. Tsai CS-J, White D, Rodriguez H, Munoz CE, Huang C-Y, Tsai C-J, Barry C, Ellenbecker MJ (2012) Exposure assessment and engineering control strategies for airborne nanoparticles: an application to emissions from nanocomposite compounding processes. Journal of Nanoparticle Research 14 (7):989

8. Morawska L, He C, Johnson G, Guo H, Uhde E, Ayoko G (2009) Ultrafine particles in indoor air of a school: possible role of secondary organic aerosols. Environmental science & technology 43 (24):9103-9109

9. Elsaesser A, Howard CV (2012) Toxicology of nanoparticles. Advanced drug delivery reviews 64 (2):129-137

10. Lin LY, Lin CY, Lin YC, Chuang KJ (2009) The effects of indoor particles on blood pressure and heart rate among young adults in Taipei, Taiwan. Indoor air 19 (6):482-488

11. Mengersen K, Morawska L, Wang H, Murphy N, Tayphasavanh F, Darasavong K, Holmes N (2011) Association between indoor air pollution measurements and respiratory health in women and children in Lao PDR. Indoor air 21 (1):25-35

12. Tan Z (2014) Air pollution and greenhouse gases: from basic concepts to engineering applications for air emission control. Springer,

13. Schnelle Jr KB, Brown CA (2016) Air pollution control technology handbook. CRC press,

14. Davies C (1945) Definitive equations for the fluid resistance of spheres. Proceedings of the Physical Society 57 (4):259

15. Subbiah T, Bhat G, Tock R, Parameswaran S, Ramkumar S (2005) Electrospinning of nanofibers. Journal of Applied Polymer Science 96 (2):557-569

16. Burger C, Hsiao BS, Chu B (2006) Nanofibrous materials and their applications. Annu Rev Mater Res 36:333-368

17. Heikkilä P, Harlin A (2008) Parameter study of electrospinning of polyamide-6. European Polymer Journal 44 (10):3067-3079

18. Nayak R, Padhye R, Kyratzis IL, Truong YB, Arnold L (2013) Effect of viscosity and electrical conductivity on the morphology and fiber diameter in melt electrospinning of polypropylene. Textile Research Journal 83 (6):606-617

19. Hekmati AH, Rashidi A, Ghazisaeidi R, Drean J-Y (2013) Effect of needle length, electrospinning distance, and solution concentration on morphological properties of polyamide-6 electrospun nanowebs. Textile Research Journal 83 (14):1452-1466

20. Angammana CJ (2011) A Study of the Effects of Solution and Process Parameters on the Electrospinning Process and Nanofibre Morphology.

21. Biber E, Gündüz G, Mavis B, Colak U (2010) Effects of electrospinning process parameters on nanofibers obtained from Nylon 6 and poly (ethylene-n-butyl acrylate-maleic anhydride) elastomer blends using Johnson S B statistical distribution function. Applied Physics A 99 (2):477-487

22. Bhardwaj N, Kundu SC (2010) Electrospinning: a fascinating fiber fabrication technique. Biotechnology advances 28 (3):325-347

23. Yang Y, Liu J, Jia Z, Wang L, Guan Z Effect of solution rate on electrospinning. In: Electrical Insulation and Dielectric Phenomena, 2007. CEIDP 2007. Annual Report-Conference on, 2007. IEEE, pp 615-618

24. Stanger J, Tucker N, Kirwan K, Staiger MP (2009) Effect of charge density on the Taylor cone in electrospinning. International Journal of Modern Physics B 23 (06n07):1956-1961

25. Son WK, Youk JH, Lee TS, Park WH (2005) Effect of pH on electrospinning of poly (vinyl alcohol). Materials letters 59 (12):1571-1575

26. Givehchi R, Li Q, Tan Z (2016) Quality factors of PVA nanofibrous filters for airborne particles in the size range of 10–125nm. Fuel 181:1273-1280

27. Lee JS, Choi KH, Ghim HD, Kim SS, Chun DH, Kim HY, Lyoo WS (2004) Role of molecular weight of atactic poly (vinyl alcohol)(PVA) in the structure and properties of PVA nanofabric prepared by electrospinning. Journal of Applied Polymer Science 93 (4):1638-1646

28. Cui W, Li X, Zhou S, Weng J (2007) Investigation on process parameters of electrospinning system through orthogonal experimental design. Journal of applied polymer science 103 (5):3105-3112

29. Costolo M, Lennhoff J, Pawle R, Rietman E, Stevens A (2007) A nonlinear system model for electrospinning sub-100 nm polyacrylonitrile fibres. Nanotechnology 19 (3):035707

30. Tong HW, Wang M (2011) An investigation into the influence of electrospinning parameters on the diameter and alignment of poly (hydroxybutyrate-co-hydroxyvalerate) fibers. Journal of Applied Polymer Science 120 (3):1694-1706

31. Buzea C, Pacheco II, Robbie K (2007) Nanomaterials and nanoparticles: sources and toxicity. Biointerphases 2 (4):MR17-MR71

32. Justino CI, Rocha-Santos TA, Duarte AC (2011) Sampling and characterization of nanoaerosols in different environments. TrAC Trends in Analytical Chemistry 30 (3):554-567

33. Hoet PH, Brüske-Hohlfeld I, Salata OV (2004) Nanoparticles – known and unknown health risks. Journal of Nanobiotechnology 2 (1):12. doi:10.1186/1477-3155-2-12

34. Oberdörster G, Oberdörster E, Oberdörster J (2005) Nanotoxicology: an emerging discipline evolving from studies of ultrafine particles. Environmental health perspectives 113 (7):823

35. Nel A, Xia T, Mädler L, Li N (2006) Toxic potential of materials at the nanolevel. science 311 (5761):622-627

36. Yang W, Peters JI, Williams III RO (2008) Inhaled nanoparticles—a current review. International Journal of Pharmaceutics 356 (1-2):239-247

37. Lee K, Kelly D, Schneider P, Trochimowicz H (1986) Inhalation toxicity study on rats exposed to titanium tetrachloride atmospheric hydrolysis products for two years. Toxicology and applied pharmacology 83 (1):30-45

38. Dowling AP (2004) Development of nanotechnologies. Materials Today 7 (12):30-35

39. Driscoll KE, Deyo LC, Carter JM, Howard BW, Hassenbein DG, Bertram TA (1997) Effects of particle exposure and particle-elicited inflammatory cells on mutation in rat alveolar epithelial cells. Carcinogenesis 18 (2):423-430

40. Oberdorster G (1999) Lung dosimetry-Considerations for noninhalation studies. Experimental lung research 25 (1):1-6

41. Brown DM, Wilson MR, MacNee W, Stone V, Donaldson K (2001) Size-dependent proinflammatory effects of ultrafine polystyrene particles: a role for surface area and oxidative stress in the enhanced activity of ultrafines. Toxicology and applied pharmacology 175 (3):191-199

42. Maynard AD, Kuempel ED (2005) Airborne nanostructured particles and occupational health. Journal of nanoparticle research 7 (6):587-614

43. Borm PJ, Kreyling W (2004) Toxicological hazards of inhaled nanoparticles—potential implications for drug delivery. Journal of nanoscience and nanotechnology 4 (5):521-531

44. Powell MC, Kanarek MS (2006) Nanomaterial health effects-part 1: background and current knowledge. WMJ-MADISON- 105 (2):16

45. Weibel ER, Cournand AF, Richards DW (1963) Morphometry of the human lung, vol 1. Springer,

46. Stone KC, Mercer RR, Gehr P, Stockstill B, Crapo JD (1992) Allometric relationships of cell numbers and size in the mammalian lung. Am J Respir Cell Mol Biol 6 (2):235-243

47. Gehr P, Bachofen M, Weibel ER (1978) The normal human lung: ultrastructure and morphometric estimation of diffusion capacity. Respiration physiology 32 (2):121-140

48. Groneberg D, Witt C, Wagner U, Chung K, Fischer A (2003) Fundamentals of pulmonary drug delivery. Respiratory medicine 97 (4):382-387

49. Courrier H, Butz N, Vandamme TF (2002) Pulmonary drug delivery systems: recent developments and prospects. Critical Reviews™ in Therapeutic Drug Carrier Systems 19 (4-5)

50. Gehr P, Green F, Geiser M, Hof VI, Lee M, Schürch S (1996) Airway surfactant, a primary defense barrier: mechanical and immunological aspects. Journal of aerosol medicine 9 (2):163-181

51. Byron PR (1986) Prediction of drug residence times in regions of the human respiratory tract following aerosol inhalation. Journal of pharmaceutical sciences 75 (5):433-438

52. Oberdörster G (2002) Toxicokinetics and effects of fibrous and nonfibrous particles. Inhalation toxicology 14 (1):29-56

53. Oberdörster G, Sharp Z, Atudorei V, Elder A, Gelein R, Lunts A, Kreyling W, Cox C (2002) Extrapulmonary translocation of ultrafine carbon particles following whole-body inhalation exposure of rats. Journal of Toxicology and Environmental Health Part A 65 (20):1531-1543

54. Tsapis N, Bennett D, Jackson B, Weitz DA, Edwards D (2002) Trojan particles: large porous carriers of nanoparticles for drug delivery. Proceedings of the National Academy of Sciences 99 (19):12001-12005

55. Gill S, Löbenberg R, Ku T, Azarmi S, Roa W, Prenner EJ (2007) Nanoparticles: characteristics, mechanisms of action, and toxicity in pulmonary drug delivery—a review. Journal of Biomedical Nanotechnology 3 (2):107-119

56. Heyder J, Gebhart J, Rudolf G, Schiller CF, Stahlhofen W (1986) Deposition of particles in the human respiratory tract in the size range 0.005–15 μm. Journal of aerosol science 17 (5):811-825

57. Heyder J, Rudolf G (1984) Mathematical models of particle deposition in the human respiratory tract. Journal of aerosol science 15 (6):697-707

58. Patton JS (2005) Unlocking the opportunity of tight glycaemic control: Innovative delivery of insulin via the lung. Diabetes, Obesity and Metabolism 7:S5-S8

59. Jaques PA, Kim CS (2000) Measurement of total lung deposition of inhaled ultrafine particles in healthy men and women. Inhalation toxicology 12 (8):715-731

60. Chalupa DC, Morrow PE, Oberdörster G, Utell MJ, Frampton MW (2004) Ultrafine particle deposition in subjects with asthma. Environmental Health Perspectives 112 (8):879

61. Bahk YK, Wang J (2014) Filtration and length determination of airborne carbon nanotubes in the submicrometer range using nanofiber filters. Aerosol and Air Quality Research 14 (5):1352-1359

62. Barhate RS, Ramakrishna S (2007) Nanofibrous filtering media: filtration problems and solutions from tiny materials. Journal of membrane science 296 (1):1-8

63. Podgórski A, Bałazy A, Gradoń L (2006) Application of nanofibers to improve the filtration efficiency of the most penetrating aerosol particles in fibrous filters. Chemical Engineering Science 61 (20):6804-6815

64. Graham K, Ouyang M, Raether T, Grafe T, McDonald B, Knauf P Polymeric nanofibers in air filtration applications. In: Fifteenth Annual Technical Conference & Expo of the American Filtration & Separations Society, Galveston, Texas, 2002. pp 9-12

65. Alivisatos P, Barbara PF, Castleman AW, Chang J, Dixon DA, Klein ML, McLendon GL, Miller JS, Ratner MA, Rossky PJ (1998) From molecules to materials: Current trends and future directions. Advanced Materials 10 (16):1297-1336

66. Grafe TH, Graham KM Nanofiber webs from electrospinning. In: Nonwovens in Filtration-Fifth International Conference, Stuttgart, Germany, 2003. pp 1-5

67. Stechkina I, Kirsch A, Fuchs N (1969) Studies on fibrous aerosol filters—iv calculation of aerosol deposition in model filters in the range of maximum penetration. Annals of Occupational Hygiene 12 (1):1-8

68. Hung C-H, Leung WW-F (2011) Filtration of nano-aerosol using nanofiber filter under low Peclet number and transitional flow regime. Separation and purification technology 79 (1):34-42

69. Yoon K, Hsiao BS, Chu B (2008) Functional nanofibers for environmental applications. Journal of Materials Chemistry 18 (44):5326-5334

70. Givehchi R (2016) Filtration of NaCl and WOx Nanoparticles using Wire Screens and Nanofibrous Filters.

71. Matulevicius J, Kliucininkas L, Prasauskas T, Buivydiene D, Martuzevicius D (2016) The comparative study of aerosol filtration by electrospun polyamide, polyvinyl acetate, polyacrylonitrile and cellulose acetate nanofiber media. Journal of Aerosol Science 92:27-37

72. Formhals A (1934) Process and apparatus for preparing artificial threads. US Patent No 1,975,504

73. Kayser JC, Shambaugh RL (1990) The manufacture of continuous polymeric filaments by the melt-blowing process. Polymer Engineering & Science 30 (19):1237-1251

74. Zhao R, Wadsworth LC (2003) Attenuating PP/PET bicomponent melt blown microfibers. Polymer Engineering & Science 43 (2):463-469

75. Medeiros ES, Glenn GM, Klamczynski AP, Orts WJ, Mattoso LH (2009) Solution blow spinning: A new method to produce micro-and nanofibers from polymer solutions. Journal of applied polymer science 113 (4):2322-2330

76. Pu Y, Zheng J, Chen F, Long Y, Wu H, Li Q, Yu S, Wang X, Ning X (2018) Preparation of Polypropylene Micro and Nanofibers by Electrostatic-Assisted Melt Blown and Their Application. Polymers 10 (9):959

77. Padron S, Fuentes A, Caruntu D, Lozano K (2013) Experimental study of nanofiber production through forcespinning. Journal of applied physics 113 (2):024318

78. Zeleny J (1914) The electrical discharge from liquid points, and a hydrostatic method of measuring the electric intensity at their surfaces. Physical Review 3 (2):69

79. Taylor G (1964) Disintegration of water drops in an electric field. Proceedings of the Royal Society of London Series A Mathematical and Physical Sciences 280 (1382):383-397

80. Hinds WC (2012) Aerosol technology: properties, behavior, and measurement of airborne particles. John Wiley & Sons,

81. Doshi J, Reneker DH (1995) Electrospinning process and applications of electrospun fibers. Journal of electrostatics 35 (2-3):151-160

82. Li D, Xia Y (2004) Electrospinning of nanofibers: reinventing the wheel? Advanced materials 16 (14):1151-1170

83. Chronakis IS (2005) Novel nanocomposites and nanoceramics based on polymer nanofibers using electrospinning process—a review. Journal of Materials Processing Technology 167 (2-3):283-293

84. Miller-Chou BA, Koenig JL (2003) A review of polymer dissolution. Progress in Polymer Science 28 (8):1223-1270

85. Tanaka F (2011) Polymer Physics: Applications to Molecular Association and Thermoreversible Gelation. Cambridge University Press,

86. Reznik S, Yarin A, Theron A, Zussman E (2004) Transient and steady shapes of droplets attached to a surface in a strong electric field. Journal of Fluid Mechanics 516:349-377

87. Cloupeau M, Prunet-Foch B (1989) Electrostatic spraying of liquids in cone-jet mode. Journal of Electrostatics 22 (2):135-159

88. Yarin AL, Koombhongse S, Reneker DH (2001) Bending instability in electrospinning of nanofibers. Journal of applied physics 89 (5):3018-3026

89. Reneker DH, Yarin AL, Fong H, Koombhongse S (2000) Bending instability of electrically charged liquid jets of polymer solutions in electrospinning. Journal of Applied physics 87 (9):4531-4547

90. Medeiros ES, Mattoso LH, Offeman RD, Wood DF, Orts WJ (2008) Effect of relative humidity on the morphology of electrospun polymer fibers. Canadian Journal of Chemistry 86 (6):590-599

91. George G, Anandhan S (2014) Glass fiber–supported NiO nanofiber webs for reduction of CO and hydrocarbon emissions from diesel engine exhaust. Journal of Materials Research 29 (20):2451-2465

92. Shao C, Guan H, Liu Y, Gong J, Yu N, Yang X (2004) A novel method for making ZrO2 nanofibres via an electrospinning technique. Journal of Crystal Growth 267 (1-2):380-384

93. Li C, Chen R, Zhang X, Shu S, Xiong J, Zheng Y, Dong W (2011) Electrospinning of CeO2–ZnO composite nanofibers and their photocatalytic property. Materials Letters 65 (9):1327-1330

94. Cao T, Li Y, Wang C, Wei L, Shao C, Liu Y (2010) Fabrication, structure, and enhanced photocatalytic properties of hierarchical CeO2 nanostructures/TiO2 nanofibers heterostructures. Materials Research Bulletin 45 (10):1406-1412

95. Yang X, Shao C, Liu Y, Mu R, Guan H (2005) Nanofibers of CeO2 via an electrospinning technique. Thin Solid Films 478 (1-2):228-231

96. Kang W, Cheng B, Li Q, Zhuang X, Ren Y (2011) A new method for preparing alumina nanofibers by electrospinning technology. Textile Research Journal 81 (2):148-155

97. Ramakrishna S (2005) An introduction to electrospinning and nanofibers. World Scientific,

98. Shin Y, Hohman M, Brenner M, Rutledge G (2001) Experimental characterization of electrospinning: the electrically forced jet and instabilities. Polymer 42 (25):09955-09967

99. Mo X, Xu C, Kotaki M, Ramakrishna S (2004) Electrospun P (LLA-CL) nanofiber: a biomimetic extracellular matrix for smooth muscle cell and endothelial cell proliferation. Biomaterials 25 (10):1883-1890

100. Megelski S, Stephens JS, Chase DB, Rabolt JF (2002) Micro-and nanostructured surface morphology on electrospun polymer fibers. Macromolecules 35 (22):8456-8466

101. Pawlowski K, Belvin H, Raney D, Su J, Harrison J, Siochi E (2003) Electrospinning of a micro-air vehicle wing skin. Polymer 44 (4):1309-1314

102. Zhao S, Wu X, Wang L, Huang Y (2004) Electrospinning of ethyl–cyanoethyl cellulose/tetrahydrofuran solutions. Journal of Applied Polymer Science 91 (1):242-246

103. Zhang C, Yuan X, Wu L, Han Y, Sheng J (2005) Study on morphology of electrospun poly (vinyl alcohol) mats. European polymer journal 41 (3):423-432

104. Tan S, Inai R, Kotaki M, Ramakrishna S (2005) Systematic parameter study for ultra-fine fiber fabrication via electrospinning process. Polymer 46 (16):6128-6134

105. Matabola K, Moutloali R (2013) The influence of electrospinning parameters on the morphology and diameter of poly (vinyledene fluoride) nanofibers-effect of sodium chloride. Journal of Materials Science 48 (16):5475-5482

106. Li D, Xia Y (2003) Fabrication of titania nanofibers by electrospinning. Nano letters 3 (4):555-560

107. Zong X, Kim K, Fang D, Ran S, Hsiao BS, Chu B (2002) Structure and process relationship of electrospun bioabsorbable nanofiber membranes. Polymer 43 (16):4403-4412

108. Demir MM, Yilgor I, Yilgor E, Erman B (2002) Electrospinning of polyurethane fibers. Polymer 43 (11):3303-3309

109. Krishnappa R, Desai K, Sung C (2003) Morphological study of electrospun polycarbonates as a function of the solvent and processing voltage. Journal of materials science 38 (11):2357-2365

110. Jarusuwannapoom T, Hongrojjanawiwat W, Jitjaicham S, Wannatong L, Nithitanakul M, Pattamaprom C, Koombhongse P, Rangkupan R, Supaphol P (2005) Effect of solvents on electro-spinnability of polystyrene solutions and morphological appearance of resulting electrospun polystyrene fibers. European Polymer Journal 41 (3):409-421

111. Teo WE, Ramakrishna S (2006) A review on electrospinning design and nanofibre assemblies. Nanotechnology 17 (14):R89

112. Theron S, Yarin A, Zussman E, Kroll E (2005) Multiple jets in electrospinning: experiment and modeling. Polymer 46 (9):2889-2899

113. Yarin A, Zussman E (2004) Upward needleless electrospinning of multiple nanofibers. Polymer 45 (9):2977-2980

114. Dosunmu O, Chase GG, Kataphinan W, Reneker D (2006) Electrospinning of polymer nanofibres from multiple jets on a porous tubular surface. Nanotechnology 17 (4):1123

115. Miloh T, Spivak B, Yarin A (2009) Needleless electrospinning: Electrically driven instability and multiple jetting from the free surface of a spherical liquid layer. Journal of Applied Physics 106 (11):114910

116. Lukas D, Sarkar A, Pokorny P (2008) Self-organization of jets in electrospinning from free liquid surface: A generalized approach. Journal of Applied Physics 103 (8):084309

117. Yarin AL, Zussman E (2004) Upward needleless electrospinning of multiple nanofibers. Polymer (45):29977-22980

118. Zhou FL, Gong RH, Porat I (2009) Mass production of nanofibre assemblies by electrostatic spinning. Polymer International 58 (4):331-342

119. Kalinová K, Jirsák O Resonance effect of nanofibrous layer. In: Proceedings of the 5th AUTEX World Textile Conference, 2005.

120. Wang X, Niu H, Wang X, Lin T (2012) Needleless electrospinning of uniform nanofibers using spiral coil spinnerets. Journal of Nanomaterials 2012:3

121. Wannatong L, Sirivat A, Supaphol P (2004) Effects of solvents on electrospun polymeric fibers: preliminary study on polystyrene. Polymer International 53 (11):1851-1859

122. Son WK, Youk JH, Lee TS, Park WH (2004) Electrospinning of ultrafine cellulose acetate fibers: studies of a new solvent system and deacetylation of ultrafine cellulose acetate fibers. Journal of Polymer Science Part B: Polymer Physics 42 (1):5-11

123. Yuan X, Zhang Y, Dong C, Sheng J (2004) Morphology of ultrafine polysulfone fibers prepared by electrospinning. Polymer International 53 (11):1704-1710

124. Haider A, Haider S, Kang I-K (2015) A comprehensive review summarizing the effect of electrospinning parameters and potential applications of nanofibers in biomedical and biotechnology. Arabian Journal of Chemistry

125. Yang J, Stewart M, Maupin G, Herling D, Zelenyuk A (2009) Single wall diesel particulate filter (DPF) filtration efficiency studies using laboratory generated particles. Chemical Engineering Science 64 (8):1625-1634

126. Huang Z-M, Zhang Y-Z, Kotaki M, Ramakrishna S (2003) A review on polymer nanofibers by electrospinning and their applications in nanocomposites. Composites science and technology 63 (15):2223-2253

127. Wei L, Zhang H, Qin X (2018) Fabricated narrow diameter distribution nanofiber for an air filtration membrane using a double rings slit spinneret. Textile Research Journal:0040517518758009

128. Hsu C-M, Shivkumar S (2004) Nano-sized beads and porous fiber constructs of poly (ε-caprolactone) produced by electrospinning. Journal of Materials Science 39 (9):3003-3013

129. Nair LS, Bhattacharyya S, Bender JD, Greish YE, Brown PW, Allcock HR, Laurencin CT (2004) Fabrication and optimization of methylphenoxy substituted polyphosphazene nanofibers for biomedical applications. Biomacromolecules 5 (6):2212-2220

130. Macossay J, Marruffo A, Rincon R, Eubanks T, Kuang A (2007) Effect of needle diameter on nanofiber diameter and thermal properties of electrospun poly (methyl methacrylate). Polymers for Advanced Technologies 18 (3):180-183

131. Shenoy SL, Bates WD, Frisch HL, Wnek GE (2005) Role of chain entanglements on fiber formation during electrospinning of polymer solutions: good solvent, non-specific polymer–polymer interaction limit. Polymer 46 (10):3372-3384

132. Kameoka J, Orth R, Yang Y, Czaplewski D, Mathers R, Coates GW, Craighead H (2003) A scanning tip electrospinning source for deposition of oriented nanofibres. Nanotechnology 14 (10):1124

133. Christanti Y, Walker LM (2001) Surface tension driven jet break up of strain-hardening polymer solutions. Journal of Non-Newtonian Fluid Mechanics 100 (1-3):9-26

134. Fong H, Chun I, Reneker D (1999) Beaded nanofibers formed during electrospinning. Polymer 40 (16):4585-4592

135. Kim SJ, Lee CK, Kim SI (2005) Effect of ionic salts on the processing of poly (2-acrylamido-2-methyl-1-propane sulfonic acid) nanofibers. Journal of Applied Polymer Science 96 (4):1388-1393

136. Choi JS, Lee SW, Jeong L, Bae S-H, Min BC, Youk JH, Park WH (2004) Effect of organosoluble salts on the nanofibrous structure of electrospun poly (3-hydroxybutyrate-co-3-hydroxyvalerate). International Journal of Biological Macromolecules 34 (4):249-256

137. Moghe A, Hufenus R, Hudson S, Gupta B (2009) Effect of the addition of a fugitive salt on electrospinnability of poly (ε-caprolactone). Polymer 50 (14):3311-3318

138. Garoz D, Bueno C, Larriba C, Castro S, Romero-Sanz I, Fernandez de La Mora J, Yoshida Y, Saito G (2007) Taylor cones of ionic liquids from capillary tubes as sources of pure ions: The role of surface tension and electrical conductivity. Journal of Applied Physics 102 (6):064913

139. Fernández de La Mora J (2007) The fluid dynamics of Taylor cones. Annu Rev Fluid Mech 39:217-243

140. Kowalewski TA, Barral S, Kowalczyk T Modeling electrospinning of nanofibers. In: IUTAM symposium on modelling nanomaterials and nanosystems, 2009. Springer, pp 279-292

141. Pinto NJ, González R, Johnson Jr AT, MacDiarmid AG (2006) Electrospun hybrid organic/inorganic semiconductor Schottky nanodiode. Applied Physics Letters 89 (3):033505

142. Pinto N, Johnson Jr A, MacDiarmid A, Mueller C, Theofylaktos N, Robinson D, Miranda F (2003) Electrospun polyaniline/polyethylene oxide nanofiber field-effect transistor. Applied physics letters 83 (20):4244-4246

143. Theron S, Zussman E, Yarin A (2004) Experimental investigation of the governing parameters in the electrospinning of polymer solutions. Polymer 45 (6):2017-2030

144. Son WK, Youk JH, Lee TS, Park WH (2004) The effects of solution and polyelectrolyte on electrospinning of ultrafine poly(ethylene oxide) fibers. polymer.

145. Lee K, Kim H, Khil M, Ra Y, Lee D (2003) Characterization of nano-structured poly (ε-caprolactone) nonwoven mats via electrospinning. Polymer 44 (4):1287-1294

146. Yuvaraj S, Fan-Yuan L, Tsong-Huei C, Chuin-Tih Y (2003) Thermal decomposition of metal nitrates in air and hydrogen environments. The Journal of Physical Chemistry B 107 (4):1044-1047

147. Shuang L, Xiaodong W, Duan W, Rui R (2015) Ceria-based catalysts for soot oxidation: a review. Journal of Rare Earths 33 (6):567-590

148. Panda P, Ramakrishna S (2007) Electrospinning of alumina nanofibers using different precursors. Journal of materials science 42 (6):2189-2193

149. Ramaseshan R, Sundarrajan S, Jose R, Ramakrishna S (2007) Nanostructured ceramics by electrospinning. Journal of Applied Physics 102 (11):7

150. Trovarelli A (1996) Catalytic properties of ceria and CeO2-containing materials. Catalysis Reviews 38 (4):439-520

151. Liu Y, Jiang G, Li L, Chen H, Huang Q, Du X, Tong Z (2017) Electrospun CeO2/Ag@ carbon nanofiber hybrids for selective oxidation of alcohols. Powder Technology 305:597-601

152. Kanzler CH, Urban S, Zalewska-Wierzbicka K, Hess F, Rohrlack SF, Wessel C, Ostermann R, Hofmann JP, Smarsly BM, Over H (2013) Electrospun metal oxide nanofibres
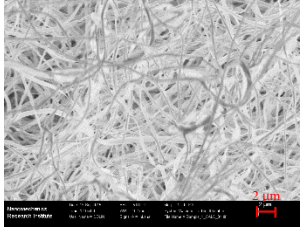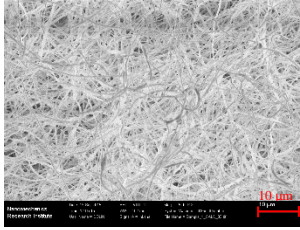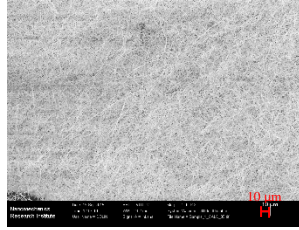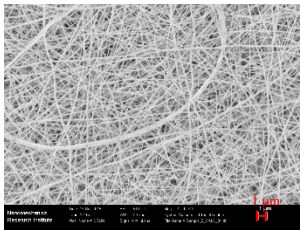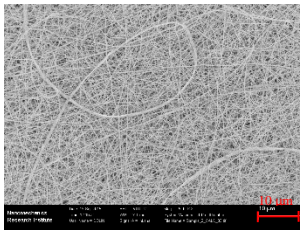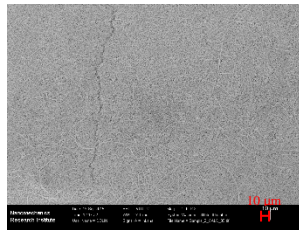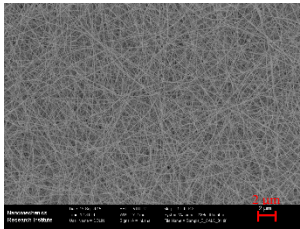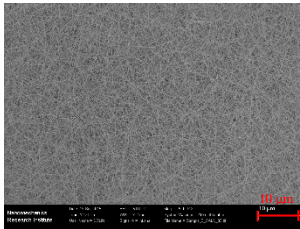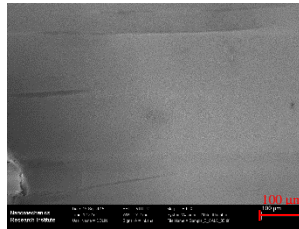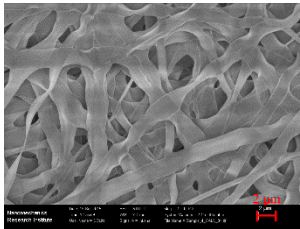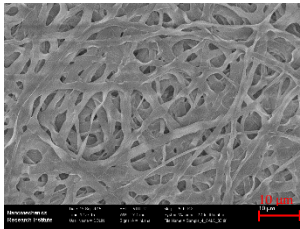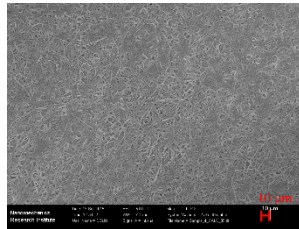
for the assessment of catalyst morphological stability under harsh reaction conditions. ChemCatChem 5 (9):2621-2626

153. Shao H, Zhang X, Liu S, Chen F, Xu J, Feng Y (2011) Preparation of pure iron nanofibers via electrospinning. Materials Letters 65 (12):1775-1777

154. Zhao Z, Li J, Yuan X, Li X, Zhang Y, Sheng J (2005) Preparation and properties of electrospun poly (vinylidene fluoride) membranes. Journal of applied polymer science 97 (2):466-474

155. Koski A, Yim K, Shivkumar S (2004) Effect of molecular weight on fibrous PVA produced by electrospinning. Materials Letters 58 (3-4):493-497

156. Küchler A (2005) Hochspannungstechnik. Springer Verlag 2:95f

157. Zhmayev E, Cho D, Joo YL (2010) Nanofibers from gas-assisted polymer melt electrospinning. Polymer 51 (18):4140-4144

158. Angammana CJ, Jayaram SH A theoretical understanding of the physical mechanisms of electrospinning. In: Proc. ESA Annual Meeting on Electrostatics, 2011. pp 14-16

159. Xu L (2009) A mathematical model for electrospinning process under coupled field forces. Chaos, Solitons & Fractals 42 (3):1463-1465

160. Liu H, Hsieh YL (2002) Ultrafine fibrous cellulose membranes from electrospinning of cellulose acetate. Journal of Polymer Science Part B: Polymer Physics 40 (18):2119-2129

161. Liu H, Tang C (2007) Electrospinning of cellulose acetate in solvent mixture N, N-dimethylacetamide (DMAc)/acetone. Polymer journal 39 (1):65-72

162. Polyvinylpyrrolidone. (2017). https://www.chemicalbook.com/ProductChemicalPropertiesCB4209342_EN.htm. 2019

163. Twigg MV (2007) Progress and future challenges in controlling automotive exhaust gas emissions. Applied Catalysis B: Environmental 70 (1):2-15

164. Shin EH, Cho KS, Seo MH, Kim H (2008) Determination of electrospun fiber diameter distributions using image analysis processing. Macromolecular research 16 (4):314-319

165. Sauvola J, Pietikäinen M (2000) Adaptive document image binarization. Pattern recognition 33 (2):225-236

166. Givehchi R, Tan Z (2015) The effect of capillary force on airborne nanoparticle filtration. Journal of Aerosol Science 83:12-24

167. Chattopadhyay S, Hatton TA, Rutledge GC (2016) Aerosol filtration using electrospun cellulose acetate fibers. Journal of materials science 51 (1):204-217

168. Tang M, Hu J, Liang Y, Pui DY (2017) Pressure drop, penetration and quality factor of filter paper containing nanofibers. Textile Research Journal 87 (4):498-508

169. Thompson C, Chase GG, Yarin A, Reneker D (2007) Effects of parameters on nanofiber diameter determined from electrospinning model. Polymer 48 (23):6913-6922

170. Poly(vinyl alcohol). (2019). https://www.chemicalbook.com/ProductList_En.aspx?kwd=polyvinyl%20alcohol&a=United%20States&left=True#J_Condition. 2019

171. Ethanol. (2019) Chemical Book. https://www.chemicalbook.com/ProductList_En.aspx?kwd=Ethanol&a=United%20States&left=True#J_Condition.

172. Water - Density, Specific Weight and Thermal Expansion Coefficient (2003) The Engineering ToolBox. https://www.engineeringtoolbox.com/water-density-specific-weight-d_595.html?vA=20&units=C#. 2019

173. Aluminum Nitrate Nonahydrate. American Elements. https://www.americanelements.com/aluminum-nitrate-nonahydrate-7784-27-2. 2019

174. Cerium(III) Nitrate Hexahydrate. American Elements. https://www.americanelements.com/cerium-iii-nitrate-hexahydrate-10294-41-4. 2019

175. Suarez S, Sahin M, Adam Y, Moussignac L, Cuffari D, Paterno D (2015) A variable temperature study of the transport properties of aqueous solutions of VOSO4 and NH4VO3 in 2 M H2SO4. Journal of Power Sources 276:153-161

176. Viscosity of Water. (2019) Anton Paar. https://wiki.anton-paar.com/en/water/. Accessed 10.02. 2019

177. Viscosity of Ethanol. (2019) Anton Paar. https://wiki.anton-paar.com/en/ethanol/. Accessed 10.02. 2019

178. Riba J-R, Esteban B (2014) A simple laboratory experiment to measure the surface tension of a liquid in contact with air. European Journal of Physics 35 (5):055003

179. Lee B-B, Ravindra P, Chan E-S (2009) New drop weight analysis for surface tension determination of liquids. Colloids and Surfaces A: Physicochemical and Engineering Aspects 332 (2-3):112-120

180. Surface Tension of Water. (2019) DDBST GmbH http://www.ddbst.com/en/EED/PCP/SFT_C174.php. Accessed 11.02. 2019

181. Montgomery DC (2017) Design and analysis of experiments. John Wiley & Sons,

182. Zohuri B (2017) Dimensional Analysis Beyond the Pi Theorem. Springer,

183. Hanche-Olsen H (2004) Buckingham's pi-theorem. NTNU: http://www math ntnu no/~ hanche/notes/buckingham/buckingham-a4 pdf

184. Ahne J, Li Q, Croiset E, Tan Z (2018) Electrospun cellulose acetate nanofibers for airborne nanoparticle filtration. Textile Research Journal:0040517518807440

185. Picq D (2015) Development of Electrospun Cellulose Acetate Nanofiber-Based Membranes for Filtration Application.

186. Christoforou T, Doumanidis C (2010) Biodegradable cellulose acetate nanofiber fabrication via electrospinning. Journal of nanoscience and nanotechnology 10 (9):6226-6233

187. Liu C, Hsu P-C, Lee H-W, Ye M, Zheng G, Liu N, Li W, Cui Y (2015) Transparent air filter for high-efficiency PM 2.5 capture. Nature communications 6:6205

188. Lee C, Park J-I, Shul Y-G, Einaga H, Teraoka Y (2015) Ag supported on electrospun macro-structure CeO2 fibrous mats for diesel soot oxidation. Applied Catalysis B: Environmental 174:185-192

189. Li Z, Fan Y, Zhan J (2010) In2O3 Nanofibers and Nanoribbons: Preparation by Electrospinning and Their Formaldehyde Gas-Sensing Properties. European journal of inorganic chemistry 2010 (21):3348-3353

190. Johnson DL, Cutler IB (1963) Diffusion sintering: I, initial stage sintering models and their application to shrinkage of powder compacts. Journal of the American Ceramic Society 46 (11):541-545

191. Ding B, Kim H-Y, Lee S-C, Lee D-R, Choi K-J (2002) Preparation and characterization of nanoscaled poly (vinyl alcohol) fibers via electrospinning. Fibers and Polymers 3 (2):73-79

192. Wang C, Zhang W, Huang Z, Yan E, Su Y (2006) Effect of concentration, voltage, take-over distance and diameter of pinhead on precursory poly (phenylene vinylene) electrospinning. Pigment & resin technology 35 (5):278-283

193. Li L, Hsieh Y-L (2005) Ultra-fine polyelectrolyte fibers from electrospinning of poly (acrylic acid). Polymer 46 (14):5133-5139

194. Zeng J, Chen X, Xu X, Liang Q, Bian X, Yang L, Jing X (2003) Ultrafine fibers electrospun from biodegradable polymers. Journal of Applied Polymer Science 89 (4):1085-1092
195. Wang C, Hsu C-H, Lin J-H (2006) Scaling laws in electrospinning of polystyrene solutions. Macromolecules 39 (22):7662-7672
196. Baker-Jarvis J, Janezic MD, DeGroot DC (2010) High-frequency dielectric measurements. IEEE Instrumentation & Measurement Magazine 13 (2):24-31
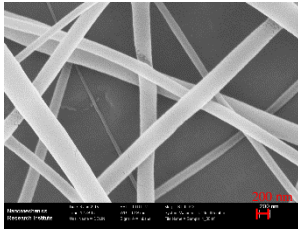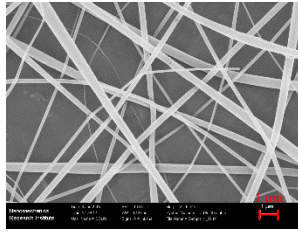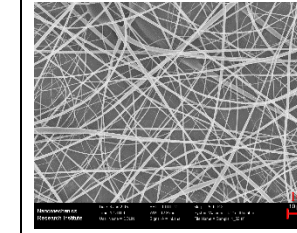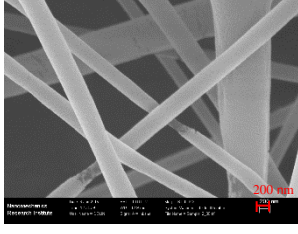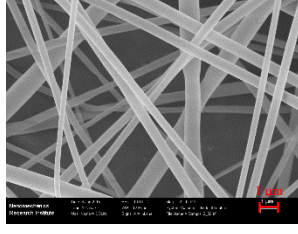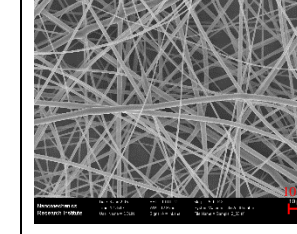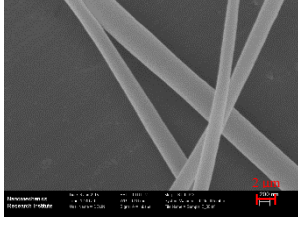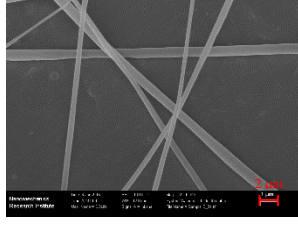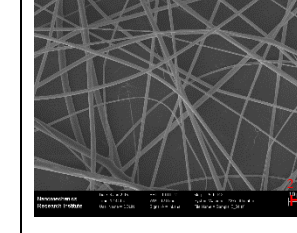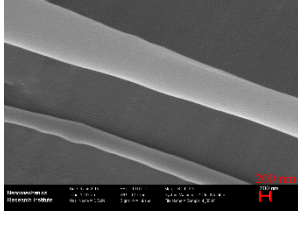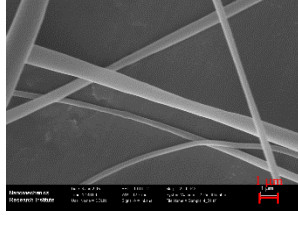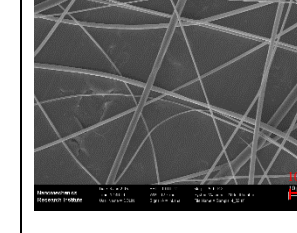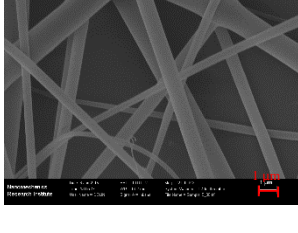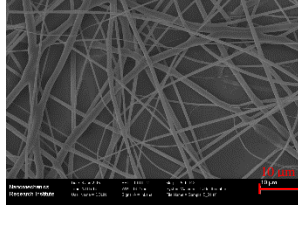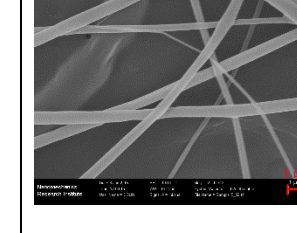
Appendix A – SEM Images

A.1. Calcined Ceria fibers with different solution composition

2:1 Ethanol:Water			
1:1 Ethanol:Water			
1:2 Ethanol:Water			
1:3 Ethanol:Water			

A.2. Cellulose Acetate Fibers

CA10_5_8_10			
CA15_5_8_10			
CA15_5_8_12.5			
CA15_5_8_15			
CA15_5_10_10			
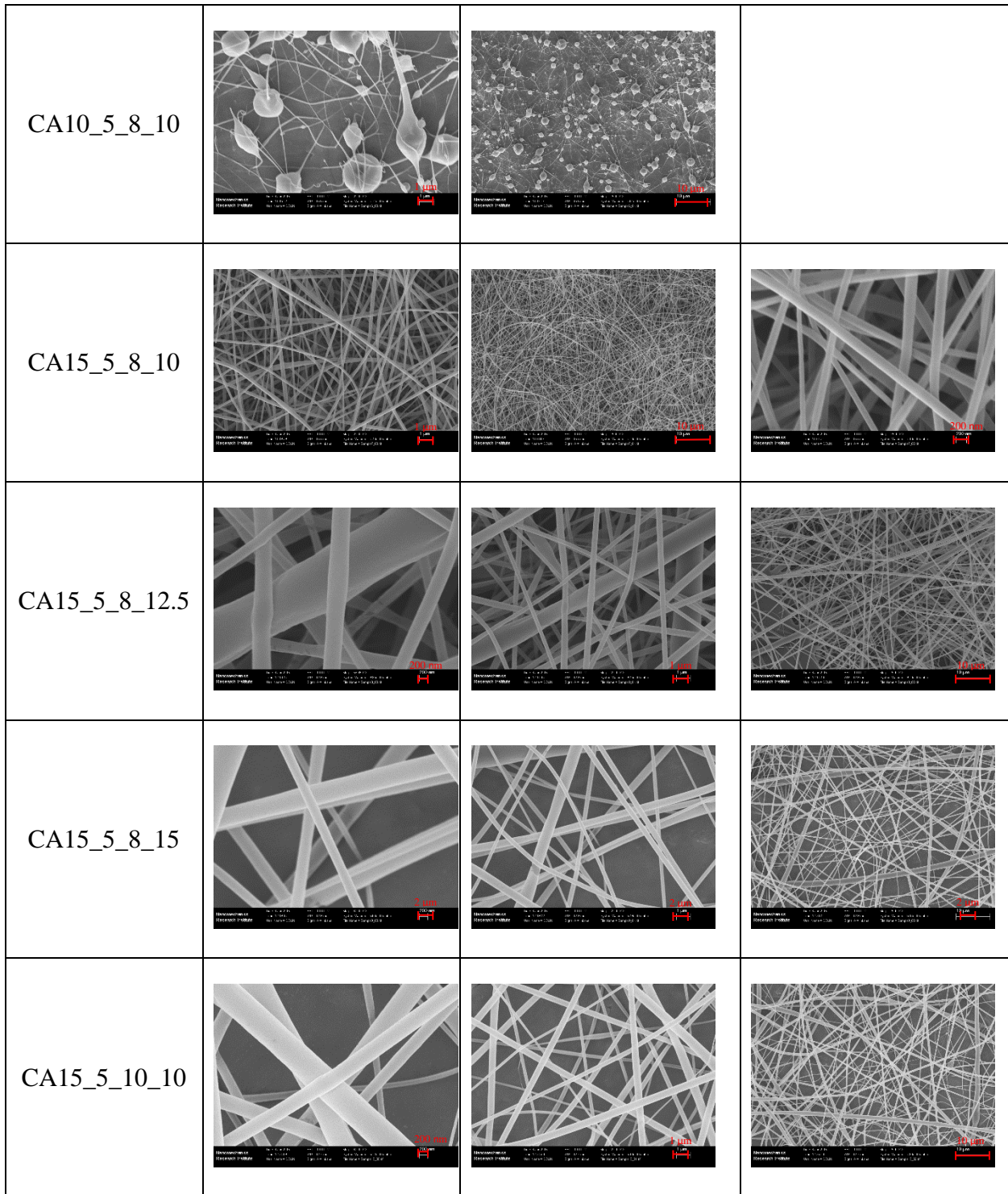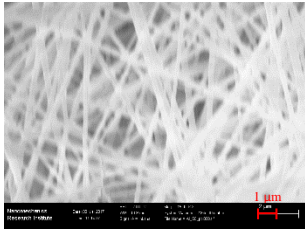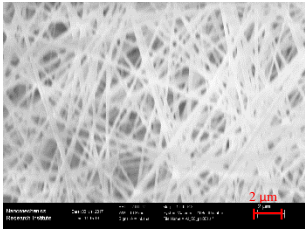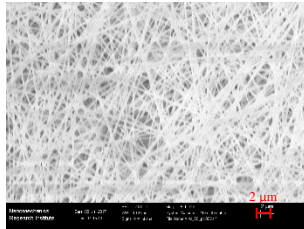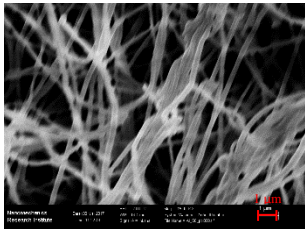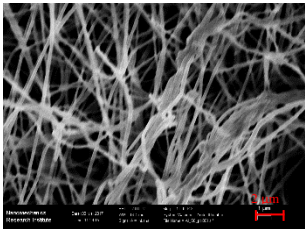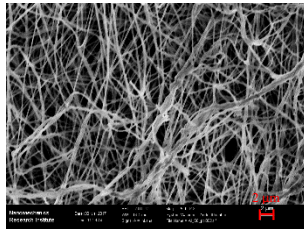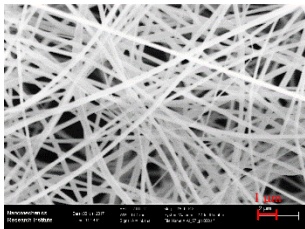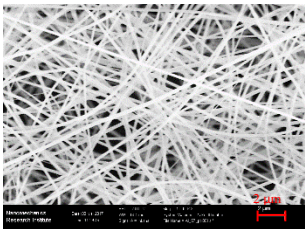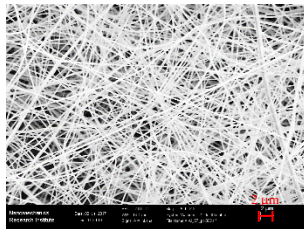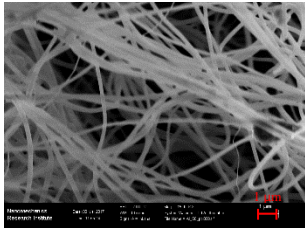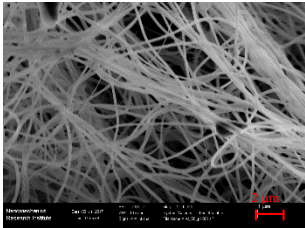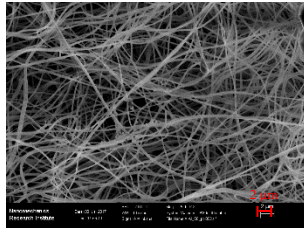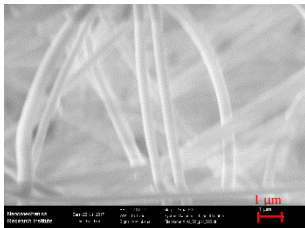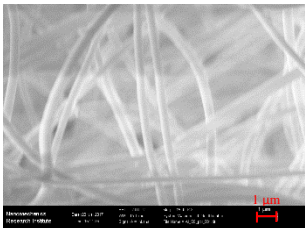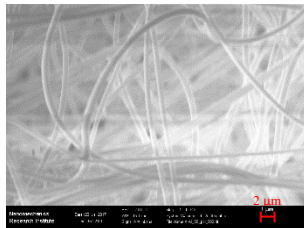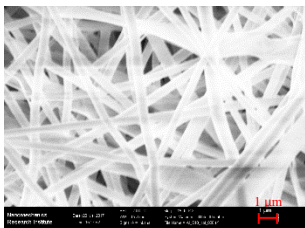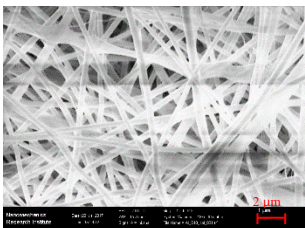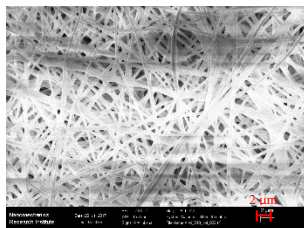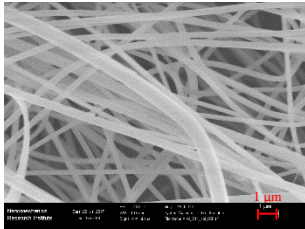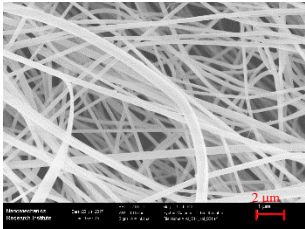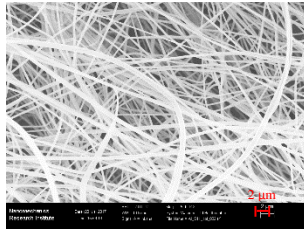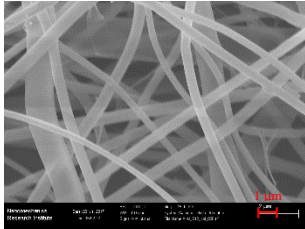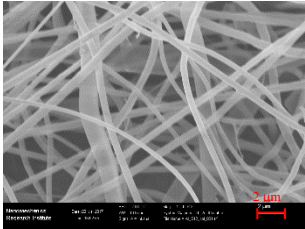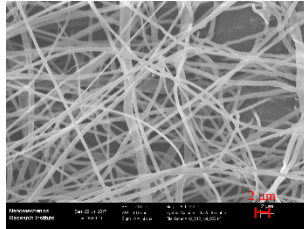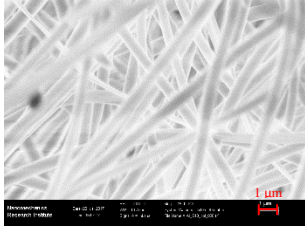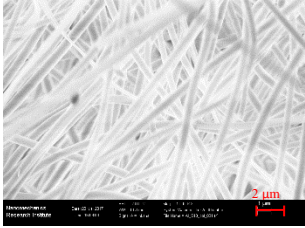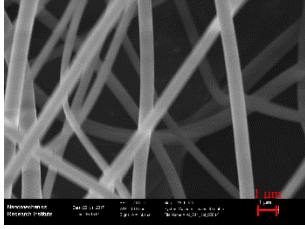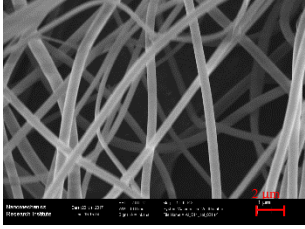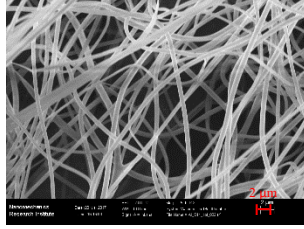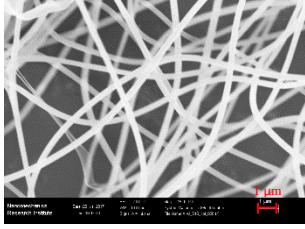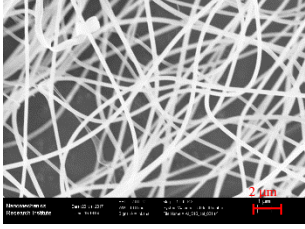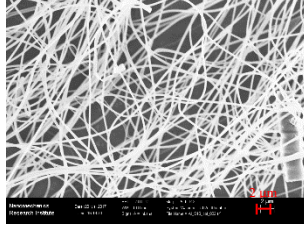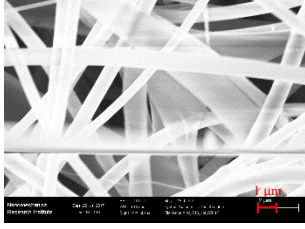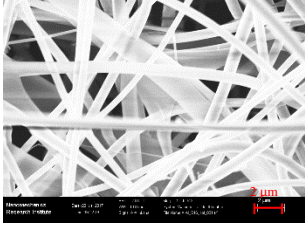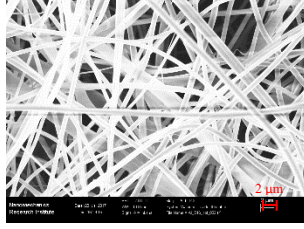
CA15_5_12_10			
CA20_5_8_10			
CA20_5_8_12.5			
CA20_5_8_15			
CA20_5_10_10			

| CA20_5_12_10 | | | |
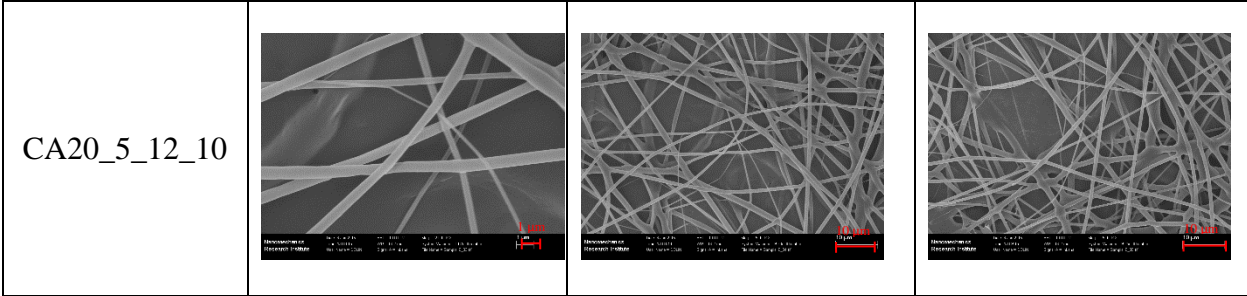
A.3. Polymerized Alumina Fibers

(1)			
a			
b			
ab			

c			
ac			
bc			
abc			
d			
ad			
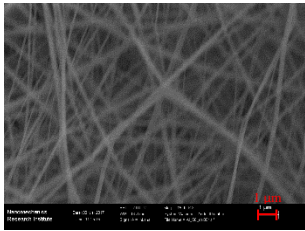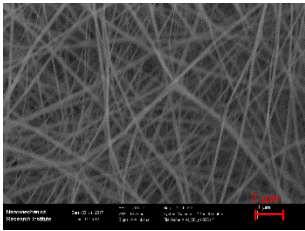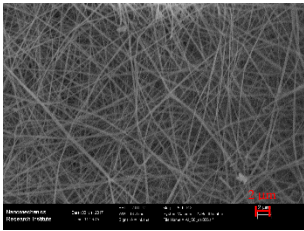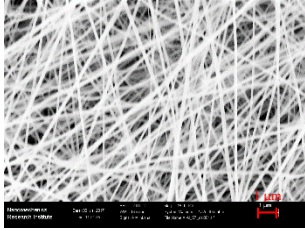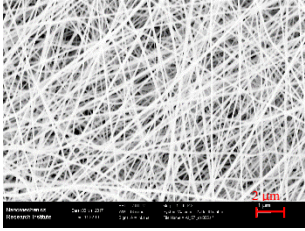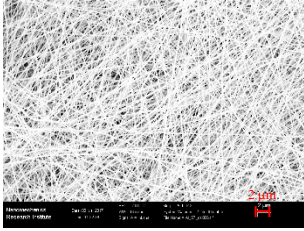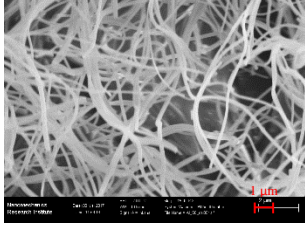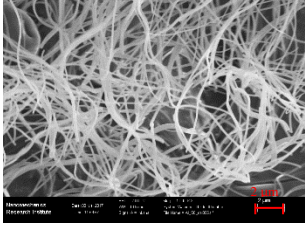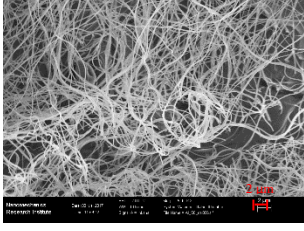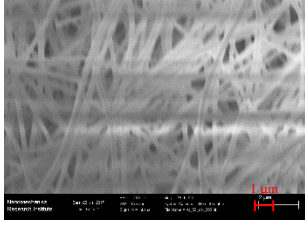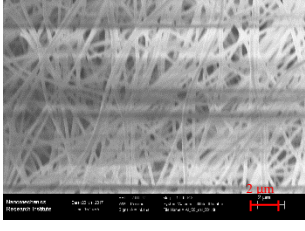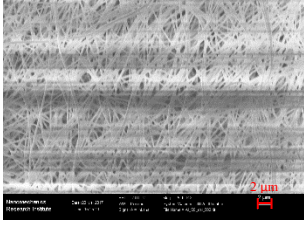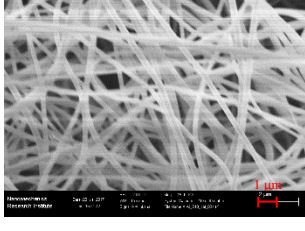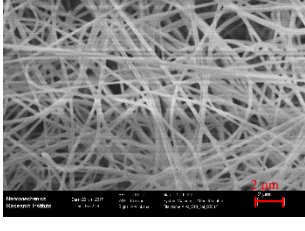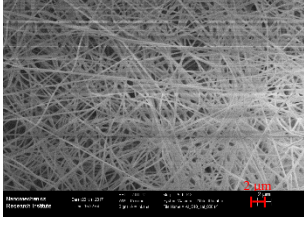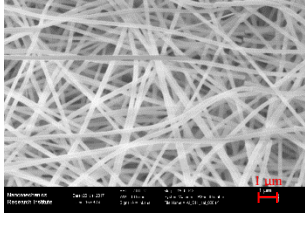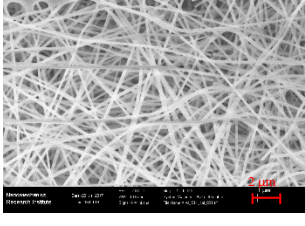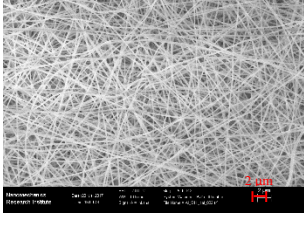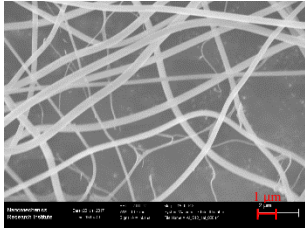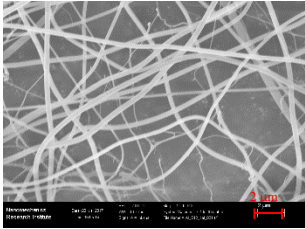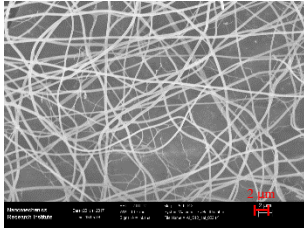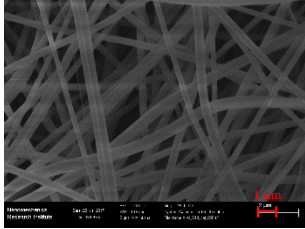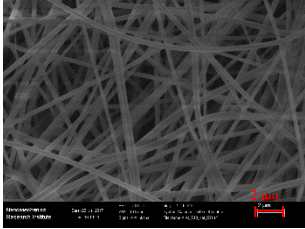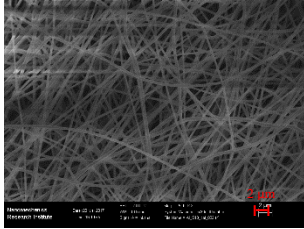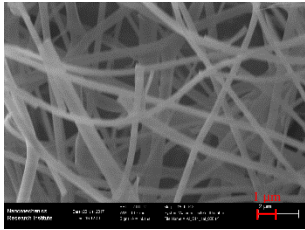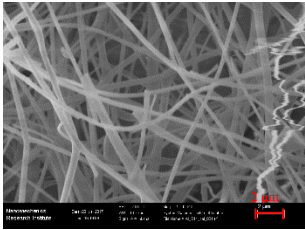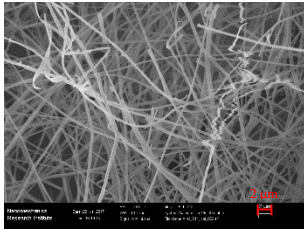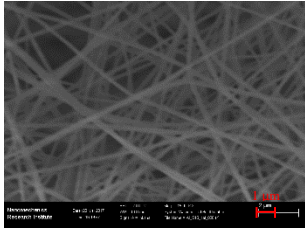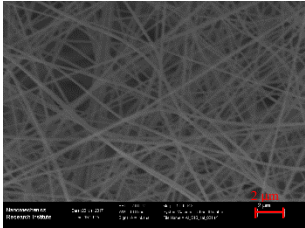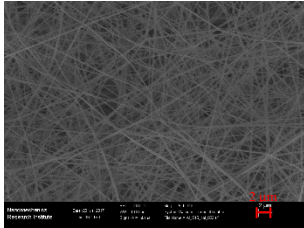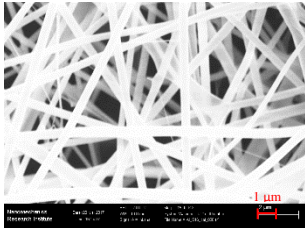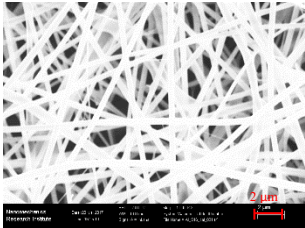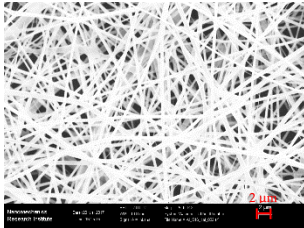
bd			
abd			
cd			
acd			
bcd			
abcd			

A.4. Calcined Alumina Fibers

ac			
bc			
abc			
d			
ad			
bd			
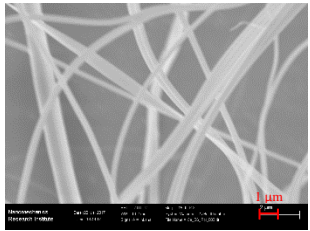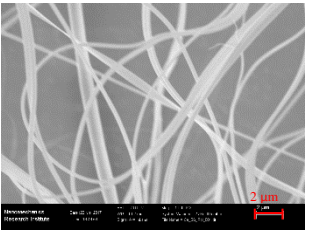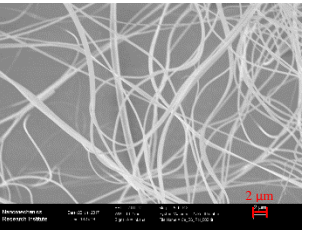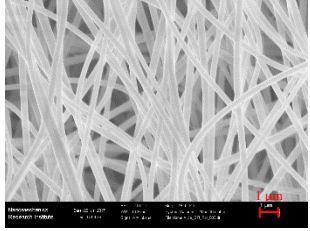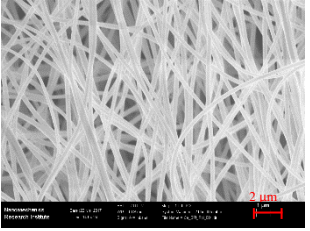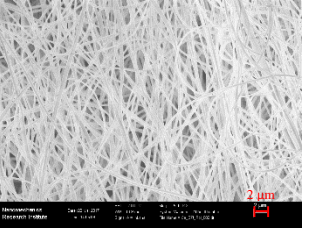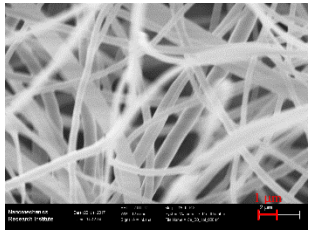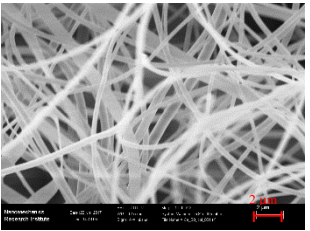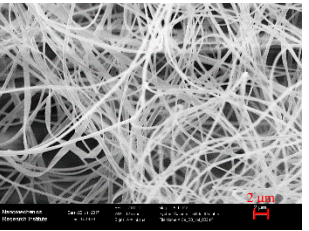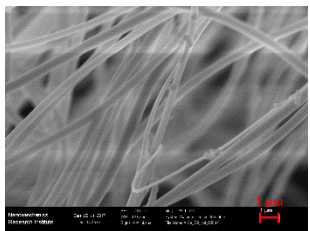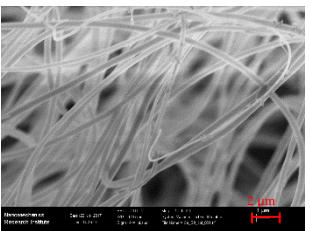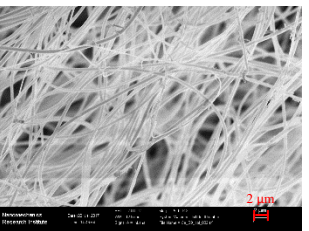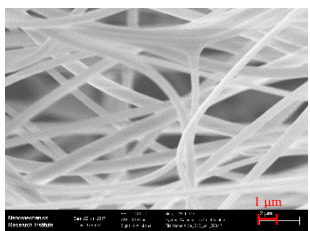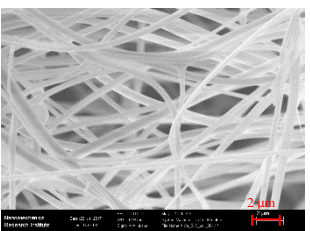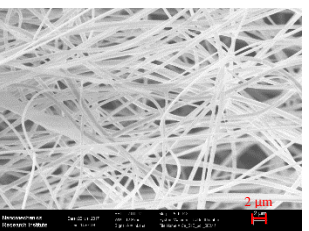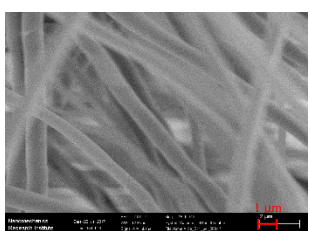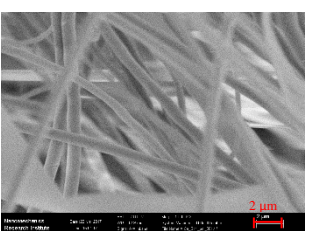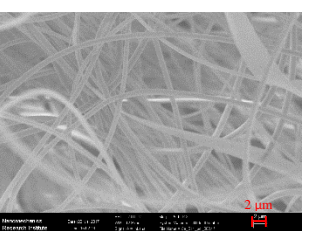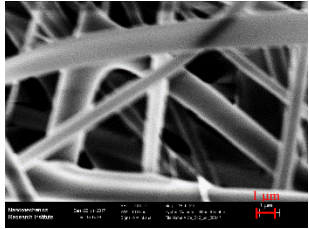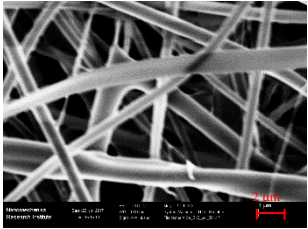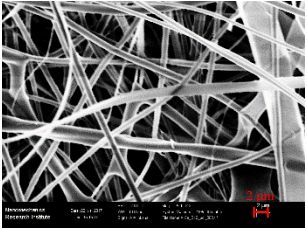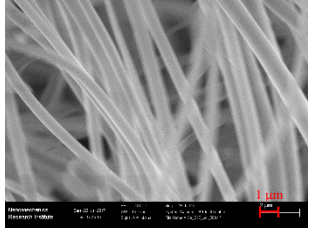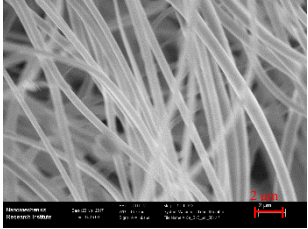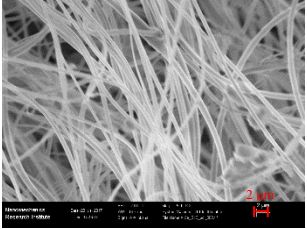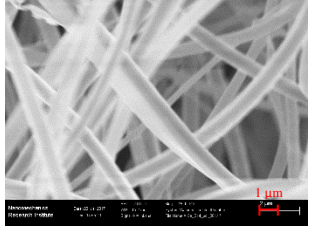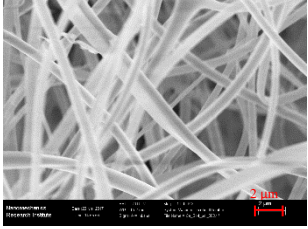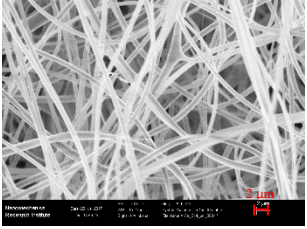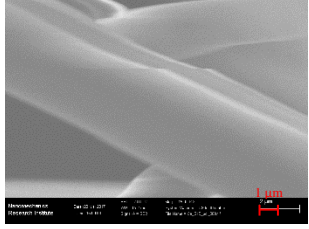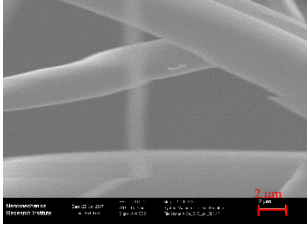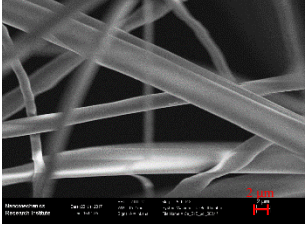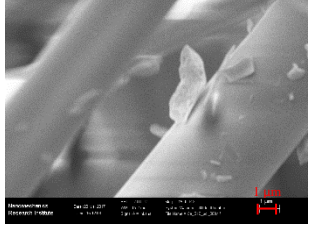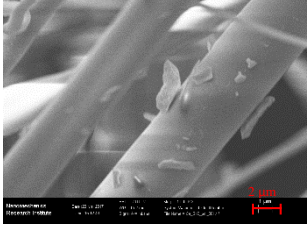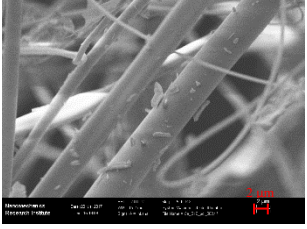
abd			
cd			
acd			
bcd			
abcd			

A.5. Polymerized Ceria Fibers

(1)			
a			
b			
ab			
c			

ac			
bc			
abc			
d			
ad			
bd			
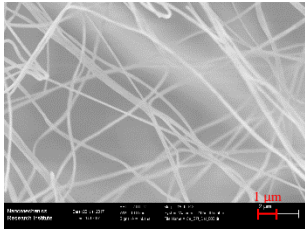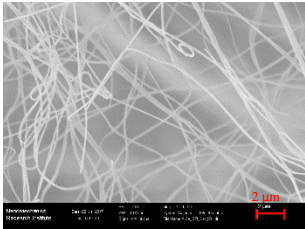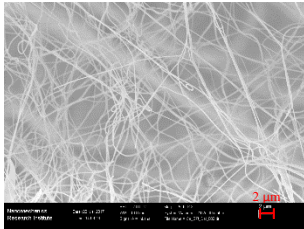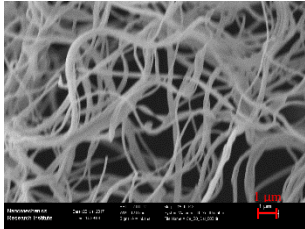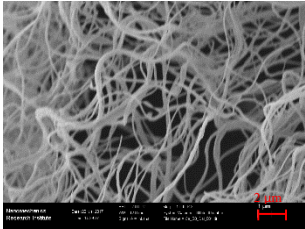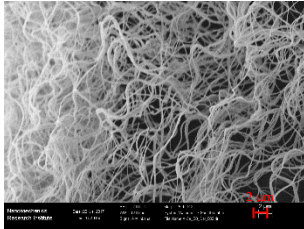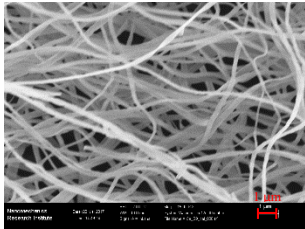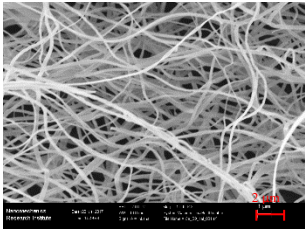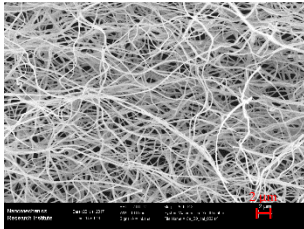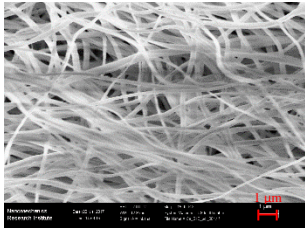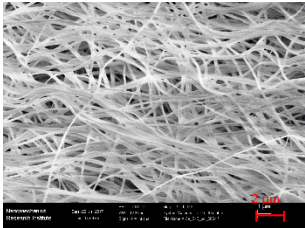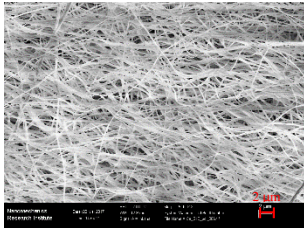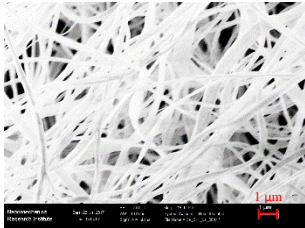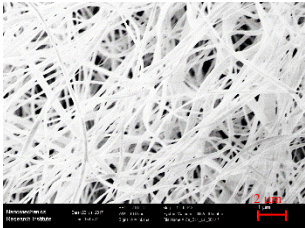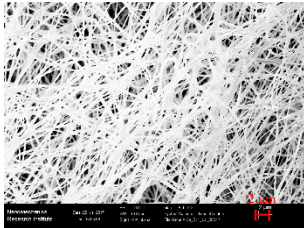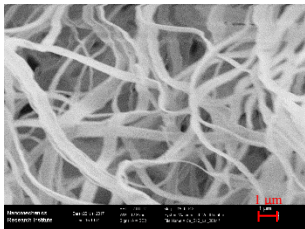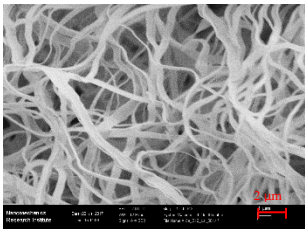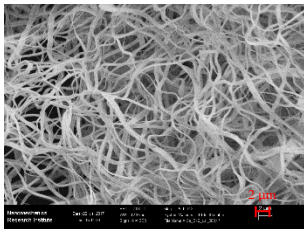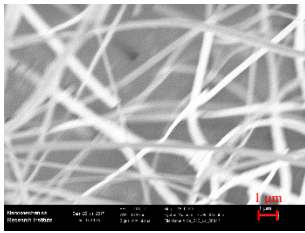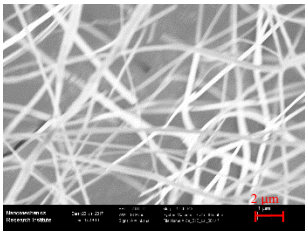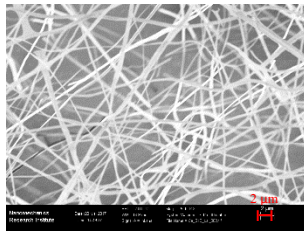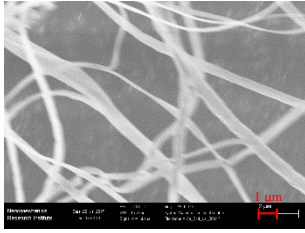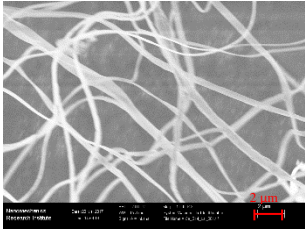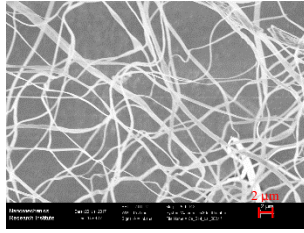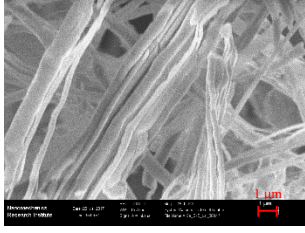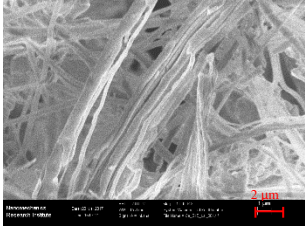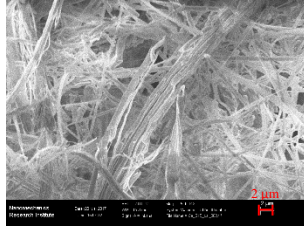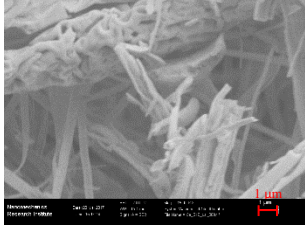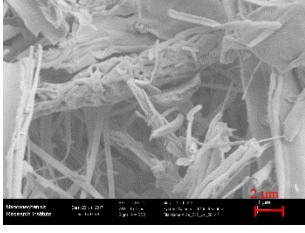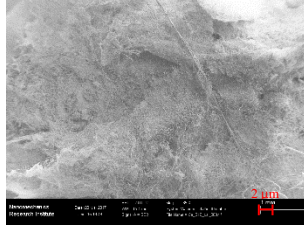
abd			
cd			
acd			
bcd			
abcd			

A.6. Calcined Ceria Fibers

a			
b			
ab			
c			
ac			

154

bc			
abc			
d			
ad			
bd			
abd			

cd			
acd			
bcd			
abcd			

Appendix B. Local distance and electric field strength between needle and collector

U= 20 kV
s= 10 cm (shortest distance between needle and collector

Bold numbers represent distance from the edge in cm, all other values are electric field strength in kV/cm

B.1. Plate Collector

10	9	8	7	6	5	4	3	2	1	0	x/y
1633	1684	1728	1761	1782	1789	1782	1761	1728	1684	1633	**0**
1684	1741	1789	1826	1849	1857	1849	1826	1789	1741	1684	**1**
1728	1789	1841	1881	1907	1916	1907	1881	1841	1789	1728	**2**
1761	1826	1881	1925	1952	1961	1952	1925	1881	1826	1761	**3**
1782	1849	1907	1952	1980	1990	1980	1952	1907	1849	1782	**4**
1789	1857	1916	1961	1990	2000	1990	1961	1916	1857	1789	**5**
1782	1849	1907	1952	1980	1990	1980	1952	1907	1849	1782	**6**
1761	1826	1881	1925	1952	1961	1952	1925	1881	1826	1761	**7**
1728	1789	1841	1881	1907	1916	1907	1881	1841	1789	1728	**8**
1684	1741	1789	1826	1849	1857	1849	1826	1789	1741	1684	**9**
1633	1684	1728	1761	1782	1789	1782	1761	1728	1684	1633	**10**

B.2. Drum Collector

17	15	13	11	9	7	5	3	2	1	0	x/y
1249	1263	1272	1278	1280	1278	1272	1263	1256	1249	1240	**0**
1372	1390	1404	1412	1414	1412	1404	1390	1382	1372	1361	**2**
1505	1530	1548	1558	1562	1558	1548	1530	1518	1505	1491	**4**
1641	1673	1696	1710	1715	1710	1696	1673	1658	1641	1622	**6**
1764	1804	1833	1851	1857	1851	1833	1804	1785	1764	1740	**8**
1853	1899	1933	1954	1961	1954	1933	1899	1877	1853	1825	**10**
1885	1934	1970	1993	2000	1993	1970	1934	1911	1885	1857	**12**
1853	1899	1933	1954	1961	1954	1933	1899	1877	1853	1825	**14**
1764	1804	1833	1851	1857	1851	1833	1804	1785	1764	1740	**16**
1641	1673	1696	1710	1715	1710	1696	1673	1658	1641	1622	**18**
1505	1530	1548	1558	1562	1558	1548	1530	1518	1505	1491	**20**
1372	1390	1404	1412	1414	1412	1404	1390	1382	1372	1361	**22**
1249	1263	1272	1278	1280	1278	1272	1263	1256	1249	1240	**24**

Appendix C – Development of Echelon Form

Initial matrix:

	U	d_{TC}	d_N	κ	ν	γ	$\dot{V}$
L	2	1	1	-3	2	0	3
M	1	0	0	-1	0	1	0
t	-3	0	0	3	-1	-2	-1
I	-1	0	0	2	0	0	0

- Divide row1 by 2

1	1/2	1/2	-3/2	1	0	3/2
1	0	0	-1	0	1	0
-3	0	0	3	-1	-2	-1
-1	0	0	2	0	0	0

- Add (-1 * row1) to row2

1	1/2	1/2	-3/2	1	0	3/2
0	-1/2	-1/2	1/2	-1	1	-3/2
-3	0	0	3	-1	-2	-1
-1	0	0	2	0	0	0

- Add (3 * row1) to row3

1	1/2	1/2	-3/2	1	0	3/2
0	-1/2	-1/2	1/2	-1	1	-3/2
0	3/2	3/2	-3/2	2	-2	7/2
-1	0	0	2	0	0	0

- Add (1 * row1) to row4

1	1/2	1/2	-3/2	1	0	3/2
0	-1/2	-1/2	1/2	-1	1	-3/2
0	3/2	3/2	-3/2	2	-2	7/2
0	1/2	1/2	1/2	1	0	3/2

- Divide row2 by -1/2

1	1/2	1/2	-3/2	1	0	3/2
0	1	1	-1	2	-2	3
0	3/2	3/2	-3/2	2	-2	7/2
0	1/2	1/2	1/2	1	0	3/2

- Add (-3/2 * row2) to row3

1	1/2	1/2	-3/2	1	0	3/2
0	1	1	-1	2	-2	3
0	0	0	0	-1	1	-1
0	1/2	1/2	1/2	1	0	3/2

- Add (-1/2 * row2) to row4

1	1/2	1/2	-3/2	1	0	3/2
0	1	1	-1	2	-2	3
0	0	0	0	-1	1	-1
0	0	0	1	0	1	0

- Swapping row4 with row3

1	1/2	1/2	-3/2	1	0	3/2
0	1	1	-1	2	-2	3
0	0	0	1	0	1	0
0	0	0	0	-1	1	-1

- Divide row4 by -1

1	1/2	1/2	-3/2	1	0	3/2
0	1	1	-1	2	-2	3
0	0	0	1	0	1	0
0	0	0	0	1	-1	1

- Add (-2 * row4) to row2

1	1/2	1/2	-3/2	1	0	3/2
0	1	1	-1	0	0	1
0	0	0	1	0	1	0
0	0	0	0	1	-1	1

- Add (-1 * row4) to row1

1	1/2	1/2	-3/2	0	1	1/2
0	1	1	-1	0	0	1
0	0	0	1	0	1	0
0	0	0	0	1	-1	1

- Add (1 * row3) to row2

1	1/2	1/2	-3/2	0	1	1/2
0	1	1	0	0	1	1
0	0	0	1	0	1	0
0	0	0	0	1	-1	1

- Add (3/2 * row3) to row1

1	1/2	1/2	0	0	5/2	1/2
0	1	1	0	0	1	1
0	0	0	1	0	1	0
0	0	0	0	1	-1	1

- **Reduced Row Echelon Form**:

1	0	0	0	0	2	0
0	1	1	0	0	1	1
0	0	0	1	0	1	0
0	0	0	0	1	-1	1